IntechOpen

Energy Conversion

Current Technologies and Future Trends

Edited by Ibrahim H. Al-Bahadly

ENERGY CONVERSION - CURRENT TECHNOLOGIES AND FUTURE TRENDS

Edited by **Ibrahim H. Al-Bahadly**

Energy Conversion - Current Technologies and Future Trends
http://dx.doi.org/10.5772/intechopen.73378
Edited by Ibrahim H. Al-Bahadly

Contributors

Giulia Massaglia, Marzia Quaglio, Olatunde Samuel Dahunsi, Munachi Enyinnaya, Youness El Mghouchi, Salman Ajib, Ali Alahmer, Songgang Qiu, Laura Solomon, Janie Ling Chin, Muhammad Burhan, Muhammad Wakil Shahzad, Kim Choon Ng, Nidal Abu-Hamdeh, Khaled Alnefaie, Debarshi Datta, Jose Palacio, José Joaquim Conceição Soares Santos, Maria Luiza Grillo Renó, Juarez Corrêa Furtado Júnior, Monica Carvalho, Dimas José Rúa Orozco, Arnaldo Martín Martínez Reyes, Nguyen The Vinh, Vo Vinh

Notice

First published in London, United Kingdom, 2019 by IntechOpen
eBook (PDF) Published by IntechOpen, 2019
IntechOpen is the global imprint of INTECHOPEN LIMITED, registered in England and Wales, registration number: 11086078, The Shard, 25th floor, 32 London Bridge Street
London, SE19SG – United Kingdom
Printed in Croatia

British Library Cataloguing-in-Publication Data
A catalogue record for this book is available from the British Library

Additional hard and PDF copies can be obtained from orders@intechopen.com

Energy Conversion - Current Technologies and Future Trends
Edited by Ibrahim H. Al-Bahadly

p. cm.

Print ISBN 978-1-78984-904-2

Online ISBN 978-1-78984-905-9

eBook (PDF) ISBN 978-1-83881-739-8

Meet the editor

Ibrahim Al-Bahadly received a B.Sc. (Eng.) degree from the Baghdad University of Technology in 1987, followed by an M.Sc. and Ph.D. from Nottingham University, in 1990 and 1994, respectively, all in electrical and electronic engineering. From 1994 to 1996, he was a research associate with the electric drives and machines group at the University of Newcastle upon Tyne, UK. Since 1996, he has been with the Massey University, where he is currently Associate Professor in electrical and electronic engineering. His research interests include power electronic applications, variable speed machines and drives, energy conversion and renewable energy system, instrumentation and automation. Ibrahim is a senior member of the Institute of Electrical and Electronics Engineers (IEEE).

Contents

Preface XI

Chapter 1 **The Solutions of DC-DC Converters for Renewable Energy System 1**
Nguyen The Vinh and Vo Thanh Vinh

Chapter 2 **Electrical Rating—Long-Term Performance Potential of Photovoltaic Systems 21**
Muhammad Burhan, Muhammad Wakil Shahzad and Ng Kim Choon

Chapter 3 **Solar Cooling Technologies 39**
Salman Ajib and Ali Alahmer

Chapter 4 **State-of-the-Art Technologies on Low-Grade Heat Recovery and Utilization in Industry 55**
Janie Ling-Chin, Huashan Bao, Zhiwei Ma, Wendy Taylor and Anthony Paul Roskilly

Chapter 5 **The Role of Material Selection and Microfluidics for Optimized Energy Conversion in Microbial Fuel Cells 75**
Giulia Massaglia and Marzia Quaglio

Chapter 6 **The Bioenergy Potentials of Lignocelluloses 93**
Olatunde Samuel Dahunsi and Munachi Enyinnaya

Chapter 7 **Free-Piston Stirling Engine Generators 105**
Songgang Qiu and Laura Solomon

Chapter 8 **Municipal Solid Waste Management and Energy Recovery 127**
José Carlos Escobar Palacio, José Joaquim Conceição Soares Santos, Maria Luiza Grillo Renó, Juarez Corrêa Furtado Júnior, Monica Carvalho, Arnaldo Martín Martínez Reyes and Dimas José Rúa Orozco

Preface

Industrialization has caused a hunger in mankind and the effects have had no equal in past history. The generation and the consumption of energy has become the basis of our global markets and has led to the formation of the largest, most powerful corporations on the planet.

Energy storage and power generation are some of the largest influences that have driven both the industrial and agricultural sectors in the developed world to what they are today. In addition, a large majority of the world is powered by finite, unsustainable resources such as fossil fuels. With growing economies and growing populations, renewable energy generation, such as solar, wind, and hydro generation is quickly growing as a means of producing electricity. These sources have great significance for consumers as they are environmentally friendly. Also, they can replace the use of oil and coal in providing energy.

Renewable energy systems are increasing in popularity nowadays in power generation systems because of the advances in the technology and the continuous increase in fuel prices. Due to the high cost of implementing individual renewable energy solutions and their low efficiency, a combination of several systems was introduced, forming a hybrid energy generation solution. The system would typically combine two or more natural energy resources to produce a steady energy flow with improved efficiencies. To ensure high quality power supply for loads, the grid is monitored constantly in real time. This includes sensing outage, over-voltage and under-voltage. Measurements are taken every cycle and compared to a threshold value.

Overall, the structure of the electrical power generation system is in the process of changing. For incremental growth, it is moving away from fossil fuel-based operations to renewable energy resources that are more environmentally friendly and sustainable. At the same time, it has to grow to meet the ever-increasing need for more energy. These changes bring very unique opportunities and obstacles at the same time. Over the past few decades, many new and innovative ideas have been explored in the broad area of energy conversion. This book encompasses a collection of selected research works in the areas of electric energy generation, renewable energy sources, hybrid system, electromechanical energy conversion, electric machines, power electronic converters and inverters, energy storage, and the smart grid. The book intends to provide academic and industry professionals working in the field of energy conversion and related applications with a n update on energy conversion technology, particularly from the applied perspective.

The editor was privileged by the invitation of INTECH to act as editor of this book “Energy Conversion: Current Technologies and Future Trends”, which contains high quality re-

search works from internationally renowned researchers in the field. The editor is glad to have this opportunity to acknowledge all contributing authors and expresses his gratitude for the help and support of INTECH staff, particularly the Author Service Managers Ms Kristina Jurdana and Ms Lada Bozic.

Dr. Ibrahim Al-Bahadly
Associate Professor in Electrical and Electronic Engineering
Massey University
Palmerston North
New Zealand

Chapter 1

The Solutions of DC-DC Converters for Renewable Energy System

Nguyen The Vinh and Vo Thanh Vinh

Additional information is available at the end of the chapter

http://dx.doi.org/10.5772/intechopen.78768

Abstract

Photovoltaic and wind systems have been used for a few years to bring a new power supply to many applications, while preserving the environment. This chapter is interested in this work at low and medium power, a few 100 W, for applications to housing and buildings. The works consider a system in which the various sources of renewable energies are connected to each other in a parallel structure which supposes the use of specialized converters accepting at the input voltages of the order of a few tens of volts, and giving out several hundred of volts. The DC-DC converters with magnetic coupling will be analyzed more particularly to show the technological limits. In particular, the influence of the magnetic circuit and the leakage flows will be studied in more detail.

Keywords: renewable energy systems, DC-DC converter, voltage step-up, coupled conductor

1. Introduction

Optimizing the use of renewable sources for the production of electrical energy is one of the possible answers that can be useful for saving exhaustible fossil energy resources. Nevertheless, the use of renewable energies induces the development of new utilities and even architectures and systems. The management and optimization of the conversion and distribution of electrical energy produced from several different renewable energy sources is a challenge for stable, sustainable energy production systems that are isolated, autonomous and stable. The choice of a high-voltage direct current bus (HVDC bus) for the distribution of energy in the energy production chain can be considered as part of an efficiency improvement strategy [1–3]. The HVDC bus has the advantage of using smaller cross sections of cables than those traditionally

used in AC networks, allowing a reduction in the costs of transport and distribution of electricity. In addition, the HVDC bus is more secure against any fraud of diversion of the produced electricity and provides a global distribution with more security. The distributed, autonomous or interconnected production units corresponding to the energy production systems considered here are generally characterized by a large input current and a low input voltage associated with a high output voltage. This HVDC bus architecture imposes a two-wire topology for the power conversion system connected to an AC distribution network. In this architecture, the distributed power is connected to an alternating current network by means of an intermediate HVDC bus. The DC-DC converters with a basic voltage ratio are integrated upstream, just behind the supply of the energy source or sensors (for example as photovoltaic panels).

Downstream of the HVDC bus is near power generation, a DC-AC inverter is inserted at the interface to convert the HVDC to standard AC, typically according to country specific standardization, 110, 220 or 380 V. In this solution, for optimum conversion efficiency, software drives the system assuming that tracking of the source's maximum power point is directly implemented in the controller of each of the individual DC-DC converters. Thus, as seen in a renewable energy production chain, the individual DC-DC converter integrated into the power generator is one of the most important electronic elements. This converter must take into account a set of characteristics and technological constraints related to the power delivered by the source, whether photovoltaic or other as:

The converter must be able to convert the energy to a range of input voltages between 12 and 60 V which is the upper limit of the no-load voltage for a panel of 60 cells, knowing that in the load the MPP is around 30 V.

The output voltage provided by the converter must be able to reach 240VDC which represents the limit set for this first converter version. An upcoming version should be proposed to have a voltage output of 400 VDC and several kV.

The power to be converted must be greater than 150 W, corresponding to the panels available in the laboratory.

The performance wished is 98%. This value is obviously an average limit, as inverter manufacturers advertise the performance of their devices for an optimal operating point.

The converter must be remotely controlled via a fieldbus.

It must be able to stop production in the event of a fault or a special order for the safety of the installation or for maintenance.

Of all the constraints, it is possible to select three main that motivate our work and are causing numerous research worldwide, that is to say, excellent performance, high voltage gain and a small volume. Other constraints are added such as thermal, mechanical, but have not been taken into account in this work which is mainly focused on the electronic properties of the converter [4]. It should be noted that the aforementioned constraints related to the integration of DC-DC converters in grid-connected electrical generators are specific to the power supply system for power from sources energy renewable.

Nevertheless, most industrial applications require efficient DC-DC converters. As examples, we can note the high intensity discharge ballasts for lamps used in automobile or the front converter with two inputs (a main AC [AC] network and a battery to support DC power supplies) to replace the common but complex emergency power supplies (UPS-uninterruptible power supply) in the computer and telecommunications industries [5]. Nevertheless, for a system of electricity generation from photovoltaic energy or another individual source, due to the variable nature of the input power of the converter, and the almost constant high voltage output hundred a set of additional features specific, necessary and are presented below.

Many works in the literature present these systems and we quote some important references [6]. In order to overcome the drawbacks of basic converters which prove to be unsuitable for photovoltaic energy production systems, as we have pointed out above, various authors, taking into account the different specific constraints of this demand, present an investigation on the many topologies of possible converters [7]. The solution considered simplest is composed of several converters in cascade to obtain the desired gain [8]. Even if we do not take into account synchronization problems inherent to active switches, this solution is not optimal from an economic point of view and the losses by the multiplication of the components and the overall efficiency of the converter low due to the number important components. In addition, this solution does not meet the constraint of reduced size.

The solution considered, which will be described below, is to adjust the high voltage gain (Step-Up), by choosing a suitable ratio of turns of a transformer or inductance coupled to an independent converter [9]. Comparing with a base of transformer converters, a coupled inductance converter in its basic configuration requires few components. Due to its less complicated structure and the smaller, larger ripple of the primary winding current, it requires filtering of input capacitance. This results in lower current stress and more conduction losses low. The converters based on the coupled inductors technique allow the adjustment of the requested voltage with respect to the input voltage by a judicious choice of the transformation ratio m between the coils, which makes it possible to keep a cyclic ratio very near to 1/2, thus guaranteeing an excellent internal energy transfer rate. Unfortunately, an increase in m results in an increase in the trapped energy in the leakage inductances, and even for the low transformation ratios, the result is a degradation of the efficiency. In this converter topology, and in order to achieve a high Step-Up gain, some authors propose efficient solutions resulting in modified topologies obtained by increasing the complexity of the basic version in **Figure 1** [10, 11].

In analyzing the performance of coupled-coupled transformers or converters, authors generally consider the coupling factor of windings to be a fixed value, theoretically equal to one. It follows from the nonpractical validity of this hypothesis that in order to make DC-DC converters effective, the current approach is often chosen, once again, to correct the defects by adding modifications to the basic topology and adding electronic components of various protections [12]. In converters based on the transformer of Forward and the push-pull as described [13–15], the transformer produces a lot of losses and the switches of these converters suffer from high voltage spikes and high power dissipation caused by the leakage inductances, and important currents.

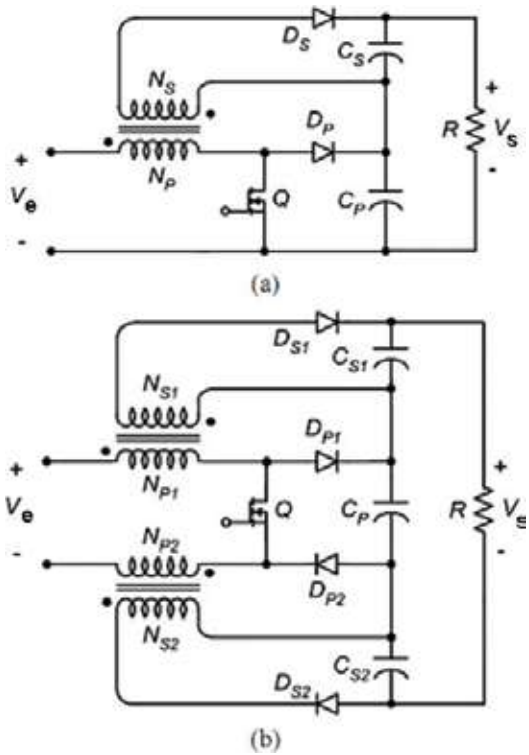

Figure 1. Unbalanced and balanced switching converter. (a) Converter balanced of conventional, (b) converter of equilibrium.

To avoid these disadvantages, some authors suggest the introduction of passive elements that diode and capacitor which gives rise to many variants of Boost, Buck-Boost, with as a direct consequence an increase in the cost due to a switch supplement of power, volume and complexity [16]. For this reason and for all the aforementioned drawbacks of converter topologies, for PV generator applications, coupled inductance converters are practical, even for transformer-based converters, to reach the high voltage ratio and conserve a small volume. With this approach, we complete the efficiency analysis proposed in this chapter and follow up on our previous study of losse on the swith in the process on–off in the converter dedicated to converting energy from photovoltaic sources. Analysis of the influence of leak inductances in the magnetic circuit for direct magnetic coupling and limiting energy leakage by circuit recovery in the DC-DC converter.

2. Analysis and calculation of leakage inductances

This type of calculation is difficult to carry out accurately, and only the finite element codes are able to give an accurate result. In the vast majority of cases, however, such precision is not useful and one can be content with an order of magnitude and sometimes even simply with a

sense of variation. For a transformer used with ETD ferrite core, where the best possible result is sought, the finalization of a transformer can hardly be done until after experimentation, rendering a "precise" calculation unattractive. It will place ourselves voluntarily in an elementary case, with the load to the reader to adapt it according to his needs. The configuration of this work will be that of two concentric circular windings [17–19].

The principle of calculating the leakage inductances in a magnetic component comprising a core can be explained from the section of **Figure 2**, corresponding to a transformer with two concentric windings wound on the central core of a magnetic circuit with three branches and separated by a layer of insulation.

In the hypothesis of a zero magnetizing current, the sum of the ampere-turns present in the coils is zero. But if we choose any closed contour passing through the window, it immediately appears that the application of Ampère's theorem highlights the existence of a nonzero magnetic module excitation vector H. We can deduce that there is an electromagnetic energy stored in the window through the relation:

$$W_{EM} = \iiint \frac{\mu_0 . H^2}{2} . dV \tag{1}$$

This energy corresponds by definition to field lines which do not enclose the entirety of the two coils. It is actually a leak energy to which we can associate a leakage inductance. Volume *"V"* of magnetic component we have shown that the product of the areas characterized the magnetic component.

Whatever the form of the component, it is necessary to retain the following first approximations:

The system is observed by freezing the currents (modules I_1 and I_2) in the coils.

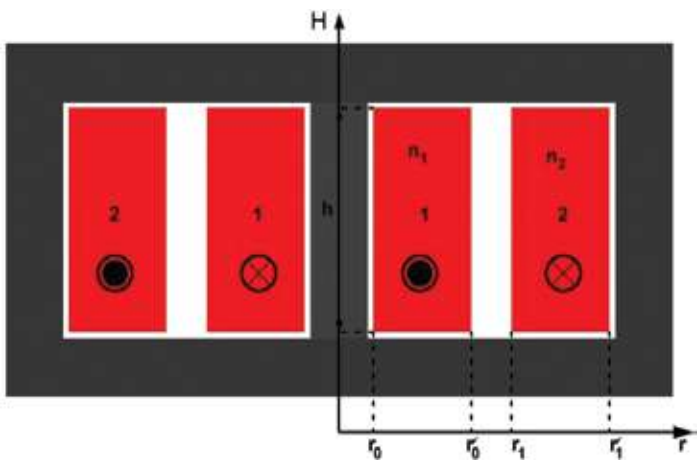

Figure 2. Cutting of a magnetic component for the calculation of leakage inductances.

The modulus H of the magnetic excitation is null (negligible) in the nucleus and, as a corollary, the magnetizing current is zero.

The field lines in the window are perfectly rectilinear and orthogonal to the direction of progression of the ampere-turns, noted overall *N. I*.

Ampere-turns are homogeneously distributed, continuous and unobtrusive in the section of the windings.

Case of concentric windings: According to these hypotheses, in the diagram of **Figure 3**. The two coils will have the same height h (the dimension of a height and the name of the average height of the field lines: this quantity is available for a given kernel in the manufacturer's documentation), start and end rays respectively H depends only on r and is written:

$$H(r) = \frac{N.I}{h} \tag{2}$$

This form results from the application of the Ampère theorem, by choosing a closed contour, of any form in the nucleus since H is zero, and closing in the window in the direction of the field lines. At the same time, we can represent, again in the case of **Figure 3**, the progression of *N.I* and H as a function of *r*:

The progression of H in the window has the same form, taking into account the expression of H(r) and the maximum value reached which is here *N1.I1 = N2.I2*.

The next problem is that of volume integration. It is clear that if the component does not show a rough symmetry of revolution, H will become a two-dimensional or even three-dimensional function, out of the context of a given section of the component. The calculation is imaginable, but would lead to totally unworkable analytical expressions. We are therefore forced to limit ourselves to magnetic structures presenting a quasi-symmetry of revolution. The so-called potted nuclei correspond relatively well to this hypothesis.

It should be noted that the principles of calculation presented here are often used in cases where there is a clear absence of any form of symmetry of revolution (structure in E for example). If it seems that the application of the described method gives, in these latter cases,

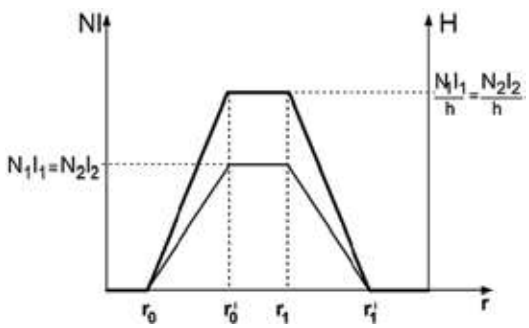

Figure 3. Progression of ampere-turns and H(r) in the window.

relatively correct results, the readers must be warned of the high level of approximation which this assumes and which is justified only by experience. Caution is therefore required [18, 19].

If we return to the hypothesis of the symmetry of revolution evoked above and always within the framework of our example, we can then express W_{EM} in the form:

$$W_{EM} = \int_{r_0}^{r'_1} \frac{\mu_0 . H^2(r)}{2} . 2\pi . h . r . dr \tag{3}$$

As mentioned above, it can be identified with the energy stored in an overall leakage inductance defined, as desired, with respect to the primary or secondary winding.

$$W_{EM} = \int_{r_0}^{r'_1} \frac{\mu_0 . H^2(r)}{2} . 2\pi . h . r . dr = \frac{1}{2} l_{f12} . I_1^2 = \frac{1}{2} l_{f21} . I_2^2 \tag{4}$$

In the concentric windings structures, on each interval of the window, H is always proportional to N1.I1 or N2.I2, depending on the chosen option. In the example of **Figure 4**, the H expressions are:

$$\text{To} \begin{cases} r_0 \le r \le r'_0 & H = \dfrac{N_1 . I_1 . (r'_0 - r)}{h(r'_0 - r_0)} = \dfrac{N_2 . I_2 . (r'_0 - r)}{h(r'_0 - r_0)} \\ r'_0 \le r \le r_1 & H = \dfrac{N_1 . I_1}{h} = \dfrac{N_2 . I_2}{h} \\ r_1 \le r \le r'_1 & H = \dfrac{N_1 . I_1 . (r'_1 - r)}{h(r'_1 - r_1)} = \dfrac{N_2 . I_2 . (r'_1 - r)}{h(r'_1 - r_1)} \end{cases} \tag{5}$$

We will then end up with general relations of the form:

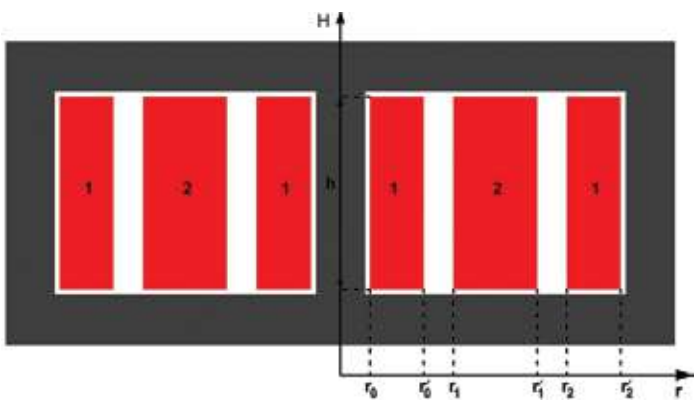

Figure 4. Types with nested concentric windings.

$$\frac{1}{2} l_{f12} . I_1^2 = \pi . \mu_0 \frac{(N_1 . I_1)^2}{h} \int_{r_0}^{r'_1} X^2(r) . r dr \tag{6}$$

$$\frac{1}{2} l_{f21} . I_2^2 = \pi . \mu_0 \frac{(N_2 . I_2)^2}{h} \int_{r_0}^{r'_1} X^2(r) . r dr \tag{7}$$

$$\text{with } X(r) = \frac{h.H(r)}{N_1 . I_1} = \frac{h.H(r)}{N_2 . I_2} \tag{8}$$

piecewise affine function from which we deduce:

$$l_{f12} = 2\pi . \mu_0 \frac{N_1^2}{h} \int_{r_0}^{r'_1} X^2(r) . r dr \tag{9}$$

$$l_{f21} = 2\pi . \mu_0 \frac{N_2^2}{h} \int_{r_0}^{r'_1} X^2(r) . r dr \tag{10}$$

At this level, one gets expressions that remain relatively heavy. A last approximation is possible if the thickness of each winding is small in front of its mean radius. We can then identify the surface element 2 μ.rdr at 2 μ.rBdr, where rB is the average radius of the considered winding (equivalent to an approximate integration by the method of the rectangles).

In the example studied, we obtain the following expression (case of l_{f12}):

$$l_{f12} = 2\pi . \mu_0 \frac{N_1^2}{h} \left[\frac{r_0 + r'_0}{2} \int_{r_0}^{r'_0} X^2(r) dr + \frac{r'_0 + r_1}{2} \int_{r'_0}^{r_1} X^2(r) dr + \frac{r_1 + r'_1}{2} \int_{r_1}^{r'_1} X^2(r) dr \right] \tag{11}$$

$$\text{with } \begin{cases} X(r) = \dfrac{r'_0 - r}{r'_0 - r_0} & \textit{for the first fiddling} \\ X(r) = 1 & \textit{for insulation} \\ X(r) = \dfrac{r'_1 - r}{r'_1 - r_1} & \textit{for the second fiddling} \end{cases} \tag{12}$$

The final result will be:

$$l_{f12} = \pi . \mu_0 . N_1^2 \frac{r'_1 2 + 2r_1^2 - 2r'_0 2 - r_0^2}{3h} \tag{13}$$

Case of l_{f21}:

$$l_{f21} = \pi.\mu_0.N_2^2 \frac{r'_1 2 + 2r_1^2 - 2r'_0 2 - r_0^2}{3h} \tag{14}$$

It would be really interesting to compare the theory with the case which concerns us concretely to see above.

In this instance concentric coils nested **Figure 5**, the method is the same as for the analysis of concentric windings. The final result will be:

$$l_{f12} = \pi.\mu_0.N_1^2 \frac{2\left(r_1^2 + r_2^2 - r'_0 2 - r'_1 2\right) + r'_2 2 - r_0^2}{12h} \tag{15}$$

This simplification can be extended to any number of winding elements. In the case of the parameters of the first and second coils, they are in fluence leakage inductance.

In the case of concentric windings nested with the four-part primary winding division, **Figure 5**:

$$\begin{aligned} l_{f12} = 2\pi.\mu_0 \frac{N_1^2}{h} \Bigg\{ & \frac{r_0 + r'_0}{2} \int_{r_0}^{r'_0} X^2(r)dr + \frac{r'_0 + r_1}{2} \int_{r'_0}^{r_1} X^2(r)dr + \\ & + \frac{r_1 + r'_1}{2} \int_{r_1}^{r'_1} X^2(r)dr + \frac{r_2 + r'_1}{2} \int_{r'_1}^{r_2} X^2(r)dr + \\ & + \frac{r'_2 + r_2}{2} \int_{r_2}^{r'_2} X^2(r)dr + \frac{r_3 + r'_2}{2} \int_{r'_2}^{r_3} X^2(r)dr + \\ & + \frac{r_3 + r'_3}{2} \int_{r_3}^{r'_3} X^2(r)dr + \frac{r'_3 + r_4}{2} \int_{r'_3}^{r_4} X^2(r)dr + \frac{r_4 + r'_4}{2} \int_{r_4}^{r'_4} X^2(r)dr \Bigg\} \end{aligned} \tag{16}$$

$$l_{f12} = \pi.\mu_0.N_1^2 \frac{2\left(r_1^2 + r_2^2 + r_3^3 + r_4^2 - r'_0 2 - r'_1 2 - r'_2 2 - r'_3 2\right) + r'_4 2 - r_0^2}{24h} \tag{17}$$

Case of superimposed windings: The physical model of this structure is obtained in the same way as previously. The flow model inside the core and the windings is derived using Ampere's law and the integration show path in **Figure 6a**. Field strength through the core and windings is shown in **Figure 6b**. The sign of the intensity of the field determines the direction flows inside the core and the windings. This at its turn determines the flow pattern within the structure which is illustrated in **Figure 6b**.

In the case of superimposed components (**Figure 6a**), the method is identical, but the assumptions are different. The leakage inductances can be estimated and the calculation of the amount of energy stored in each of the winding can be done by shorting the secondary "mathematically."

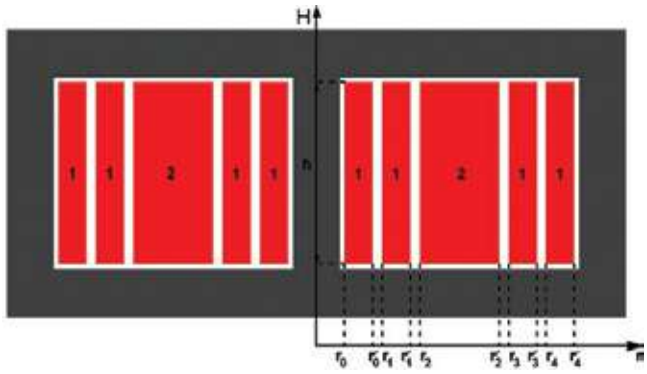

Figure 5. Types with nested concentric windings (winding primary four part).

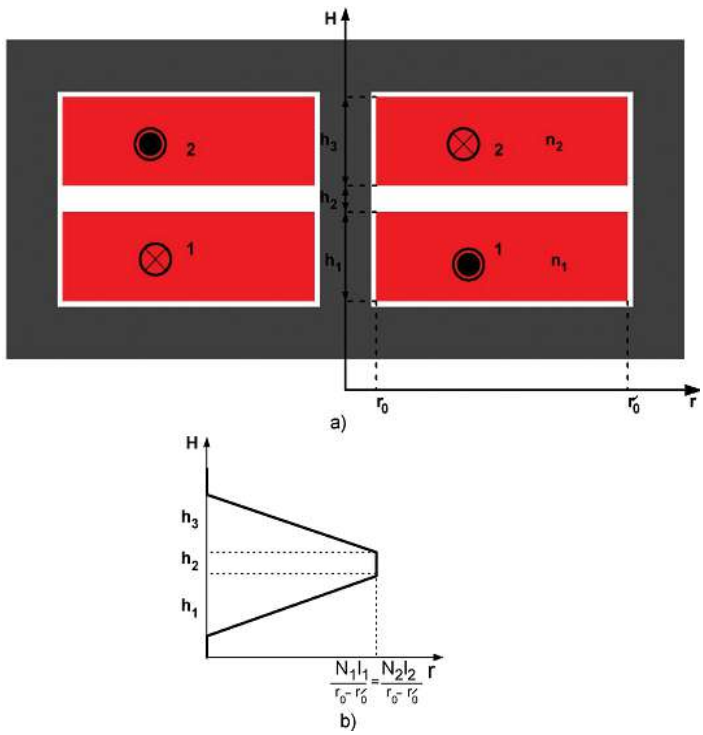

Figure 6. Case of superimposed windings.

The field strength with the short-circuited secondary is similar to that of **Figure 6b**, with the mutual flow reduced to about 0.

Compared to the previous case, the progression of Ampere-turns is done according to the vertical axis. H now depends only on h. The expression of W_{EM} becomes:

$$W_{EM} = \int_0^{hT} \frac{\mu_0 . H^2(h)}{2} . \pi \left(r_0' 2 - r_0^2 \right) . dh \tag{18}$$

We obtain:

$$W_{EM} = \int_0^{hT} \frac{\mu_0 . H^2(h)}{2} . \pi \left(r_0' 2 - r_0^2 \right) . dh = \frac{1}{2} . l_{f12} . I_1^2 = \frac{1}{2} . l_{f21} . I_2^2 \tag{19}$$

The calculation is then quite similar to the previous one, initially expressing H(h) on the different zones.

In the concentric windings structures, on each interval of the window, H is always proportional to *N1I1* or *N2I2*, depending on the chosen option. In the example of **Figure 6b**, the expressions of H are:

$$\begin{cases} height\ \mathrm{h}_1 \quad H = \dfrac{N_1 . I_1 . h}{h_1 \left(r_0' - r_0 \right)} = \dfrac{N_2 . I_2 . h}{h_1 \left(r_0' - r_0 \right)} \\ height\ \mathrm{h}_2 \quad H = \dfrac{N_1 . I_1}{\left(r_0' - r_0 \right)} = \dfrac{N_2 . I_2}{\left(r_0' - r_0 \right)} \\ height\ \mathrm{h}_3 \quad H = \dfrac{N_1 . I_1 . h}{h_3 \left(r_0' - r_0 \right)} = \dfrac{N_2 . I_2 . h}{h_3 \left(r_0' - r_0 \right)} \end{cases} \tag{20}$$

In the example studied, we obtain the following expression (case of l_{f12}):

$$l_{f12} = \pi . \mu_0 . \frac{N_1^2}{\left(r_0' - r_0 \right)^2} \left\{ \int_0^{h_1} H^2(h) . \left(r_0' 2 - r_0^2 \right) . dh + \int_0^{h_2} H^2(h) . \left(r_0' 2 - r_0^2 \right) . dh + \int_0^{h_3} H^2(h) . \left(r_0' 2 - r_0^2 \right) . dh \right\} \tag{21}$$

The final result will be:

$$l_{f12} = \pi . \mu_0 . N_1^2 . \frac{\left(r_0' + r_0 \right) \left(h_1 + 3h_2 + h_3 \right)}{3 \left(r_0' - r_0 \right)} \tag{22}$$

This type of calculation, be it overlapping concentric overlapping or overlapping structures, presents no particular difficulty but is not extremely light. We give the result for four typical two-part superimposed overlapping windings with two-part primary winding division in **Figure 6**, and superimposed overlapping windings with four-part primary winding splitting. The method of analysis is the same as that of concentric windings. The final result will be:

$$l_{f12} = \pi . \mu_0 . N_1^2 . \frac{\left(r_0' + r_0 \right) \left(h_1 + 3h_2 + h_3 + 3h_4 + h_5 \right)}{12 \left(r_0' - r_0 \right)} \tag{23}$$

In the case of nested concentric windings with four-part primary winding division:

$$l_{f12} = \pi.\mu_0.N_1^2.\frac{\left(r'_0 + r_0\right)(h_1 + 3h_2 + h_3 + 3h_4 + h_5 + 3h_6 + h_7 + 3h_8 + h_9)}{24\left(r'_0 - r_0\right)} \tag{24}$$

The final comparison with the theoretical calculations will follow to confirm the veracity of the theoretical approach with the experience of measurement.

In order to accurately predict the behavior of the converter, a preliminary measurement of the transformer coupling coefficient is necessary. The method used to determine the inductance of the two inductance coils consists of two sequential measurements on the basis of taking into account the additive and subtractive contribution of the magnetic flux of the inductor windings connected in series. So, we obtained two inductor values, named respectively L12M and L12m defined by

$$L_{12M} = L_1 + L_2 + 2M \tag{25}$$

$$L_{12m} = L_1 + L_2 \tag{26}$$

With:

L_{12M}: the measurement of the series inductance with the opposite direction windings.

L_{12m}: the series measurement with the same direction windings.

Thus, it is possible to deduce the value of M representing the coupling inductance

$$M = \frac{L_{12M} - L_{12m}}{4} \tag{27}$$

In carrying out our experiments $L_{12M} = 168mH$ and $L_{12m} = 75mH$. So, we deduce the value of M = 23.25 mH representing a coupling factor k given by the classical formula:

$$k = \frac{M}{\sqrt{L_1.L_2}} = 0,981 \tag{28}$$

This high value of k corresponds to a transformer quality and allows a good performance of the converter.

According to magnetic circuit EDT54 in the transformer (the inductance $L_1 = 31.6mH$ measured; $N_1 = 32spires$) and Eq. (24) we gave factor k calculated such that:

$$l_{f12-calculate} = 0,812mH$$

$$k_{caculate} \simeq 0.987$$

It is easy to see that the total leakage inductance brought back to the primary is reduced in the concentric coils and superimposed coils. This technique is one that is commonly used in energy conversion in DC-DC converters to reduce the leakage inductance and thus extend the

bandwidth to high frequencies. In practice, we will meet from two to four interlacing, larger numbers posing major problems of realization. It is of course also possible to reduce the leakage inductance by decreasing the number of turns of the windings, which is possible if the permeability of the core is increased. This generally requires the use of nickel alloys, permalloys and derivatives or mumetal. The extra cost generated by these materials makes it possible to justify this technique only for link transformers and for realizations the cost price of which does not count for very little. Still for the link transformers, and in some output transformers, it is possible to use multi-wire windings wound together, which further improve the primary-secondary coupling but having the defect of a low electrical isolation. Very careful achievements can achieve a high cut of (30–100) kHz.

3. Solution for DC-DC Flyback converter

3.1. Flyback converter with nonlinear magnetic coupling

When the switch is conducting, the energy is stored in the primary inductance as well as in the corresponding leakage inductance. The leakage flux associated with the leakage inductance of the primary winding is not transferred to the secondary winding, and it is therefore necessary to manage the energy associated with this leakage flow either by dissipating it in an external circuit (known as damping), or by recycling it. Unless this energy finds a path, it will occur at a peak voltage across the windings that could destroy the switching circuit (see **Figure 7**). The greater the leakage inductance of all transformer isolated DC-DC converters can lead to ring, an increase in voltage constraints, and an increase in power loss, resulting in a significant degradation of the performance of the circuit.

Figure 7 shows a practical Flyback converter modeled. The solution for the recovery circuit consists of a fast recovering series diode in the output winding with a combination of a

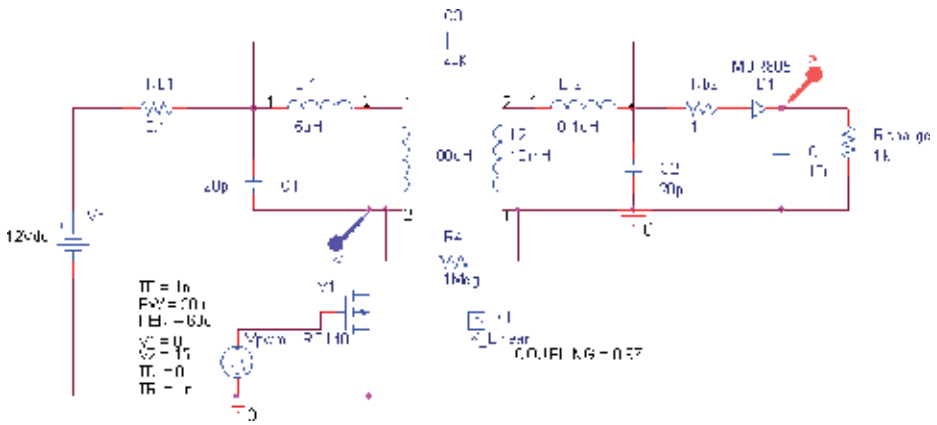

Figure 7. Basic diagram of a Flyback converter with leakage inductance in the transformer.

damping capacitor and a parallel resistor [13, 20] making load for the simulation. The current of the primary winding of leakage inductance has a low impedance path during the conduction of M1. It can be seen that at the end of the conduction of the diode D1, the voltage across the output filter capacitor will be at the higher potential. To check for excessive build-up voltage across the damping capacitor a resistor is placed across. According to the equilibrium state of this resistor is intended to dissipate the leakage flux energy.

The waveforms described above are only valid if all components are considered perfect. In fact, one can observe an overvoltage when opening the transistor operating as a controlled switch. This overvoltage comes from the energy stored in the leakage inductance Lf at the primary of the transformer. The energy it contains at the time of opening of the transistor cannot be transferred to the secondary. The evacuation of the energy stored in this parasitic inductance will be transferred to the parasitic capacitances of the transistor and the primary of the transformer by creating an overvoltage at the terminals of the transistor. As the primary has an inductive impedance, the cancelation of the current passing through the switch cannot be done under a zero voltage, so it will generate switching losses The effects damaging these overvoltages are detrimental to the transistor and therefore require the addition of switching assistance circuits. There is also secondary leakage inductance. This inductance will also cause losses and decrease the energy supplied by the power supply to the load. In the case of power supply having multiple outputs, secondary leakage inductances will create different losses on each of the outputs.

In this case, however, the locking of the switch interrupts the current through the leakage inductance of the transformer, and this will produce a voltage spike on the drain of MOSFET. The inductance will then resonate with the parasitic capacitances of the circuit, producing a high frequency high frequency wave as shown in **Figures 8** and **9**. On the Flyback primary, the measured leakage inductance resonates with the primary capacitances.

Many application and design notes ignore the resonance and make the converter work without addressing the issue. There are two problems related to resonance phenomena: first, the voltage, when excessive on the MOSFET drain, can cause the entail breaking of the transistor, and finally the failure of the device. Secondly, the resonance energy will be radiated and

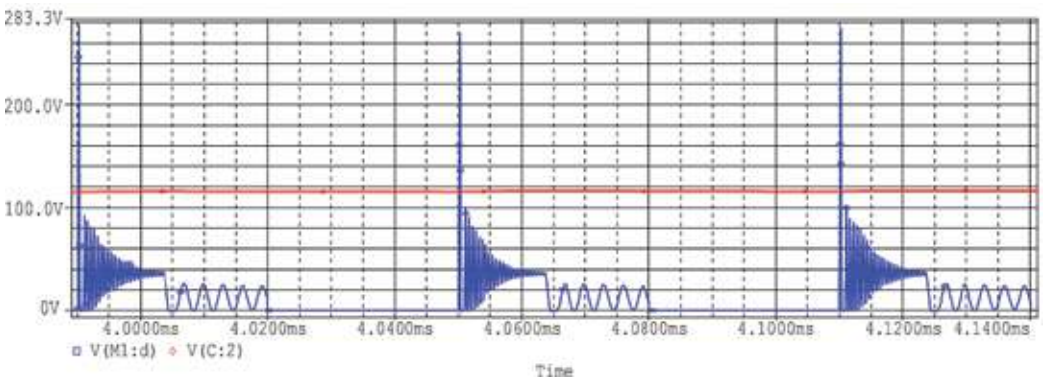

Figure 8. Simulation of the voltages obtained on a fly-back with a non-ideal transformer. The output voltage remains close to that on the transistor.

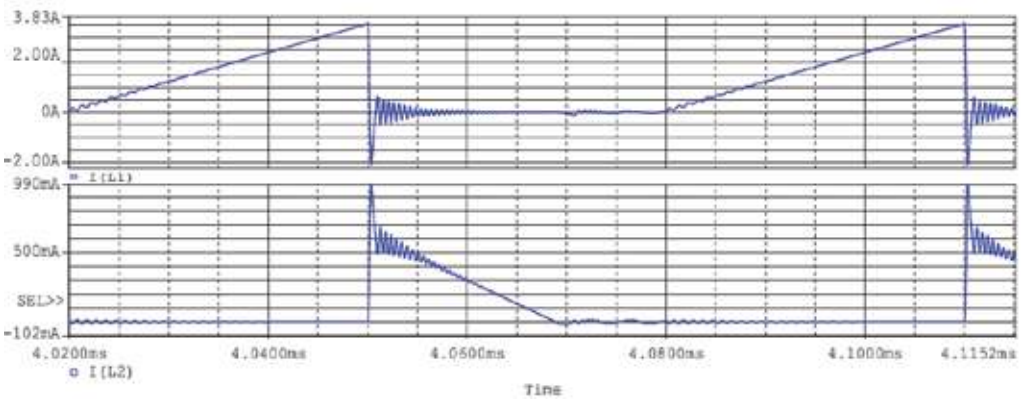

Figure 9. The current passed primary and secondary transformer inductance obtained modeling modeled with leakage inductance.

conducted everywhere in the power supply, load, and electronic control system, which creates noise problems and even random errors or failures in the logic part. Therefore, the frequency of the resonance will appear as a peak in the IEM spectrum and will be propagated in both "radiated" and "led" modes.

3.2. Flyback converter with recovery stage

Figure 10 shows the Flyback converter with the recovery stage (F-RS converter), the F-RS converter scheme in **Figure 10** shows the two main active inductors, L8, L9 and the two additional leakage inductors, constituted by a diode D5 in series, and a capacitor in parallel,

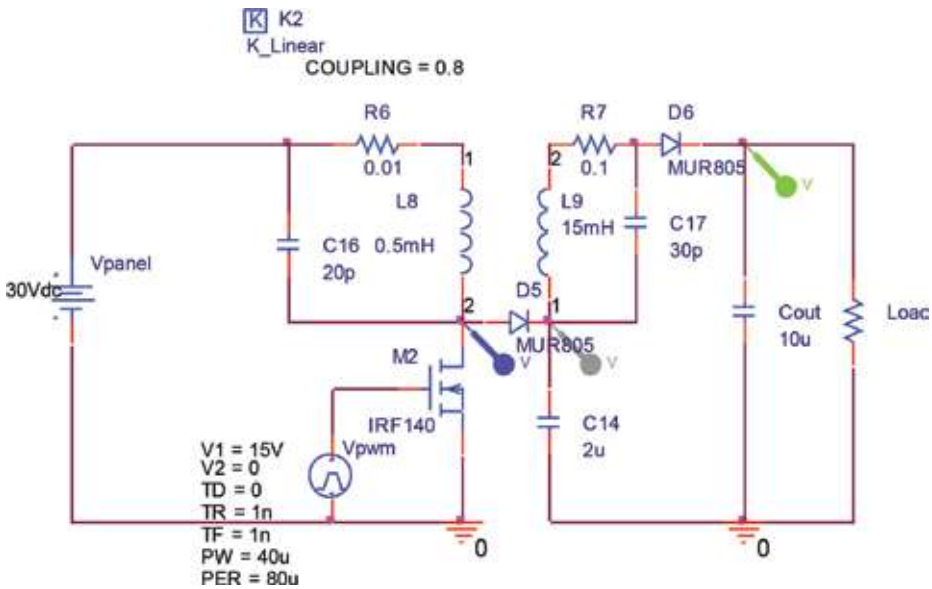

Figure 10. Model diagram for the simulation of the F-RS converter.

inserted between the two coupled inductance coils. Finally, the principle of the F-RS converter is based on an Flyback converter, voltage step-up base arrangement as described above, a recovery stage, and a second output amplifier stage. This recovery step should recover all normally lost energies in the standard basic MCB structure. This recovery step should recover all normally lost energies in the standard basic Flyback structure. In fact, even if the energy lost in the leakage inductances is only a small but significant percentage of the total transferred energy, this energy must be recycled during the shutdown time when there is an increase in efficiency overall conversion.

In this converter principle, the capacitor C is charged by the recovery energy initially stored in the leakage inductance coil L8 via the diode D5. It remains to ensure that the recovered leakage energy stored in the first pulse is not too large to cause a local increase of the voltage V_{C14}, which limits the voltage across the switch, Vds below an acceptable value.

We performed simulations of the MCB-RS converter under OrCad software. Magnetic coupling was deliberately chosen at a low value (k = 0.8) for the purpose of highlighting the effect of magnetic leakage. The transformation ratio was chosen as m = 20 in accordance with the prototype F-RS converter developed in our laboratory and previously tested in photovoltaic energy conversion [21]. The value of the capacitor must provide a quasi-constant value of V_{C14} throughout the cycle, while offering the possibility of accepting relatively fast variations of the voltage across it. For this reason, in this simulation, the capacitor C is chosen with a low value equal to 2 μF. Finally, to comply with a high power of the studied system, the voltage of the bus HVDC was set at (200–400)V.

Figure 10 shows the electrical diagram, developed under OrCad, of a Flyback F-RS type matching stage inserted between a PV and an HVDC bus. In the simulation diagram are given the values of the parameters. To provide a means for displaying the progress when the effect of the transformer leakage inductance to the transistor parameters M2. Furthermore, the recovery of the stage voltage RS of this converter is also shown. It can be seen that the magnetic coupling has deliberately been chosen at a low value (k = 0.8) that the transformation ratio is m = 20 to comply with the PV panels for increasing the output voltage).

The results of the simulation of the different voltages in the converter, the output of V_{D6}, on the capacitor V_{C14}, and on the switch Vds of the M2 in **Figure 11**. If these transient phenomena are considered negligible, one can idealize these variations of the main current inside F-RS converter as the linear ones. In spite of a converter considered with a low value of the coupling coefficient, which in the general high voltage Flyback converter can also be seen in **Figure 11** that the voltage is the V_{C14} trend across the capacitor C14 is stable throughout the cycle, a value of approximately V_{C14} = 125 V. A positive consequence is that the switching voltage, Vds, does not exceed the damage threshold value of the MOSFET IRF140 chosen for these simulations.

During the time has pulse to M2, we can observe parasitic pseudo oscillations on V_{D6} in **Figure 11**. During the entire duration of this mode, the diode D6 is blocked and, consequently, the secondary stage of the converter is in an open circuit state. With this time in state, at a primary voltage corresponds a secondary voltage proportional to the transformation ratio m, which comes into resonance due to the parasitic capacitance of D6. The influence of the

http://dx.doi.org/10.5772/intechopen.78768

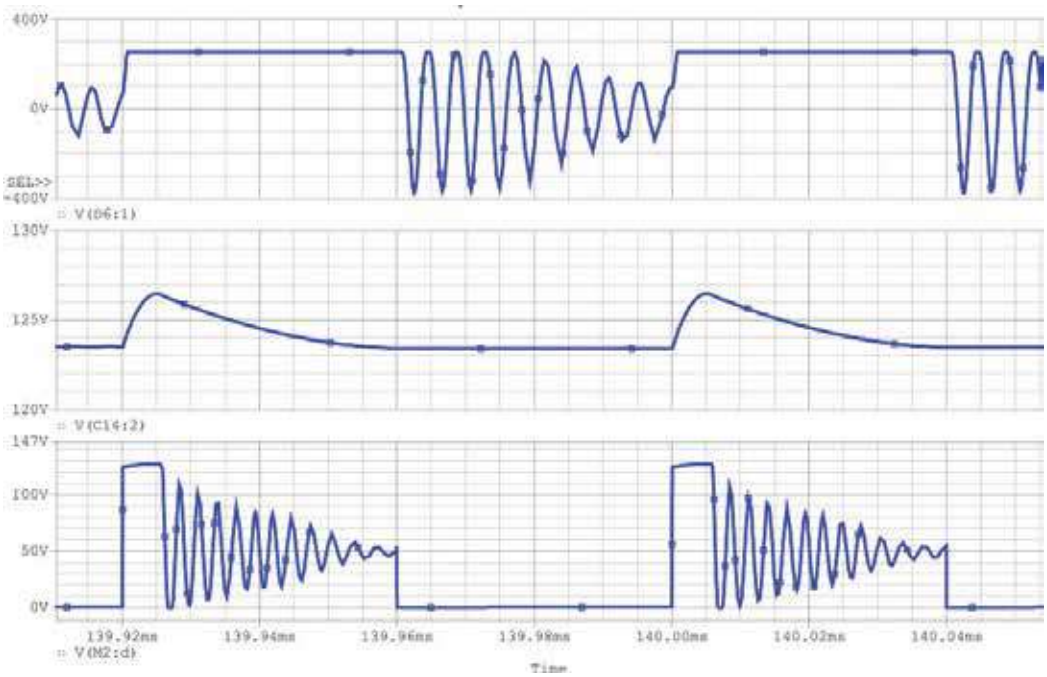

Figure 11. Simulation of the main voltage V_{D6}, V_{C14}, and Vds in the F-RS.

capacitance and values of the coupling coefficient on the shape of the different converter voltages is also highlighted in **Figure 11**. For the selected low value of the intermediate storage capacity, C14 = 2 μF, associated with the small chosen value of the coupling factor k = 0.8, we can observe during all the stopping state (time no pulse) a slight ripple of the voltage V_{C14} around its average value (equal to 125 V in this application). This ripple is due to the transfer of the leakage energy during the turn-off time of the switch. On the other hand, at the beginning of the off state mode of the switch, a transient voltage appears on Vds, followed during the intermediate mode by a huge decrease to zero. Finally (time not pulse), the time main starts with high frequency ripples due to resonance phenomena between the primary inductance and the parasitic capacitances.

Now, we compare the transition from opening to closing at switching time, namely the transition between the two modes, for the basic Flyback and the F-RS converters. We note that during this transition in the Flyback basic system, a very high voltage pulse is applied to the switch. Whereas, in an F-RS, this pulse is immediately transferred via the diode D5 to the recovery capacitor once it reaches a determined threshold value as a function of the capacitor itself, and therefore of V_{C14}, and all other parameters system. As we can see in the above presentation for the fixed experimental parameters selected for this simulation to explain the different modes of the F-RS converter, all these parameters, such as component values, cyclic, transformation ratio and coupling factor, have a huge interdependent influence on the overall behavior of the converter.

4. Conclusion

In this chapter, we presented a specific analysis and calculation leakage inductor in the transformer of individual DC-DC magnetically coupled converters for use in a renewable energy conversion system, including an HVDC bus converter. The DC-DC converter with a high voltage ratio and used upstream, just behind the power source: PV, wind turbine, compressed air storage generator. This solution makes it possible to reduce the voltage Vds applied to the MOSFET transistor. We have shown that in an F-RS converter, even with a low value of the coupling factor, a lower voltage is applied to the transistor which can then be selected from a family of components having a low maximum voltage Vdsmax with a Rdson accordingly low. This choice will increase the performance of the converters. In addition, the energy transfer is improved by a better balance of the service cycle, which is an additional factor of a better efficiency.

Acknowledgements

This work has been funded by Quang Ninh University of Industry, Quang Ninh, Vietnam and Electric power University, Ha noi, Vietnam.

Author details

Nguyen The Vinh[1]* and Vo Thanh Vinh[2]

*Address all correspondence to: dhcnqn@qui.edu.vn

1 Quang Ninh University of Industry, Vietnam

2 Dong Thap University, Vietnam

References

[1] Liang Z, Hung JC, L S, Guo R, Li J, Huang AQ. A high-efficiency pv module-integrated DC/DC converter for pv energy harvest in FREEDM systems. IEEE Transactions on Industrial Electronics. 2011;**26**(3):898-909

[2] Petit P, Zegaoui A, Sawicki JP, Aillerie M, Charles JP. New architecture for high efficiency DC-DC converter dedicated to photovoltaic conversion. Energy Procedia. 2011;**6**:688-694

[3] Petit P. Optimisation du transfert d'énergie dans les systèmes photovoltaïques. thèse, Universitèe de Lorraine. 2011

[4] Wai RJ, Lin CY, Duan RY, Chang YR. High-efficiency power conversion system for kilowatt-level stand-alone generation unit with low input voltage. IEEE Transactions on Industrial Electronics. 2008;**55**(10):3702-3714

[5] Sun J, Sen PC. A general unified large signal model for current programmed DC-to-DC converters. IEEE Transactions on Power Electronics. 1998;**9**(4):414-424

[6] Bidram A, Davoudi A, Balog RS. Control and circuit techniques to mitigate partial shading effects in photovoltaic arrays. IEEE Journal of Photovoltaics. 2012;**2**(4):532-546

[7] Petit P, Aillerie M, Sawicki JP, Charles JP. Push-pull converter for high efficiency photovoltaic conversion. Energy Procedia. 2012;**18**:1583-1592

[8] Petibon S, Alonso C, Estibals B, Seguier L. Multiphase converter structures applied to integrated micro-power application circuits. European Conference on Power Electronics and Applications. 2007;**2007**:1-9

[9] Axelrod B, Berkovich Y, Ioinovici A. Switched coupled-inductor cell for DC-DC converters with very large conversion ratio. In: Proceedings of the Conference of IEEE Industrial Electronics Society; 2006. pp. 2366-2371

[10] Dumrongkittigule V. Tarateeraseth, and W. Khan-Ngern. A new integrated inductor balanced switching technique for common mode EMI reduction in high step-up DC-DC converter. In: Proceedings of the International Zurich Symposium on Electromagnetic Compatibility; 2006. pp. 541-544

[11] Zhao Q, Lee FC. High-efficiency, high step-up DC-DC converters. IEEE Transactions on Power Electronics. 2003;**18**(1):65-73

[12] Park KB, Seong HW, Kim HS, Moon GW, Youn MJ. Integrated boost-sepic converter for high step-up applications. In: Proceedings of the Power Electronics Spec. Conf.; Rohode, Greece; 2008. pp. 944-950

[13] Hariharan S, Schie D. Designing single-switch forward converters. Power Electronics Technology. 2005:38-43

[14] Ryan MJ, Brumsickle WE, Divan DM, Lorenz RD. A new ZVS LCL-resonant push–pull DC–DC converter topology. IEEE Transactions on Industry Applications. 1998;**34**(5):1164-1174

[15] Tomaszuk A, Krupa A. High efficiency high step-up DC/DC converters—A review. Bulletin of the Polish academy of Sciences Technical Sciences. 2011;**59**(4):475-483

[16] Watson R, Lee FC. Utilization of an active-clamp circuit to achieve soft switching in Flyback converters. In: Proc. IEEE Power Electron. Spec. Conf.; 1994. pp. 909-916

[17] Naderian Jahromi A, Faiz J, Mohseni H. A fast method for calculation of transformers leakage reactance using energy technique. Archive of SID. 2003;**16**(1):41-48

[18] William GH, Wilcox DJ. Calculation of leakage inductance in transformer windings. IEEE Transactions on Power Electronics. 1994;**9**(1):121-126

[19] Dauhajre AA. Modelling and estimation of leakage phenomena in magnetic circuit [Thesis]. Pasadena, California: California Institute of Technology. Vol. 22; 1986

[20] Barbosa PM, Barbi I. A single-switch Flyback-current-fed DC–DC converter. IEEE Transactions on Power Electronics. 1998;**13**(3):466-475

[21] Sawicki JP, Petit P, Zegaoui A, Aillerie M, Charles JP. High efficiency step-up hvdc converter for photovoltaic generator. Energy Procedia. 2012;**18**:1593-1600

Chapter 2

Electrical Rating—Long-Term Performance Potential of Photovoltaic Systems

Muhammad Burhan,
Muhammad Wakil Shahzad and Ng Kim Choon

Additional information is available at the end of the chapter

http://dx.doi.org/10.5772/intechopen.78952

Abstract

Owing to diverse photovoltaic technology and dynamic nature of meteorological data, a number of factors affect the performance of photovoltaic systems. The highly efficient concentrated photovoltaic (CPV) system can only respond to beam radiations of solar energy, unlike stationary silicon-based conventional photovoltaic (PV) panels. The availability of solar energy, and share of beam/diffuse radiations, varies from region to region, depending upon weather conditions. However, the rated performance as instantaneous maximum efficiency at STC (standard testing conditions) or NOCT (nominal operating cell temperature) in the laboratory, does not depict the true system performance under changing field conditions. The energy planners are interested in actual field performance, in terms of total delivered energy. Therefore, despite highest efficiency, CPV installations seem to be limited to desert regions, with high beam radiations availability and favorable working conditions. In this chapter, the performance potential and feasibility of CPV system is reported for long term operation in tropical weather conditions, in terms of proposed electrical rating parameter, giving total energy delivered as kWh/m^2.year. From 1-year field operation of two in-house built CPV units, electrical rating of 240.2 kWh/m^2. year is recorded for CPV operation in Singapore, the first ever reported CPV performance in this region, which is two folds higher than the stationary PV.

Keywords: electrical rating, CPV, concentrated photovoltaic, long term performance, solar tracker, MJC

1. Introduction

For the sustainable future environment, the renewable energy sources have been hailed as promising solution for primary energy supply. The rise in the global temperature can be

expected to reach to an alarming level if the dependency on fossil fuels is unabated [1–5]. Solar energy is believed to be the only renewable energy source with highest energy potential among all energy sources, which is many time than the global energy demand [6, 7]. However, to solar energy useful energy, photovoltaic systems provide the simplest configuration to produce electricity by the direct utilization of solar radiations [8–10].

The photovoltaic market is having a huge diversity of photovoltaic technology which is ranging from simple single junction, non-concentrating, stationary flat plate panels, to advanced, multi-junction cell based concentrated photovoltaic systems. Such diversity depicts many different system configurations with different working conditions and parameters. The third generation multi-junction solar cell (MJC) concentrated photovoltaic (CPV) system provide highly efficient photovoltaic technology, available hitherto [11]. As we know, solar energy consists of two type of radiations i.e. beam and diffuse. Concentrated photovoltaic system relies onto low cost solar concentrators which can only respond and concentrate solar beam radiations [12] onto the smaller area of solar cell, unlike flat plate PV panels which can respond to both beam and diffuse part of solar radiations. The share of beam radiations in coming energy depends upon the sky conditions and the local climate. As solar concentrators can only respond to beam radiations, therefore, the conventional CPV systems were designed as gigantic unit which huge solar tracking unit, to be installed in the open desert regions. The main reason for such desert region design and application, was due to the clear sky condition with high beam share which is ideal for CPV.

The manufactures of PV and CPV system only furnish the catalogues of such system with rated and maximum capacity. Such rated performances are measured under controlled laboratory conditions and at certain optimum energy input. The standard testing procedure for such rated performance measurements are carried out under STC (Standard Testing Conditions, IEC 60904-3) parameters or NOCT (Nominal Operating Cell Temperature, IEC 61215 and IEC 61646) conditions [13]. Such laboratory testing conditions are totally different that the actual field operating conditions [14, 15]. The field conditions fluctuate throughout the day with different intensities. There are three factors responsible for such fluctuating field conditions. Firstly, the share of beam and diffuse radiations in the received solar energy is changing throughout the day, due to clod cover and changing sun position. Secondly, the cell operating temperature changes drastically throughout the operation due to daily and seasonal change in ambient temperature. Thirdly, the dust particles present in the air [16] and the dust storms reduce the incoming solar radiations thereby, affecting the performance output of photovoltaic modules. However, the customers and plat designers are interested in the actual output of the system which can be obtained during their filed operation and life period. Therefore, the rated performance of CPV and PV systems, available in the overwhelming catalogues of manufacturers, does not reflect the true performance of the system as the rated conditions are far different than the actual conditions [17, 18].

In addition, every system requires different operating conditions. Therefore, despite being highly efficient photovoltaic technology, concentrated photovoltaic (CPV) are only targeted to be installed in open desert regions due to favorable conditions as due to clear sky, these regions have high beam radiation share in solar energy and CPV can only respond to beam radiations.

http://dx.doi.org/10.5772/intechopen.78952

Therefore, it can be understood that the feasibility and potential of a system cannot be judged by rated performance parameters and conditions. The real field output of the system must the real performance indicator of the system and to be used by the plant designers and the customers. Therefore, this chapter introduces the long term electrical rating as true performance parameter of Photovoltaic system. In addition, the real field performance data of CPV and conventional PV systems is also presented, for tropical weather condition, to compare and analyze the performance under different scenarios of electrical rating method.

2. Development of CPV system

In order to investigate the performance of the CPV system, two CPV units, one with double reflective cassegrain based concentrating assembly and other with Fresnel lens based concentrating assembly, were developed with two axis solar tracker.

Figure 1 shows the schematic and the concentrating assembly arrangement of the two developed CPV systems for current study. The CPV unit shown in **Figure 1(a)**, named as mini dish CPV unit, is using cassegrain arrangement of parabolic and hyperbolic reflectors, for double stage concentration. The other CPV unit, named as Fresnel lens CPV unit, as shown in **Figure 1(b)**, is designed for single stage concentration by using Fresnel lens as solar concentrator. In both designs, the solar radiations are concentrated at the inlet of glass homogeniser, which further guides and uniformly distributes the solar radiations onto multi-junction solar cell (MJC), placed at the outlet aperture of the glass homogeniser. The back side of the MJC is attached to heat spreader and heat sink, for heat rejection, in order to keep cell temperature within the operational range. For Fresnel lens based CPV unit, the glass homogeniser is place at the focal point of the Fresnel lens. While for mini dish CPV unit, primary parabolic reflector first try to concentrate solar radiations at its focal point f1, however, due to secondary hyperbolic reflector, the solar radiations are again reflected to be focused at its focal point f2, where glass homogenizer is placed.

The specifications and materials of the developed CPV prototypes are also shown in **Figure 1** [12]. The concentrated light spot that can be seen at center of the glass homogenizer, verifies the perfect design of the concentrating assemblies. Both CPV modules are mounted onto the aluminum frame of two axis solar tracker, controlled by atmega128 microcontroller. The developed CPV systems have acceptance angle of 0.3–0.4° for mini dish and 0.6–0.7° for Fresnel Lens CPV unit. The control box of the two axis solar tracker, as shown in **Figure 1**, is based upon AVR ATmega128 microcontroller which is connected to two stepper motor drivers, power supply and GPS module. The developed two axis solar tracker works on a hybrid tracking algorithm, astronomical and optical tracking. At first, astronomical tracking is executed according to azimuth and zenith angles computed through solar geometry, as explained in [19]. For astronomical tracking to compute azimuth and zenith angles, data regarding local latitude, longitude, date and time, is received through GPS. The calculated azimuth and zenith angles are then compared with the actual position of the tracker, with reference to north or south plane and horizontal plane. If the difference is more than the required tracking accuracy i.e. 0.1° then

the tracker is moved accordingly otherwise it remains stationary. The tracking algorithm and tracking path are shown in **Figure 2**. According to the tracking path, the solar tracker is always kept within the tracking accuracy of ±0.1°. When astronomical tracking method completes, feedback from the solar tracking sensor is obtained based upon the actual position of sun, with sensitivity of 0.1°. The solar tracking sensor consists of an array of photo-sensors and if feedback from any of the photo-sensor is high, then tracker is adjusted accordingly otherwise it remains stationary, depicting tracker is accurately facing the sun. This tracking algorithm loop then starts again from the astronomical tracking.

To verify reliability and accuracy of the astronomical tracking algorithm, the calculated azimuth and zenith angles were compared with the azimuth and zenith angles data, obtained from Astronomical Applications Department of the U.S. Naval Observatory for January 1,

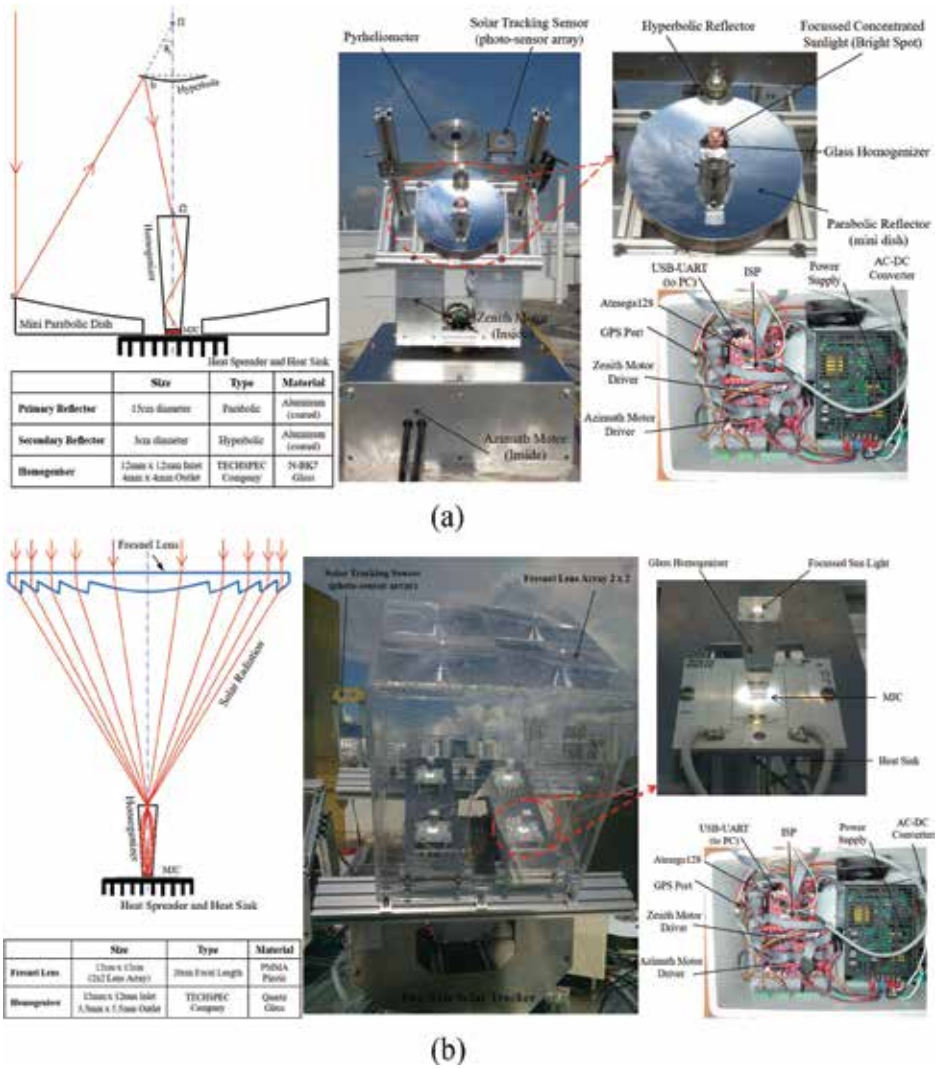

Figure 1. Developed prototypes of CPV system (a) mini dish CPV unit and (b) Fresnel lens CPV unit.

http://dx.doi.org/10.5772/intechopen.78952

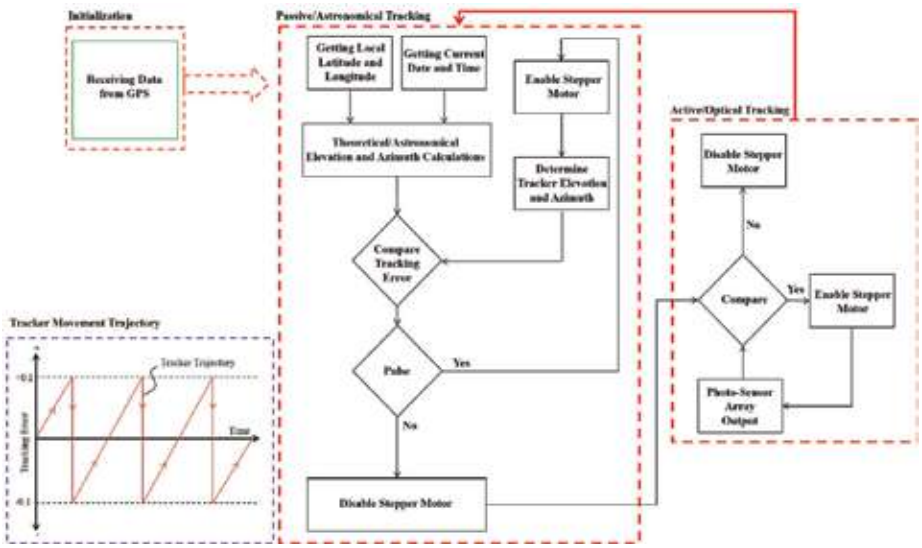

Figure 2. Hybrid tracking algorithm.

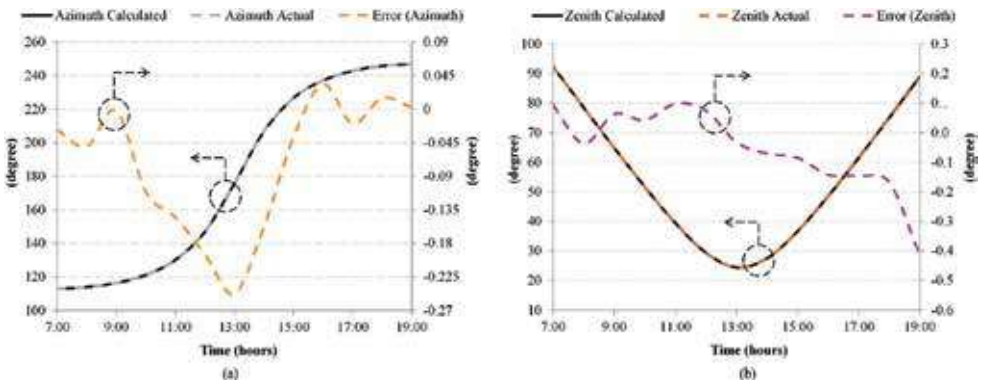

Figure 3. Comparison of calculated and actual (a) azimuth (b) zenith angles.

2015 [20] with latitude of 1.299°N and longitude of 103.771°E (for NUS EA-building). The comparison of the tracking angles is shown in **Figure 3**, for which calculated and obtained azimuth and zenith angle lines are overlapping. The difference in tracking angles is not more than 0.25 and 0.4 for azimuth and zenith angles respectively. This difference is within the acceptance angles of both of the CPV units and can be handled through solar tracking sensor.

3. Testing methodology

In order to analyze the actual field performance of the CPV system and to compare it with the conventional stationary PV, irrespective of their operating conditions, total energy output of the system for long term period of operation is taken as the common reference to compare the

performance and feasibility of the photovoltaic technologies. For this purpose, an electrical rating parameter is proposed and used to demonstrate the long term performance of the photovoltaic system in terms of total energy output, expressed in kWh/m^2.year. The main significance of comparison over total energy output, instead of instantaneous efficiency, is that it accommodates all of the effects of system operating condition, configuration and efficiency, and it is the main parameter of interest for the customers from any power plant. In addition, the normalization of energy output over per m^2 area will help plant designers to determine the size of the plant as per required energy requirements. Furthermore, the consideration of long term performance comparison is to mitigate the effect of solar intermittency and weather condition as the average annual solar insolation and weather condition remain same. In current study, the system testing is carried out in tropical weather of Singapore, for 1 year from September, 2014 to August, 2015. Complete detail regarding the methodology of experiment and the calculation of electrical rating and its associated parameters, is discussed further in this section.

3.1. System description

The CPV system analysis is based upon the electrical power output, calculated from CPV current and voltage output through maximum power point tracking (MPPT). The CPV units were operated for whole day, from sun rise to sunset and the power output from the systems was recorded through Agilent data logger at an interval of 1sec. The solar energy input data of direct normal irradiance (DNI) was collected by using Pyrheliometer. The system description of current experimental setup is shown in **Figure 4**. To analyze the recorded data, the power output from the system and solar energy received were integrated over the whole day period by using OriginPro software, to obtain the total energy input and output of the system.

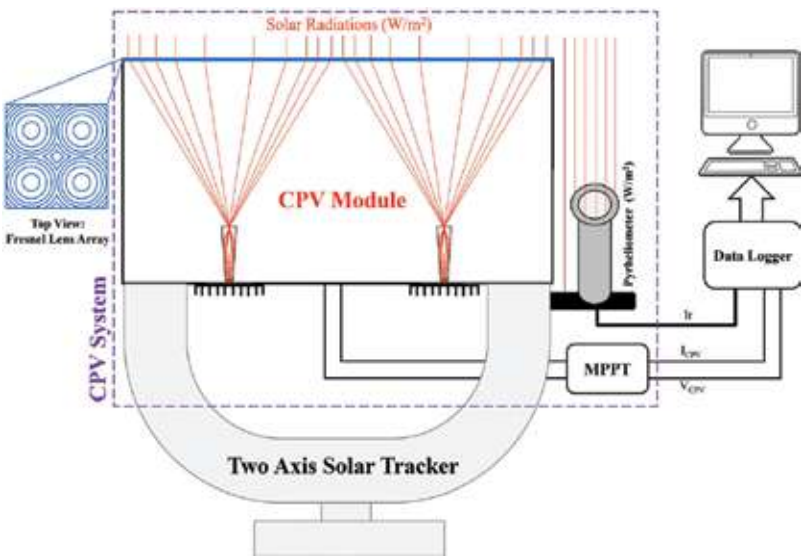

Figure 4. Experimental setup description of CPV system [12].

3.2. Electrical rating

To investigate short and long term performance of CPV system, monthly and overall electrical rating can be determined by using Eqs. (1) and (2).

$$Monthly\ Electrical\ Rating, R_{e,m} = \left(\sum_{j=1}^{n} E_i\right).\ \frac{365}{n} \qquad \left(\frac{kWh}{m^2.\ year}\right) \tag{1}$$

$$Overall\ Electrical\ Rating, R_e = \left(\sum_{j=1}^{m} E_i\right).\ \frac{365}{m} \qquad \left(\frac{kWh}{m^2.\ year}\right) \tag{2}$$

where 'n' represent the maximum number of days, for that particular month, and 'm' represents the overall total number of days for which the experiment was performed and data was recorded. The parameter 'E' represents the daily total electrical energy output of the CPV system, given by Eq. (3). Similarly, daily total solar energy received by CPV system is given by Eq. (4).

3.3. Daily electrical energy output and solar insolation

$$E = \int_1^t \left(\frac{V_{CPV}.\ I_{CPV}}{A_C}\right)dt = \sum_{i=1}^{t} \left(\frac{(V_{CPV}.\ I_{CPV})_i - (V_{CPV}.\ I_{CPV})_{i-1}}{2 \times A_C}\right).\ S \qquad \left(\frac{kWh}{m^2}\right) \tag{3}$$

$$D_m = \int_1^t (Ir)dt = \sum_{i=1}^{t} \left(\frac{(Ir)_i - (Ir)_{i-1}}{2}\right).\ S \qquad \left(\frac{kWh}{m^2}\right) \tag{4}$$

where 'V_{CPV}' and 'I_{CPV}' are voltage and current of the CPV units at maximum power point, obtained from multi-junction solar cells, A_C is the area of concentrator and 'Ir' represents the DNI received in W/m^2. The parameter 't' represents the time of operation in seconds for that particular day and 'S' is scanning interval between two recordings, which is 1sec for current study.

3.4. System average DNI efficiency

Based upon the total daily energy input and output of the CPV system, daily, monthly and overall average efficiency of the system are given by Eqs. (5)–(7).

$$Daily\ Averge\ DNI\ Efficiency = \frac{E}{D_m} \times 100 \qquad (\%) \tag{5}$$

$$Monthly\ Averge\ DNI\ Efficiency = \frac{\sum_{j=1}^{n} E_i}{\sum_{j=1}^{n} D_m} \times 100 \qquad (\%) \tag{6}$$

$$Overall\ Averge\ DNI\ Efficiency = \frac{\sum_{j=1}^{m} E_i}{\sum_{j=1}^{m} D_m} \times 100 \qquad (\%) \tag{7}$$

3.5. System average GHI efficiency

As CPV system can only accept beam radiations of solar energy, so the average efficiency mentioned above is based upon the DNI input. In order to have comparison with the conventional stationary PV system, average efficiency based upon the global horizontal irradiance (GHI) is given by Eq. (8).

$$Overall\ Averge\ GHI\ Efficiency = \frac{\sum_{j=1}^{m} E_i}{\sum_{j=1}^{m} GHI} \times 100 \qquad (\%) \tag{8}$$

3.6. Percentage share of beam radiations

The percentage share of beam radiations received against global irradiance is given by Eq. (9).

$$DNI\ Share = \frac{\sum_{j=1}^{n} D_m}{\sum_{j=1}^{n} GHI} \times 100 \qquad (\%) \tag{9}$$

3.7. CO_2 emissions saving

In addition, CO_2 emissions saving for each kWh electric produced, can also be computed by using the carbon emission factor provided by International Energy Agency (IEA) and is given by (10):

$$CO_2\ Emissions\ Saving = R_e \times 0.635 \qquad \left(\frac{kg}{m^2.\ year}\right) \tag{10}$$

where 0.635 CO_2 tons/MWh_e is the value for crude oil taken from International Energy Agency (IEA) [21], for calculations in current chapter. The value of CO_2 emissions saving depends upon the carbon emission factor which is different for different fuels and depends upon their calorific values.

4. Maximum performance characteristics of systems under comparison

In this section, the characteristics, maximum performance rating and installed location of the systems under comparison is described. **Table 1** shows the maximum performance rating of the used multi-junction solar cell, by Arima Photovoltaic and Optical Co., and the developed CPV Units. The maximum efficiency of both CPV systems is based upon the real field testing at EA-Building NUS Singapore and the performance graphs with back plate or heat sink temperature, during testing, are shown in **Figures 5** and **6**.

http://dx.doi.org/10.5772/intechopen.78952

Sr. no.	Photovoltaic technology	Performance	
1	Multi-junction solar cell (InGaP/InGaAs/Ge)	Concentration ratio = 500	Efficiency = 39.5% @ 25°C cell temperature
			Efficiency = 35.2% @ 90°C cell temperature
		Concentration ratio = 100	Efficiency = 38.5% @ 25°C cell temperature
			Efficiency = 33.6% @ 90°C cell temperature
2	Fresnel lens CPV unit	Geometric concentration ratio = 476	Maximum module efficiency = 28% Tested at NUS EA-building rooftop
3	Mini dish CPV unit	Geometric concentration ratio = 492	Maximum module efficiency = 18% Tested at NUS EA-building rooftop

Table 1. Maximum performance rating of multi-junction solar cell and developed CPVs [12].

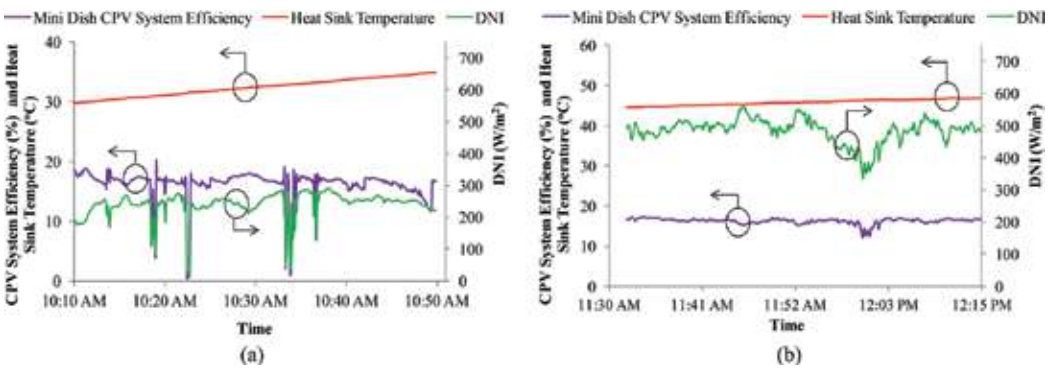

Figure 5. Mini dish CPV system performance. (a) Test 1 and (b) Test 2 [12].

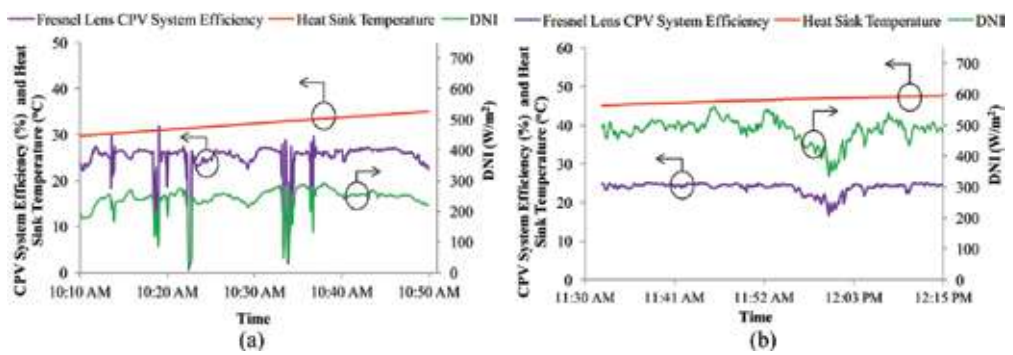

Figure 6. Fresnel lens CPV system performance. (a) Test 1 and (b) Test 2 [12].

It can be seen that the Maximum efficiency of Fresnel lens CPV unit is same as commercial CPV systems i.e. 28%. For both CPV prototypes, same type of multi-junction solar cell is used. However, lower conversion efficiency of mini dish CPV unit is due to aluminum reflecting coating on both reflectors, which had lower reflectance due to surface imperfections, causing

Figure 7. Conventional monocrystalline, polycrystalline and thin film (CIS) PV systems at CITI (BCA), Singapore [22].

Sr. no.	Photovoltaic technology	Performance	Location
1	Mono-crystalline (16.86 m^2)	17.2% @ STC [23]	CITI (BCA), Singapore.
2	Poly-crystalline (19.4 m^2)	16.2% @ STC [24]	
3	Thin film (CIS) (21.27 m^2)	17% @ STC [25]	

Table 2. Performance characteristics of conventional PV systems at CITI (BCA), Singapore.

lower optical efficiency of the mini dish concentrating assembly. The reason for testing the CPV efficiency at different time zones, is to show the effect of temperature on the system performance. It is evident from the **Figures 5** and **6** that the CPV efficiency is decreasing with increase in the heat sink temperature in the noon time, due to higher DNI received.

In order to show the feasibility and the potential of CPV system operation in tropical region, the performance of the CPV units is compared with the other conventional stationary PV system installed in Singapore, shown in **Figure 7**. The details of these PV units regarding their maximum rating, the cell type and the installed location, are given in **Table 2**.

5. Results and discussion

The field operating conditions in form of daily average ambient temperature and the solar energy input as direct normal irradiance (DNI) and global horizontal irradiance (GHI), are shown in **Figure 8** for the period of 1 year. The presented DNI data is the actual recorded measurements taken at the rooftop of NUS EA-building, Singapore with an interval of 1 s. The data was recorded for 1-year period from September 2014 to August 2015. The GHI and the daily average ambient temperature data were obtained from National Environment Agency (NEA) Singapore [26], for 3-year period from 2012 to 2014. However, the presented data is the 3-year average value for GHI and ambient temperature. From **Figure 8**, it can be seen that the

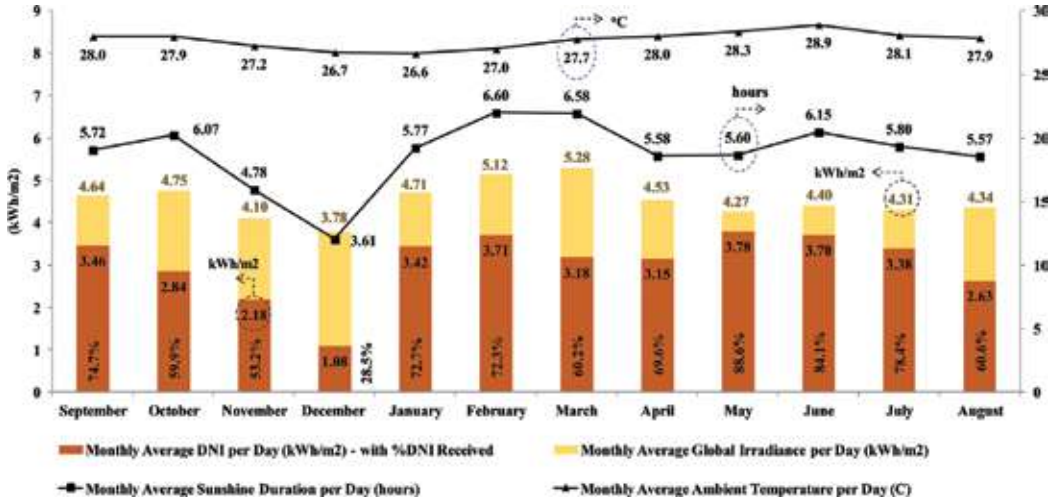

Figure 8. Monthly average values of solar irradiance (Global and DNI) and sunshine duration data per day [12].

longer sunshine period is observed for the month with larger amount of received solar energy. For March, the received GHI in kWh/m^2/day is highest with longest sunshine period. On the other hand, for the rainy season period of November and December, the lowest amount of solar energy was received, for tropical weather of Singapore.

The field performance potential of developed CPV systems in form of monthly average DNI efficiency and monthly electrical rating, against percentage of DNI share in total received solar energy, is shown in **Figure 9**. At first glance, it can be seen that the monthly average electrical rating is proportional to the direct normal irradiance share. For May and June, it can be ordered that the highest electrical rating value was recorded as 297.6 and 296.2 kWh/m^2.year for Fresnel Lens CPV system and 235 and 227.2 kWh/m^2.year for mini dish CPV system, respectively. It's due to larger share DNI in received solar radiations. On the other hand, for November and December, very poor output was recorded from both CPV systems due to low DNI availability. It is important to mention here that the main reason for higher electrical rating of Fresnel lens than the mini dish CPV, is due to its higher system efficiency as explained in **Figure 5**. The monthly average efficiencies of 22 and 16% were recorded for Fresnel lens and mini dish CPV systems, respectively. The highest efficiency was recorded for February, which is due to the longest sunshine duration and lowest ambient; the favorable conditions for CPV system.

In order to compare the field performance of CPV system with conventional flat plate PV panels, in tropical urban region, the electrical rating is presented for both developed CPV systems and three PV system, based upon single junction solar cells, installed at the rooftop of CITI (BCA), Singapore [27]. The yearly performance data is shown in **Figure 10**. The Fresnel lens CPV system showed the highest electrical rating of 240.21 kWh/m^2.year which is about 2 folds higher than the conventional PV systems. The annual average efficiency of 22% was also recorded during 1-year operation. Such long term efficiency includes all of the performance affecting parameters and that is why, it provide most meaningful and reliable performance

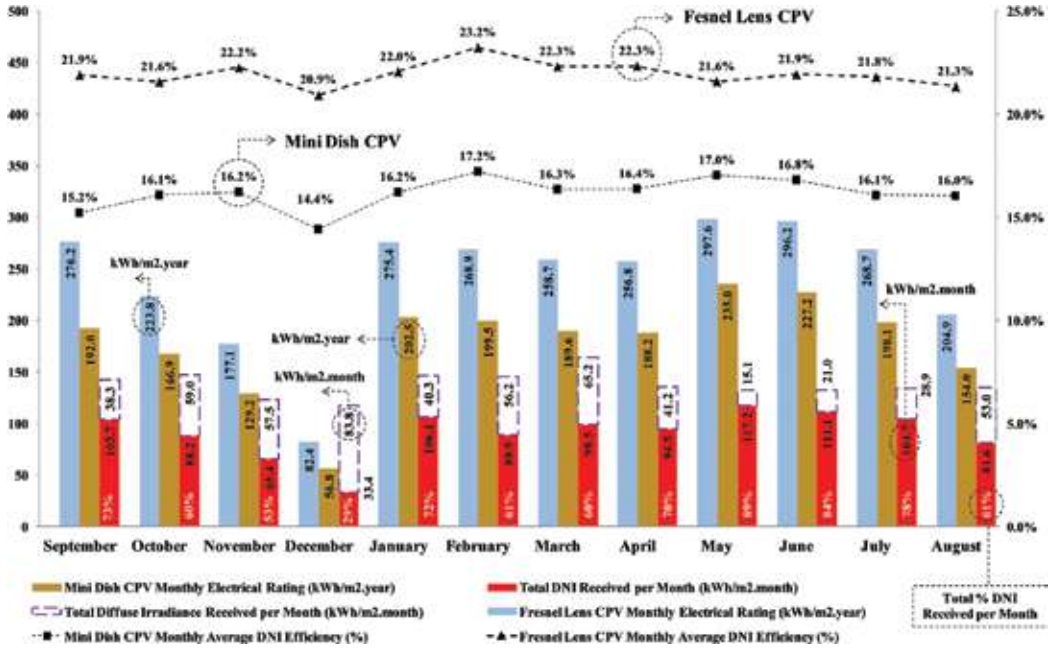

Figure 9. Monthly electrical rating and monthly average efficiency of CPV systems with the DNI received [12].

indicating parameter for photovoltaic systems, as compared to the instantaneous rated efficiency. It is important to mention here that the CPV system showed twice the power output than the conventional PV system, indicating the superiority and feasibility of CPV technology even in tropical region, other than the open desert fields.

So far, the presented efficiency of CPV system is based upon direct normal irradiance (DNI) as solar energy input. Because concentrated photovoltaic (CPV) system can only respond to beam radiations of solar energy. This means that another big portion of solar energy in form of diffuse radiations, which is very high in tropical climates, is not considered in the efficiency calculations of CPV as solar energy input. However, conventional PV systems can respond to both, beam and diffuse radiations. Therefore, in order to compare the performance of CPV with conventional PV, diffuse radians must also be considered as solar energy input. For such scenario, based upon global horizontal irradiance, the GHI efficiency of photovoltaic systems is shown in **Figure 10**. An average solar insolation of 1700 kWh/m^2.year is considered as global solar energy input to the photovoltaic system. The CPV system showed 14% GHI efficiency which is still 2 folds higher than conventional PV, even in tropical weather conditions. The summary of annual field performance of CPV systems is shown in **Table 3**. It can be seen that only 66.1% of total solar energy was received in form of beam radiations which were converted into electricity by CPV system, but still two times the power output of conventional PV. For comparison purpose, the long term energy output of conventional PV units, across the globe, is also given in **Table 4**.

Figure 11 shows the plot of monthly electrical rating against monthly received solar energy, to analyze the synergy of proposed method of electrical rating. For CPV system, monthly electrical rating is plotted against received DNI. On the other hand, the overall electrical rating

http://dx.doi.org/10.5772/intechopen.78952

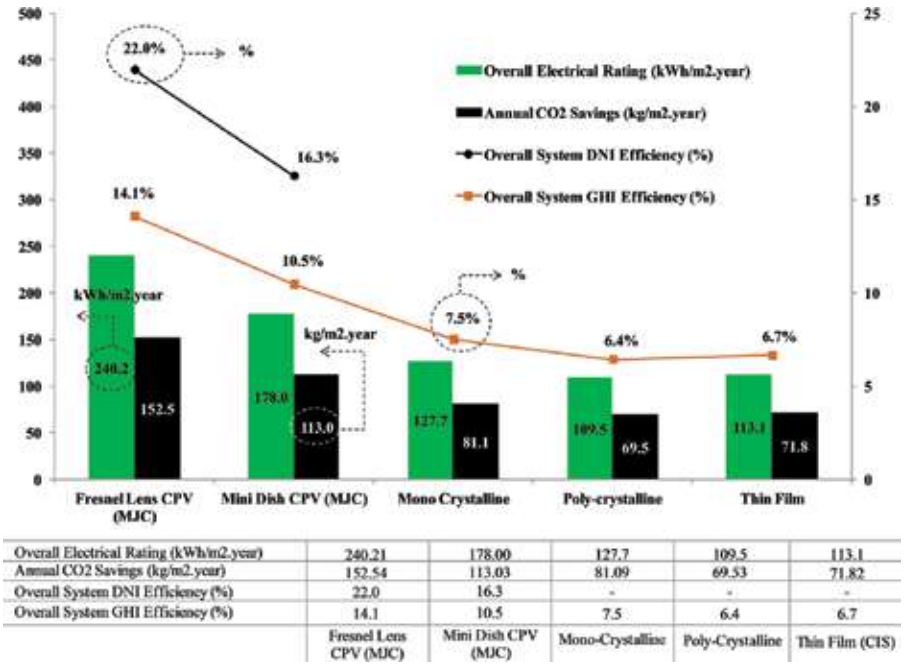

Overall Electrical Rating (kWh/m2.year)	240.21	178.00	127.7	109.5	113.1
Annual CO2 Savings (kg/m2.year)	152.54	113.03	81.09	69.53	71.82
Overall System DNI Efficiency (%)	22.0	16.3	-	-	-
Overall System GHI Efficiency (%)	14.1	10.5	7.5	6.4	6.7
	Fresnel Lens CPV (MJC)	Mini Dish CPV (MJC)	Mono-Crystalline	Poly-Crystalline	Thin Film (CIS)

Figure 10. CPV systems and conventional PVs and their CO_2 savings comparison [12].

Month	Solar input			Fresnel Lens CPV		Mini Dish CPV	
	GHI*	DNI	DNI share	Total power delivered	Average DNI efficiency	Total power delivered	Average DNI efficiency
	GHI	D_m		E		E	
	kWh/m²/month	kWh/m²/month	%	kWh/m²/month	%/month	kWh/m²/month	%/month
September	142.04	103.75	73.0	22.70	21.89	15.78	15.2
October	147.20	88.19	59.9	19.00	21.6	14.17	16.1
November	122.97	65.44	53.2	14.55	22.2	10.62	16.2
December	117.21	33.45	28.5	7.00	20.9	4.82	14.4
January	146.37	106.10	72.5	23.39	22.0	17.20	16.2
February	145.17	88.83	61.3	20.63	23.2	15.30	17.2
March	163.73	98.52	60.2	21.97	22.3	16.10	16.3
April	135.77	94.55	69.6	21.10	22.3	15.47	16.4
May	132.31	117.19	88.6	25.28	21.6	19.96	17.0
June	132.08	111.11	84.1	24.35	21.9	18.67	16.8
July	133.68	104.75	78.4	22.83	21.8	16.82	16.1
August	134.59	81.58	60.6	17.40	21.3	13.08	16.0
Annual Average	**1653.12** kWh/m²/year	**1093.46** kWh/m²/year	**66.1**%	**240.2** kWh/m²/year	**22.0**%	**178.0** kWh/m²/year	**16.3**%

*from NEA [26].

Table 3. Summary of long-term (12 months) performance data of CPV systems [12].

Sr. no.	Plant location	Solar cell type	Average efficiency
1	JNU, JEJU, Korea	Poly-crystalline	6.5% [27]
2	Malaga, Spain	-	6.1–8.0% [28]
3	Jaen, Spain	-	7.8% [29]
4	Calabria, Italy	Poly-crystalline (Si)	7.6% [30]
5	Warsaw, Poland	Thin film (amorphous-Si)	4.0-5.0% [31]
6	Umbertide, Italy	Poly-crystalline (Si)	6.2-6.7% [32]
7	Khatkar Kalan, India	Poly-crystalline (Si)	8.3% [33]
8	United Kingdom	Thin film (amorphous-Si)	3.2% [34]
9	United Kingdom	Poly-crystalline (Si)	7.5% [34]
10	United Kingdom	-	8.4% [34]
11	Brazil	Thin film (amorphous-Si)	5% [34]

Table 4. Overall average efficiencies of conventional PV plants installed worldwide.

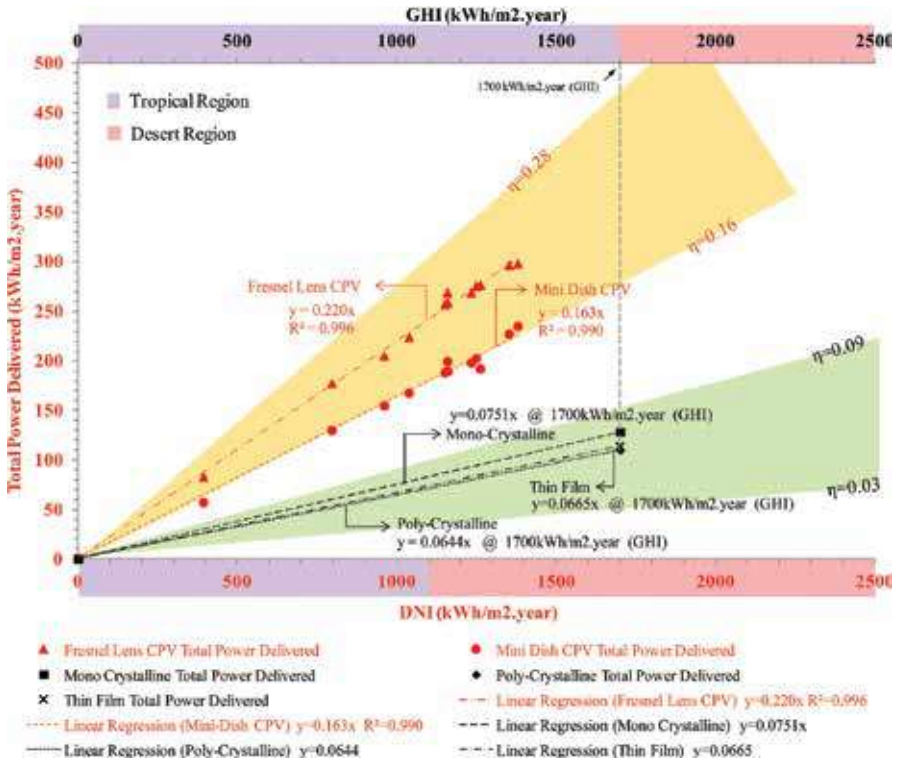

Figure 11. Total power delivered by assorted PV Systems against DNI and global irradiance [12].

of conventional PV i.e. mono crystalline, poly-crystalline and thin film, is plotted against annual average GHI of 1700 kWh/m^2.year [27]. From linear regression, it can be seen that the electrical rating of photovoltaic systems is directly proportional to corresponding received

solar energy i.e. DNI for the case of CPV and GHI for the case of conventional PV. In addition, it can also be seen that the slope of linear regression line gives the long term average efficiency of respected photovoltaic technology. For Fresnel lens CPV, the slope of regressed line is 0.22 which is equal to the long term average efficiency of 22%, given in **Table 3**. The significance of **Figure 11** in the design of photovoltaic system, is that if the total DNI or GHI availability of particular region is known then the actual output of the system can be roughly estimated to have quick production potential of system in form of its electrical rating. Higher the value of solar energy input, higher the electrical rating of the system. However, for such field production estimation, only average efficiency of the system must be considered, instead of rated maximum efficiency. For desert region of Saudi Arabia, with GHI availability of 2300 kWh/m^2.year [35] and assuming 90% share of beam radiations, overall output of 476 kWh/m^2.year and 184 kWh/m^2.year can be expected to be received from the operation of CPV and PV system, respectively, with average system efficiencies of 23 and 8%.

6. Summary of the chapter

The long-term electrical rating of two in-house built CPV units i.e. the mini dish and the Fresnel lens CPVs, has been successfully analyzed under the outdoor tropical weather of Singapore, which is the first ever CPV performance reporting in this region. Based on the local tropical climate conditions, the mini-dish and the Fresnel lens CPVs achieved electric ratings of 178.0 and 240.2 kWh/m^2.year, which is about two folds higher than the conventional PVs (mono-crystalline, poly-crystalline and thin CIS films) of 118 $\pm$ 10 kWh/m^2.year, operating under the same tropical weather conditions, with only 66.1% DNI share. In addition, the average system efficiency based on the total energy input and output, for long term operation, is recommended over instantaneous maximum efficiency, as the true field performance indicator, accommodating all performance affecting parameters. The CPV system showed long term average efficiency of 22 $\pm$ 0.5% in the tropical climate, with maximum efficiency of 28%. The plot of electric rating (in kWh/m^2.year) versus the annual insolation is also suggested as its slope gives the long term average efficiency, which can be used to estimate the CPV field performance against the available solar energy (DNI). To conclude, this study demonstrates a strong potential and feasibility of CPV system operation in the tropical weather conditions. It is also emphasized that the electrical rating parameter is more accurate and reliable when conducting a performance evaluation of photovoltaic systems.

Author details

Muhammad Burhan*, Muhammad Wakil Shahzad and Ng Kim Choon

*Address all correspondence to: muhammad.burhan@kaust.edu.sa

Water Desalination and Reuse Centre, King Abdullah University of Science and Technology, Saudi Arabia

References

[1] Shafiei E, Davidsdottir B, Leaver J, Stefansson H, Asgeirsson EI. Comparative analysis of hydrogen, biofuels and electricity transitional pathways to sustainable transport in a renewable-based energy system. Energy. 2015;**83**:614-627

[2] Burhan M, Shahzad MW, Ng KC. Development of performance model and optimization strategy for standalone operation of CPV-hydrogen system utilizing multi-junction solar cell. International Journal of Hydrogen Energy. 2017;**42**(43):26789-26803

[3] Burhan M, Chua KJE, Ng KC. Electrical rating of concentrated photovoltaic (CPV) systems: Long-term performance analysis and comparison to conventional PV systems. International Journal of Technology. 2016;**7**(2):189-196. DOI: 10.14716/ijtech.v7i2.2983

[4] Ng KC, Burhan M, Shahzad MW, Ismail ABA. Universal isotherm model to capture adsorption uptake and energy distribution of porous heterogeneous surface. Scientific Reports. 2017;**7**(1):10634

[5] Burhan M, Chua KJE, Ng KC. Sunlight to hydrogen conversion: Design optimization and energy management of concentrated photovoltaic (CPV-Hydrogen) system using micro genetic algorithm. Energy. 2016;**99**:115-128

[6] IPCC. Renewable energy sources and climate change mitigation. In: Edenhofer O, Pichs-Madruga R, Sokona Y, Seyboth K, Matschoss P, Kadner S, Zwickel T, Eickemeier P, Hansen G, Schlömer S, von Stechow C, editors. IPCC Special Report on Renewable Energy Sources and Climate Change Mitigation. Cambridge, United Kingdom and New York, NY, USA: Cambridge University Press; 2012

[7] Burhan M, Chua KJE, Ng KC. Simulation and development of a multi-leg homogeniser concentrating assembly for concentrated photovoltaic (CPV) system with electrical rating analysis. Energy Conversion and Management. 2016;**116**:58-71

[8] Burhan M, Oh SJ, Chua KJ, Ng KC. Solar to hydrogen: Compact and cost effective CPV field for rooftop operation and hydrogen production. Applied energy. 2017;**194**:255-66

[9] Burhan M, Oh SJ, Chua KJE, Ng KC. Double lens collimator solar feedback sensor and master slave configuration: Development of compact and low cost two axis solar tracking system for CPV applications. Solar Energy. 2016;**137**:352-363

[10] Burhan M, Chua KJE, Ng KC. Long term hydrogen production potential of concentrated photovoltaic (CPV) system in tropical weather of Singapore. International Journal of Hydrogen Energy. 2016;**41**(38):16729-16742

[11] Burhan M, Shahzad MW, Choon NK. Hydrogen at the rooftop: Compact CPV-hydrogen system to convert sunlight to hydrogen. Applied Thermal Engineering. 2018;**132**:154-164

[12] Burhan M, Shahzad MW, Ng KC. Long-term performance potential of concentrated photovoltaic (CPV) systems. Energy Conversion and Management. 2017;**148**:90-99

[13] Arndt R, Puto IR. Basic Understanding of IEC Standard Testing for Photovoltaic Panels. TUV SUD America Inc. http://www.tuvamerica.com/services/photovoltaics/articlebasicunderstandingpv.pdf [Retrieved: October 21, 2015]

[14] Burhan M, Shahzad MW, Ng KC. Sustainable cooling with hybrid concentrated photovoltaic thermal (CPVT) system and hydrogen energy storage. International Journal of Computational Physics Series. 2018;**1**(2):40-51

[15] Burhan M, Shahzad MW, Oh SJ, Ng KC. A pathway for sustainable conversion of sunlight to hydrogen using proposed compact CPV system. Energy Conversion and Management. 2018;**165**:102-112

[16] Said SAM. Effects of dust accumulation on performances of thermal and photovoltaic flat-plate collectors. Applied Energy. 1990;**37**(1):73-84

[17] Muhammad B, Seung JO, Ng KC, Chun W. Experimental investigation of multijunction solar cell using two axis solar tracker. Applied Mechanics and Materials. 2016;**819**:536-540. Trans Tech Publications

[18] Riffonneau Y, Bacha S, Barruel F, Ploix S. Optimal power flow management for grid connected PV systems with batteries. IEEE Transactions on Sustainable Energy. 2011;**2**(3): 309-320

[19] Oh SJ, Burhan M, Ng KC, Kim Y, Chun W. Development and performance analysis of a two-axis solar tracker for concentrated photovoltaics. International Journal of Energy Research. 2015;**39**(7):965-976

[20] Astronomical Applications Department of the U.S. Naval Observatory. Available from: http://aa.usno.navy.mil/data/docs/AltAz.php [Retrieved: May 10, 2015]

[21] International Energy Agency, CO_2 Emissions from Fuel Combustion Highlights, France: International Energy Agency; 2013

[22] Burhan M. Theoretical and experimental study of concentrated photovoltaic (CPV) system with hydrogen production as energy storage [Doctoral dissertation]. Singapore: National University of Singapore (NUS); 2015

[23] Yingli Green Energy Holding Co. Ltd. PANDA 60 CELL SERIES 2. Available from: www.yinglisolar.com

[24] Yingli Green Energy Holding Co. Ltd. YGE 48 Cell 40mm SERIES. Available from: www.yinglisolar.com

[25] MiaSolé Hi-Tech Corp. FLEX–02N SERIES CIGS MODULE. Available from: www.miasole.com

[26] National Environment Agency (NEA) Singapore. Available from: www.nea.gov.sg

[27] Lin-Heng L, Lok-Ming C, Chia A, Gunawansa A, Harn-Wei K. Sustainability Matters, Challenges and Opportunities in Environmental Management in Asia. Singapore: Pearson Education South Asia Pte Ltd; 2011

[28] Sidrach-de-Cardona M, Lopez LM. Performance analysis of a grid-connected photovoltaic system. Energy. 1999;**24**(2):93-102

[29] Drif M, Pérez PJ, Aguilera J, Almonacid G, Gomez P, De la Casa J, Aguilar JD. Univer Project. A grid connected photovoltaic system of at Jaén University. Overview and performance analysis. Solar Energy Materials and Solar Cells. 2007;**91**(8):670-683

[30] Cucumo M, De Rosa A, Ferraro V, Kaliakatsos D, Marinelli V. Performance analysis of a 3kW grid-connected photovoltaic plant. Renewable Energy. 2006;**31**(8):1129-1138

[31] Pietruszko SM, Gradzki M. Performance of a grid connected small PV system in Poland. Applied Energy. 2003;**74**(1):177-184

[32] Ubertini S, Desideri U. Performance estimation and experimental measurements of a photovoltaic roof. Renewable Energy. 2003;**28**(12):1833-1850

[33] Dobaria B, Pandya M, Aware M. Analytical assessment of 5.05 kWp grid tied photovoltaic plant performance on the system level in a composite climate of western India. Energy. 2016;**111**:47-51

[34] Mondol JD, Yohanis Y, Smyth M, Norton B. Long term performance analysis of a grid connected photovoltaic system in Northern Ireland. Energy Conversion and Management. 2006;**47**(18):2925-2947

[35] Almarshoud AF. Performance of solar resources in Saudi Arabia. Renewable and Sustainable Energy Reviews. 2016;**66**:694-701

Chapter 3

Solar Cooling Technologies

Salman Ajib and Ali Alahmer

Additional information is available at the end of the chapter

http://dx.doi.org/10.5772/intechopen.80484

Abstract

This chapter describes different available technologies to provide the cooling effect by utilizing solar energy for both thermal and photovoltaic ways. Moreover, this chapter highlights the following points: (i) the main attributes for different solar cooling technologies to recognize the main advantages, challenges, disadvantages, and feasibility analysis; (ii) the need for further research to reduce solar cooling chiller manufacture costs and improve its performance; (iii) it provides useful information for decision-makers to select the proper solar cooling technology for specific application. Furthermore, some references, which include investigation results, will be included. A conclusion about the main gained investigation results will summarize the investigation results and the perspectives of such technologies.

Keywords: cooling, air conditioning system, solar cooling, performance, absorption machines, adsorption machines

1. Introduction

Today, the increase of requirements for indoor cooling demands improves thermal human comfort inside residential buildings, reduces the divergence between the energy supply and energy demand by the use of low-grade heat sources such as solar energy and industrial waste heat, lowers the CO_2 emissions in the building sector due to the use of air condition systems, and finally reduces the peak of energy consumption of air conditioning processes generated by the use of conventional vapor compression system especially during summer period for the buildings and spaces that have high latent loads. All above reasons make the solar cooling that has been received much more attention as innovative, promising, efficient, and environmentally friendly air conditioning systems as alternative options for conventional air conditioning systems [1, 2]. The building sector is considered as a major contributor

to energy consumption in the world. Numerically, 41.1% of the total energy in the United States in 2011 was consumed in the building sector, and this state is expected to increase to 42.1% in 2035 [3]. In Europe, buildings consumed for 39% of total energy consumption, which 26% is for residential buildings and 13% for commercial architectures [4]. In China, 25–30% of the total energy is consumed by civil and industrial buildings [5]. A same scenario in Australia which the building industry consumes 40% of the total energy produced [6]. According to the report issued by EU strategy on heating and cooling 2016, the energy consumption for cooling and heating in buildings demonstrated about 80%. Although less than 20% is presently exploited for cooling purposes, the domestic cooling building still has a high potential for growth. Moreover, the use of the innovative low-energy cooling technologies for heating and cooling will bring fuel savings of 5 Mtoe per year in 2030, corresponding to 9 million ton of CO_2 [7]. Therefore, the annual energy for air-conditioning purposes for a room was increased considerably, which was 1.7 GWh in 1990 and it reached 44 GWh in 2010 [8]. The Mediterranean countries have saved 40–50% of their energy consumed for refrigeration and air-conditioning by using solar-driven air-conditioning system techniques [9, 10]. It is stated that the solar system was able to contribute up to 70% of total energy consumption for heating and air-conditioning for domestic buildings. Many solar cooling technologies such as solar absorption, solar adsorption, desiccant, and ejector systems have been studied by researchers. Among these technologies, solar absorption is the most widely used technology with 59% of the installed systems in Europe against 11% for solar adsorption and 23% for desiccant cooling [11]. Many investigations have been done on solar thermal-driven absorption refrigeration machines in the small range of refrigeration capacity (5–30 kW). Some of the investigation results have been published in [12–14]. A design guide for solar cooling systems is presented in [15].

2. Classification of solar cooling technologies

Solar cooling systems can be classified into two main categories according to the energy used to drive them: solar thermal cooling systems and solar electric cooling systems. In solar thermal cooling systems, the cooling process is driven by solar collectors collecting solar energy and converting it into thermal energy, and uses this energy to drive thermal cooling systems such as absorption, adsorption, and desiccant cycles; whereas in solar electric cooling systems, electrical energy that is provided by solar photovoltaic (PV) panels is used to drive a conventional electric vapor compressor air-conditioning system. Both types of solar cooling can be used in industrial and domestic refrigeration and air-conditioning processes, with up to 95% saving in electricity [16].

2.1. Electricity-driven solar refrigeration systems

In general, the solar electrical cooling system consists of two parts: photovoltaic panel and electrical refrigeration device. Photovoltaic cells transform light into electricity through photoelectric effect. The power generated by solar photovoltaic panel is supplied either to the vapor compression systems, thermoelectrical system, or Stirling cycle.

http://dx.doi.org/10.5772/intechopen.80484

2.1.1. Solar-powered vapor compression systems

Photovoltaic powered refrigerators are an alternative option to produce cooling in remote areas of developing countries. Photovoltaic cell converts the incident solar radiation to DC power which can drive the compressor of vapor compression system. This system as depicted in **Figure 1** consists of a DC compression refrigerator connected to controller, a battery to supply and store energy, and a photovoltaic (PV) generator which supplies the refrigerator and charges the battery with excess energy. The main advantage of this system compared to the other air-conditioning systems is that it does not require an outside fuel supply. In order to run the system at highest efficiency, the voltage should be close to the voltage produced at the maximum possible power.

2.1.2. Thermoelectric cooling systems (the Peltier cooling system)

Thermoelectric device utilizes the Peltier effect to make a temperature gradient by creating heat flux between two different types of semiconductors materials. Riffat and Qiu [17] defined the Peltier effect as presence of cooling or heating effect at junction of two different conductors due to electricity flow. The main principle of working thermoelectric cooling systems is shown in **Figure 2** and follows these steps: an electric current flows across the joint of n- and p-type semiconductor materials by applying a voltage. When the current passes through the junctions of the

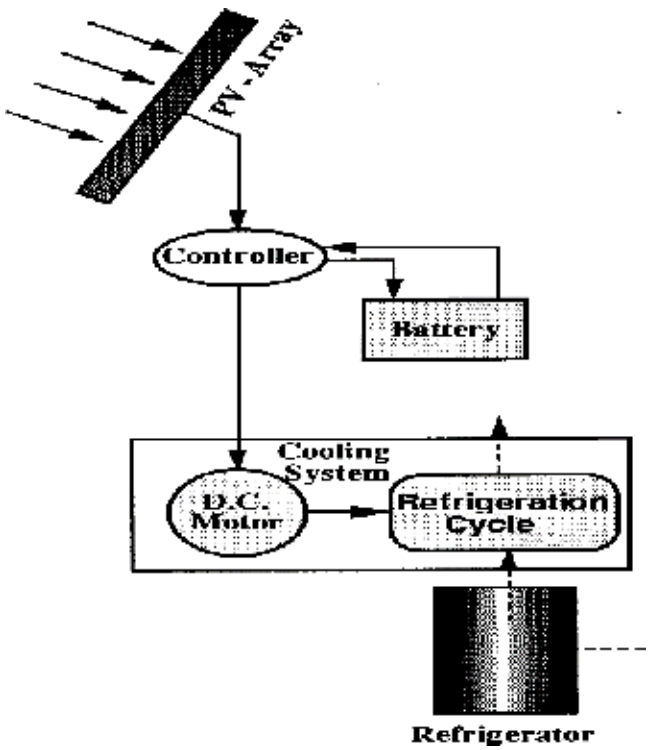

Figure 1. A configuration of a PV solar-powered vapor compression systems.

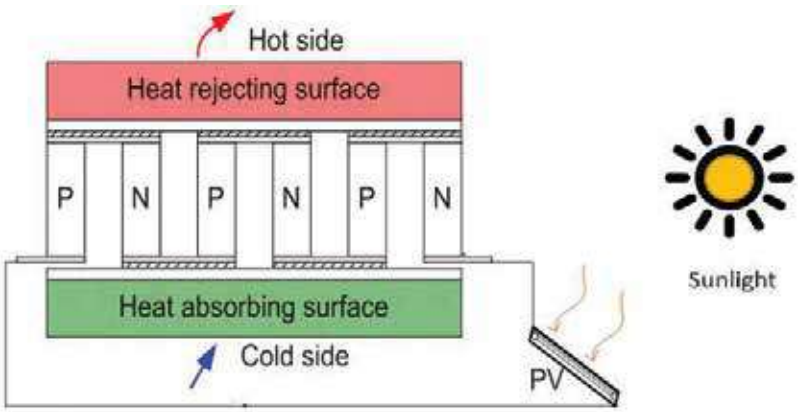

Figure 2. Thermoelectric cooling configuration.

two conductors, heat is removed at one junction and absorbs the heat from its surrounding space to create a cooling effect. Heat is deposited at the other junction. When a direction of the current is reversed, the air-conditioning system operates in the heating manner due to reverse of the heat flow direction. The main advantages of using thermoelectric cooling compared to vapor compression cycle are as follows: (a) compact and lightweight due to no bulky compressor units needed; (b) no moving parts; (c) environment friendly due to no hazardous gases; (d) silent operation; (e) high reliability in which a mean time between failures (MTBF) is more than 100,000 h; (f) precise temperature stability in which a tolerance of better than +/−0.1°C; and (g) finally cooling/heating mode option, which is fully reversible with switch in polarity and supports rapid temperature cycling. But on the other side, high cost and low efficiency are the main disadvantages.

2.1.3. Stirling systems

The cooling cycle is split into four steps as depicted in **Figure 3**. The cycle starts when the two pistons are in their most left positions:

- Process (a→b): Isothermal compression process and heat rejection to the surrounding. Initially, the left warm piston moves to the right while the cold piston is fixed. The isothermal compression process was occurred and the pressure rises, so the heat transfer Q_a is taken to the surroundings at ambient temperature T_a.
- Process (b→c): Constant volume. The two pistons move to the right at the same rate to keep the volume constant, so the volume between the two pistons is kept constant. The hot gas enters the regenerator with temperature T_a and leaves it with temperature T_L. The heat is transferred to the regenerator material.
- Process (c→d): Isothermal expansion process and heat addition from the external source. The cold piston moves to the right while the warm piston is fixed. The isothermal expansion was occurred and the pressure decreases, so the heat transfer Q_L is taken up. This is the useful cooling power.

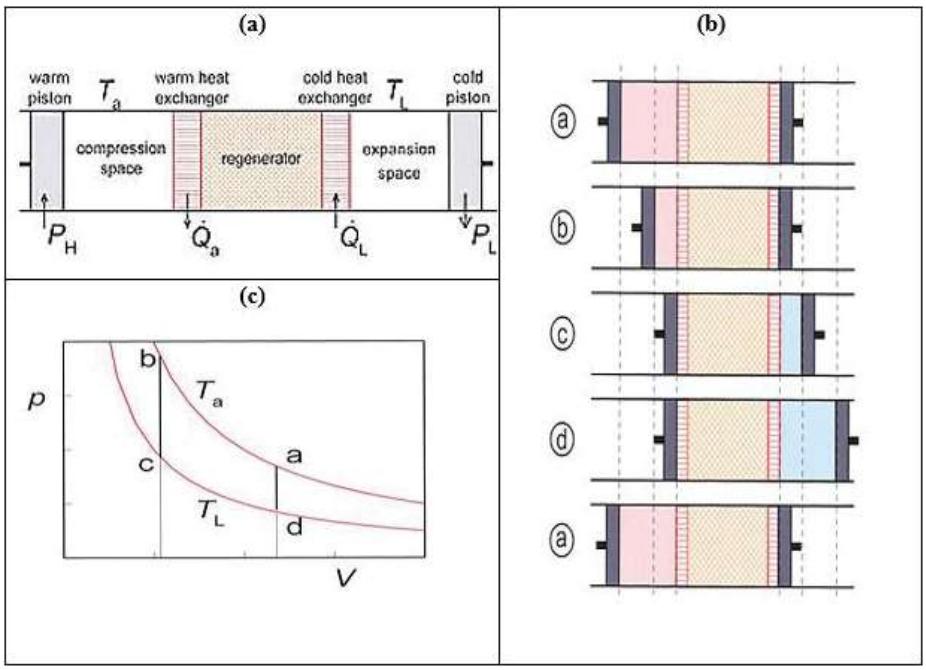

Figure 3. (a) Schematic diagram of a Stirling cooler; (b) four states in the Stirling cycle; and (c) PV-diagram of the ideal Stirling cycle.

- Process (d→a): Constant volume. The two pistons move to the left to keep the total volume constant.
- The gas temperature rises from *TL* to *Ta* so heat is taken up from the regenerator material. This completes the cycle.

2.2. Solar thermal cooling systems

2.2.1. Absorption systems

The absorption refrigeration cycle is one of the oldest refrigeration technologies. Absorption refrigeration cycle operates under the same principle as the conventional vapor compression refrigeration cycle in the refrigerant side. The mechanical compressor in the conventional vapor compression refrigeration cycle is replaced by the thermal compressor in the absorption refrigeration cycle. The thermal compressor consists of absorber and generator. **Figure 4** shows the general schematic of a single effect absorption cycle [18]. The absorption chiller cycle consists of the following steps:

1. The rich solution (rich on coolant) will be pumped from the absorber to the generator passing the solution heat exchanger (economizer).

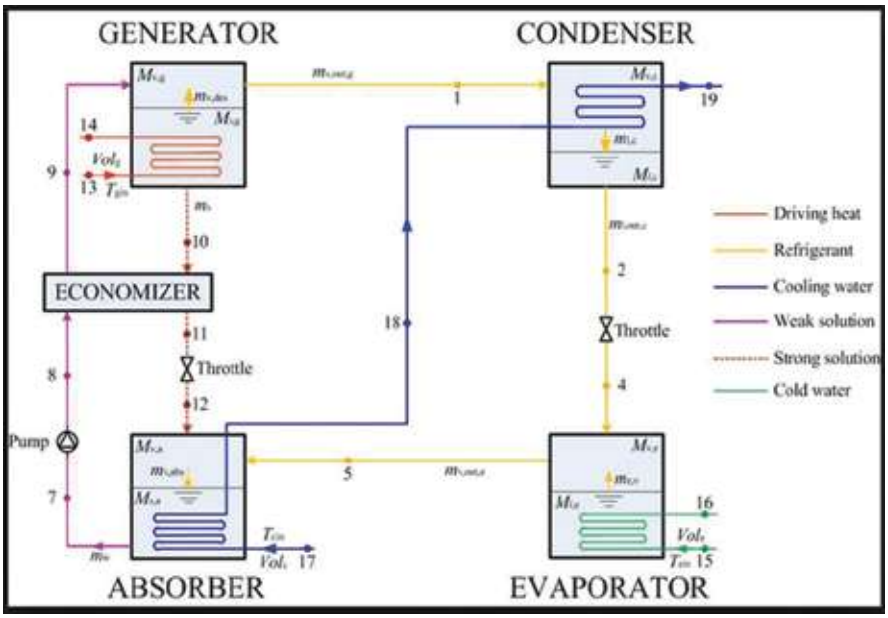

Figure 4. Schematic of the absorption chilling cycle [18].

2. Through the heat supply in the generator from a driving heat source (solar collectors), a part of the coolant will be driven out from the rich solution and flows to the condenser. After that, the remaining poor solution (poor on coolant) flows back to the absorber.
3. In the condenser, the refrigerant vapor from the generator condenses in the condenser. The heat of condensation must be rejected at an intermediate temperature level by the use of the cooling water supplied from a cooling tower.
4. The refrigerant condensate flows back to the evaporator at low pressure through an expansion device. The cycle of the coolant then repeats.
5. In the evaporator, the refrigerant is vaporized at very low pressure to produce the cooling power by extracting heat from the low-temperature medium. The coolant vapor flows to the absorber.
6. In the absorber, refrigerant vapor is absorbed by the poor solution, which flows back from the generator passing the economizer and the throttle. Then, the heat of absorption and mixing is rejected by the cooling water stream supplied from a cooling tower. After that, the cycle of the solution will repeat again.

The two main pairs of refrigerant/absorbent that are widely used are water/lithium bromide (H_2O/LiBr) and ammonia/water pair (NH_3/H_2O), where water is the refrigerant (coolant) and LiBr is the absorbent; while for the second pair, ammonia and water are the refrigerant and absorbent, respectively.

List of advantages of using water/LiBr pair, which is the most common for solar air-conditioning application, is as follows:

- uses nontoxic substances;
- low working pressures; and
- nonvolatile absorbent, i.e., there is no need of rectification of the refrigerant.

However, there are disadvantages associated with the water/LiBr pair and are as follows:

- Water cooling is required, which is commonly accomplished by a cooling tower. Cooling towers have the risk of legionella;
- Systems have bigger sizes which are due to the large volume of the water vapor;
- Risk of corrosion of the components; and
- Risk of the crystallization of the solution at very low cooling temperatures.

2.2.2. Adsorption systems

Adsorption refrigeration cycle is similar to absorption refrigeration cycle. The main difference in the former is that the refrigerant is adsorbed on the internal surface of highly porous solid material instead of the refrigerant being absorbed by a liquid solution. In the adsorption refrigeration cycle, the solid sorbent and the refrigerant form the adsorption pairs such as activated carbon-ammonia, activated carbon-methanol, activated carbon-ethanol, silica gel-water, and zeolite-water.

Adsorption is a physical or chemical process that is different from absorption, which is a chemical process. Just as there is an attraction between a liquid and a solid at a surface, there is also an attraction between a gas and a solid at a surface. Adsorption is a surface phenomenon which can be divided into physical adsorption (physisorption) and chemical adsorption (chemisorption). Physical adsorption generally resulted by the Van der Waals forces through physical process, and chemical adsorption usually achieved by valency forces through chemical process. The heat of adsorption is usually large in chemical adsorption and small in physical adsorption. Adsorbent substances can be retained to original properties by a desorption process under the application of heat.

The adsorption refrigeration cycle consists of two sorption chambers, a condenser, and an evaporator, as illustrated in **Figure 5**. The adsorption cycle achieves a COP of 0.3–0.7, depending upon the driving heat temperature of 55–90°C.

The working cycle of 5–7 min consists of the following four steps [19]:

1. In the first step, the adsorbed water is desorbed after the application of thermal energy (as example from solar energy). The collector becomes the generator (1).

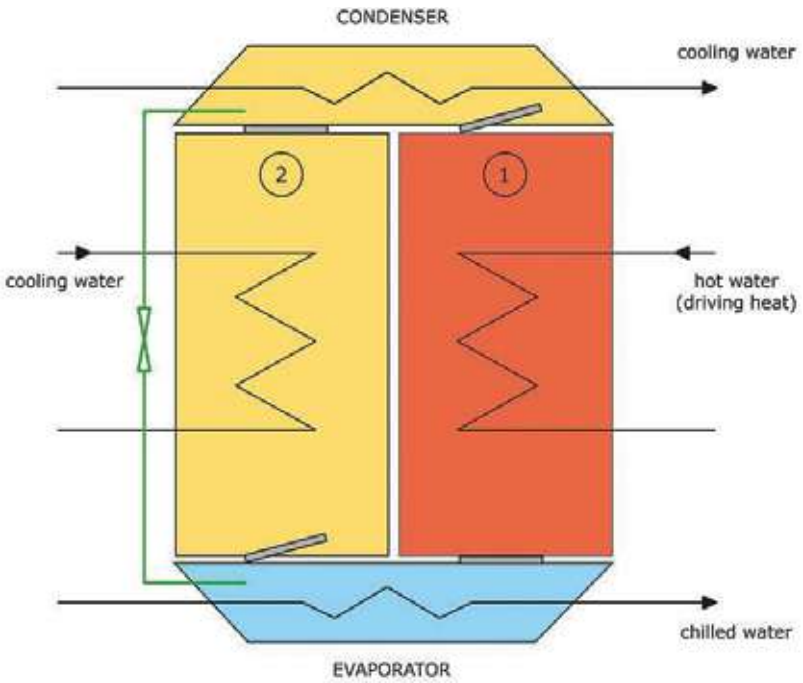

Figure 5. Schematic of adsorption cycle solar cooling system.

2. In the second step, the desorbed refrigerant (water) is cooled and condensed to liquid in the condenser by rejecting the heat through the cooling water supplied from a cooling tower.
3. In the third step, the condensed water flows through the expansion valve to the evaporator, where it vaporizes under low partial pressure and low temperature in the evaporator while the useful cooling is produced, then heat is taken away from the chilled water.
4. In the fourth and final step, the vaporized water is adsorbed in the collector (2) until the silica gel is saturated, then it is switched to the second adsorber chamber.
5. The circuit is completed as the condensed water is fed back into the evaporator through a valve.
6. The functions of two sorption chambers are reversed by alternating the opening of the butterfly valves and the direction of the heating and cooling refrigerants. In this way, the chilling refrigerant is obtained continuously. The cycle then repeats.

Advantages of adsorption chiller systems compared to absorption chiller systems [20, 21] are as follows:

1. The operating temperatures can be lower, e.g., 55–90°C as compared to 70–120°C for absorption chillers.

2. There is no low limit to the temperature reservoir.
3. There is no limitation for the low cooling water temperature, because there is no risk of crystallization problem as in the case of absorption chillers.
4. No risk of corrosion problem as in the case of absorption chillers, because there are heat sources with temperature close to 500°C that can be used directly.
5. The adsorption systems have flexibility in regeneration temperature and do not require frequent replacement of adsorbent.
6. The adsorption systems do not need a rectifier for the refrigerant or solution pump in comparison with absorption systems.

The disadvantages of adsorption chiller systems include [22]:

1. Adsorption technology is more expensive than absorption technology.
2. The average COP of adsorption chillers is lower than the absorption chillers.
3. The adsorption chillers are both heavy weight and larger than the absorption chillers.
4. Heat recovery is very complex, because the adsorption system is intermittent system.

Advantages of absorption and adsorption chiller systems compared to vapor compression systems:

1. Absorption and adsorption systems are environmentally friendly. The equipment uses completely harmless working fluids.
2. The maximum cooling load can be achieved with the maximum available solar radiation and hence potential of the refrigeration system.
3. Maintenance costs are lower due to fewer moving parts like solenoid valves and vacuum pumps. It is almost noiseless system, where there are not many moving parts, other than the solution pump in the absorption refrigeration systems.
4. Taking advantage of solar thermal plants in the sorption refrigeration technology even when there is no heat demand.
5. Operation costs are lower due to low electricity consumption in comparison with vapor compression systems.

2.2.3. Desiccant systems

The desiccant air-conditioning system utilizes the capability of desiccant materials in removing the air moisture content by sorption process. All materials that attract moisture at different capacities are called desiccant [4]. The desiccant cooling system can be a suitable selection for thermal comfort especially in climates with high humidity. Moreover, this

technique allows us to utilize renewable energy or low-temperature gains from solar energy, waste heat, and cogeneration to drive the cooling cycle. The comparison between desiccant system and conventional systems is listed in **Table 1**. There are many required properties for any desiccant materials selected in open-cycle cooling based on [23]: (i) mechanical and chemical stability; (ii) large moisture capacity per unit weight; (iii) low heat of adsorption/absorption to regenerate; (iv) sorption rate; (v) large adsorption/absorption capacity at low water vapor pressures; (vi) cheap cost; (vii) sorption at low relative humidity; and (viii) finally ideal isotherm shape.

Two configurations were described in detail below: ventilation and recirculation modes. The schematic of the ventilation mode representation is demonstrated in **Figure 6a**. On the conditioning side of the system (air processing side), warm and humid air enters the slowly rotating desiccant wheel and is dehumidified by adsorption of water (1–2). Since the air is heated up by the adsorption heat, a heat recovery wheel is passed (2–3), resulting in a significant precooling of the supply air stream. Subsequently, the air is humidified and thus further cooled by a controlled humidifier (3–4) according to the set-values of supply air temperature and humidity. In order to control the sensible heat factor, the remix air is introduced by the mix evaporatively cooled room air with the cooled and dried room make-up air (5–6). On the regeneration side of the system, the exhaust air stream of the rooms is humidified (6–7) close to the saturation point to exploit the full cooling potential in order to allow an effective heat recovery (7–8). After that, the sorption wheel has to be regenerated (8–9) by applying heat in a comparatively low temperature range from 50 to 75°C and to allow a continuous operation of the dehumidification process. Finally, the cold and humid air is exhausted to the atmosphere (9–10) and the cooling cycle is completed.

Parameter	Conventional system	Desiccant system
Operation cost	High	Low
Performance	High	Low
Energy source	Mainly electricity	Low-grade energy
Environmental safety	Less	High
System care	Less	High
Control over humidity	Average	Accurate
Indoor air quality	Less	More
System installation	Simple	More complicate
Energy storage capacity	Mainly not applicable	Applicable
Installation cost	High	Low
System control	Average	Complicate

Table 1. The comparison between desiccant system and conventional systems.

http://dx.doi.org/10.5772/intechopen.80484

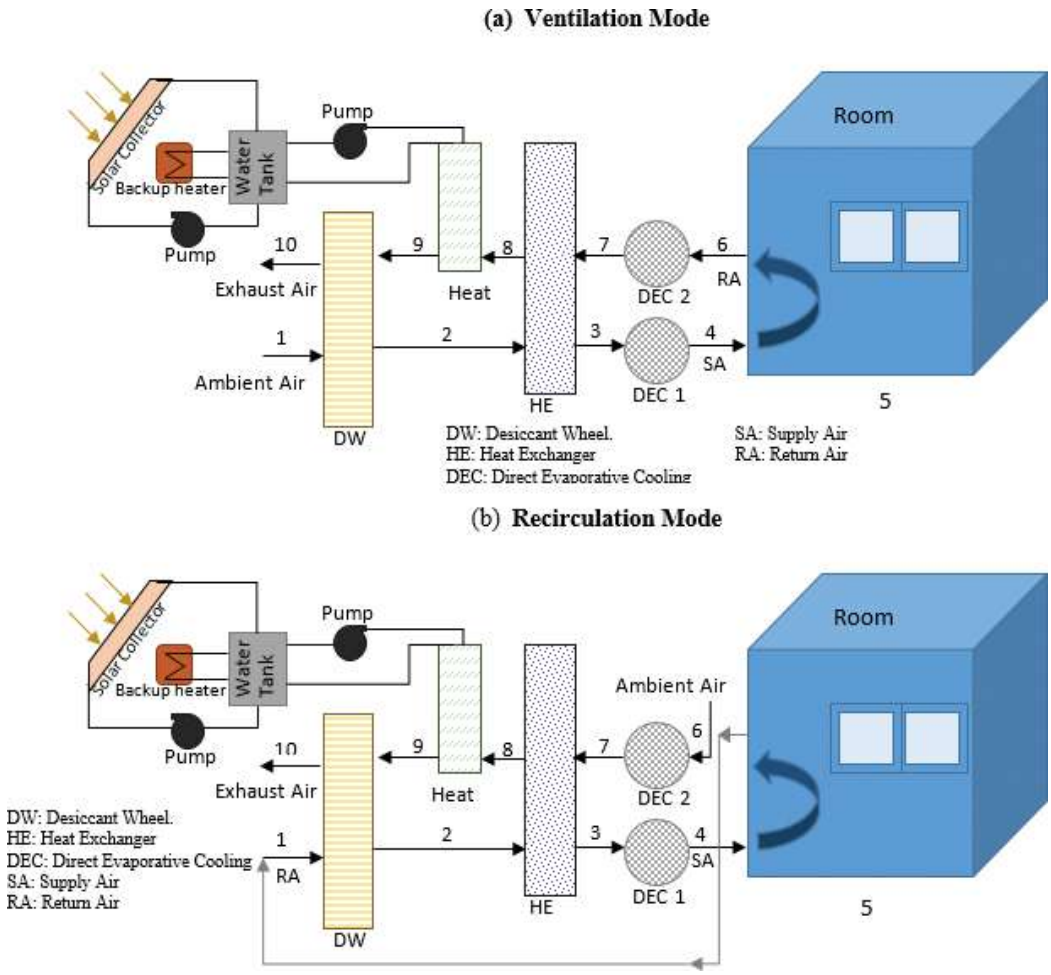

Figure 6. Schematic of desiccant cooling system in (a) ventilation mode and (b) recirculation mode.

The recirculation mode representation is depicted in **Figure 6b**. It uses the same components as the ventilation mode except the process air side in the recirculation mode is a closed loop, whereas the regeneration air side is an open cycle where the outdoor air is used for regeneration.

2.2.4. Ejector systems

A solar-driven ejector cooling system consists of an ejector cooling cycle and a collector circuit. The main components of the system are collector array, generator, ejector, condenser, expansion valve, evaporator, and cycle pump. A schematic diagram of the solar ejector cooling system and its component is presented in **Figure 7**. The working principle of the ejector systems follows the below states [24, 25]:

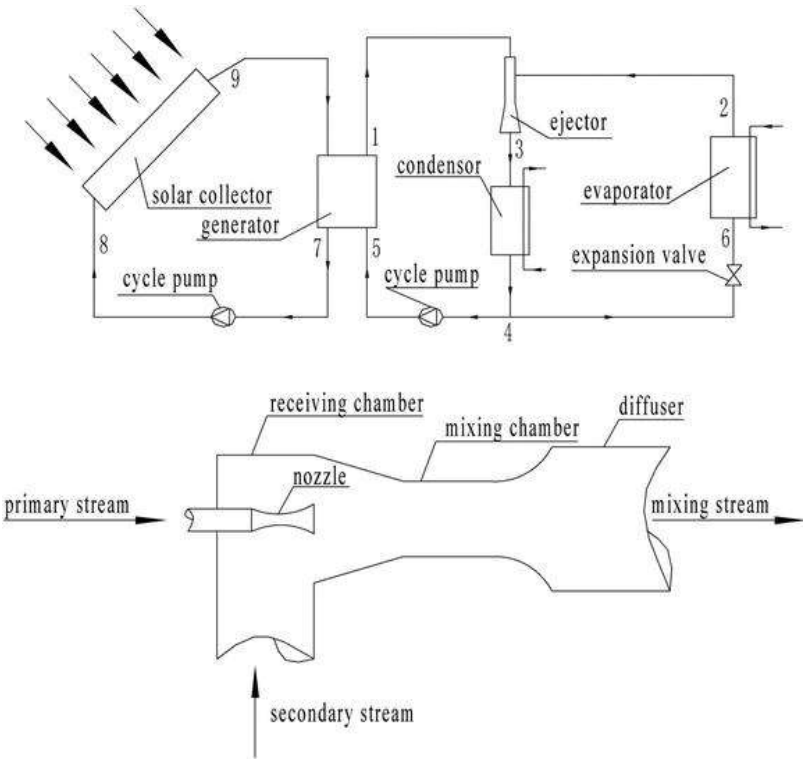

Figure 7. Schematic presentation of the solar ejector cooling configuration.

In the generator, the refrigerant is vaporized as a primary steam by utilizing the solar energy coming from the solar collector. This primary steam leaves the generator at a relatively high pressure and enters the supersonic nozzle of the ejector to accelerate it at supersonic velocity and creating low pressure at the nozzle exit section. This low pressure draws the secondary flow coming from the evaporator into the chamber. The primary and secondary streams are mixed in the mixing chamber. These mixing steams enter into diffuses where increases its pressure to the condensing pressure. The mixing stream discharges from the ejector to the condenser, where the stream is converted into liquid refrigerant by rejection heat to the surrounding. Some part of the liquid refrigerant pumps to the generator and the remaining liquid part leaves the condenser and enters the evaporator through expansion value.

In expansion value, the refrigerant pressure is dropped and this refrigerant enters the evaporator to absorb heat from space that required to cool and the refrigerant is converted into vapor and enters to the ejector.

2.2.5. Rankine systems

One of the promising methods that utilize solar heat to produce mechanical work and then use it to drive a conventional vapor compression cycle is solar Rankine cooling systems. Two different configurations of solar Rankine cooling systems were suggested by different scholars [26]. One

http://dx.doi.org/10.5772/intechopen.80484

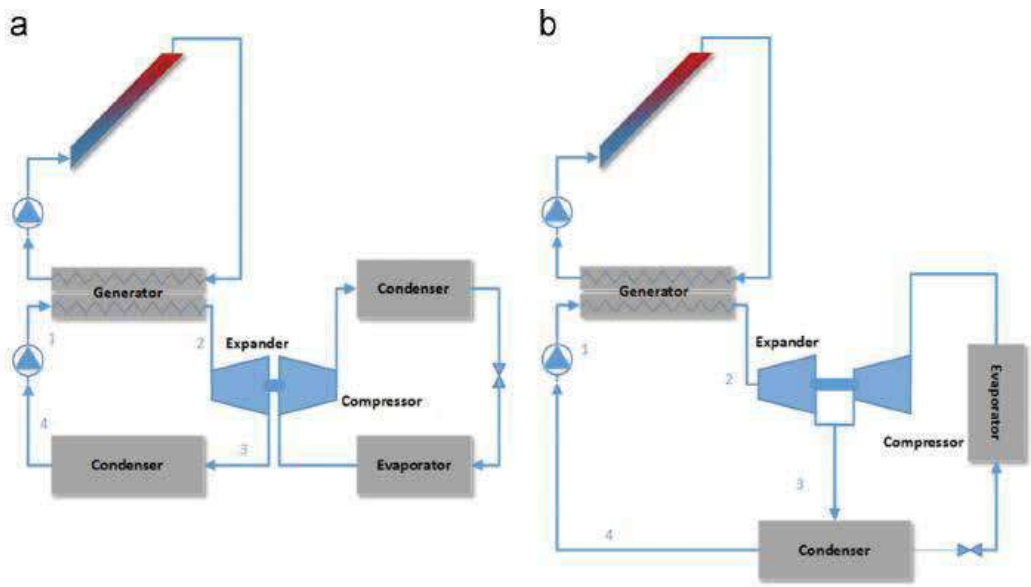

Figure 8. Representation of a Rankine solar cooling system as (a) separate configuration for power and refrigeration cycles and (b) integrated configuration for power and refrigeration cycle.

arrangement is using separate power and cooling system where the compressor of the vapor compression cycle is mechanically coupled with the expander of organic Rankine cycle. Another arrangement is an integrated system by the use of one joint condenser for both cycle coupled with the expander-compressor.

The main advantages of a second configuration are the use of a same working fluid in both loops to remove a leakage and mixing problems. Moreover, the integrated design is simpler but on the other side reduces the system flexibility.

Figure 8 depicts a schematic for two widely solar Rankine cooling system arrangements. In the first loop of organic Rankine cycle, high-pressure liquid coming from the pump is vaporized inside the boiler (state 1) that absorbs the heat from solar collector. The vapor (state 2) enters the expander and produces a useful work which is used to drive a compressor of a conventional refrigeration cycle. The working fluid pressure from the expander outlet is same to the condenser pressure (state 3). After that, a rejection heat to the surrounding inside the condenser converts the working fluid to saturated fluid. Subsequently, a pressure of the working fluid is increased by using pump to enter a boiler as subcooled liquid (state 1).

3. Conclusion

The executed investigations on the field of solar thermal-driven cooling systems and the gained results can be concluded as follows:

- The investigations on solar thermal-driven systems show that solar thermal refrigeration systems are promised technologies, especially in the small and middle cooling capacity ranges.
- The work temperatures have a big impact on the refrigeration capacity of the chiller.
- The higher is the required chilled water temperature, the higher are the refrigeration capacity and the coefficient of performance (COP) of the absorption refrigeration machine.
- The lower is the cooling water temperature; the higher are the refrigeration capacity and the COP of the absorption refrigeration machine.
- There are a big potential for further research at this field to optimize the system operation and to reduce the specific costs (€/kW cooling capacity).

Author details

Salman Ajib[1]* and Ali Alahmer[2]

*Address all correspondence to: salman.ajib@hs-owl.de

1 Department of Renewable Energies and Decentralized Energy Supplying, Hochschule Ostwestfalen-Lippe, Höxter, Germany

2 Department of Mechanical Engineering, Tafila Technical University, Tafila, Jordan

References

[1] Alahmer A, Wang X, Al-Rbaihat R, Alam KA, Saha BB. Performance evaluation of a solar adsorption chiller under different climatic conditions. Applied Energy. 2016;**175**:293-304

[2] Ajib S. An overview on solar thermal energy for cooling and air conditioning. Annals of Arid Zone. 2010;**49**(3 & 4):275-284

[3] Henning HM. Solar assisted air conditioning of buildings—An overview. Applied Thermal Engineering. 2007;**27**(10):1734-1749

[4] El-Samadony Y, Hamed AM, Kabeel AE. Dynamic performance evaluation of single bed desiccant dehumidification system. International Journal of Renewable and Sustainable Energy. 2013;**2**(1):18-25

[5] U.S. Department of Energy. 2011 Buildings Energy Data Book, Table 1.1.3. D & R International Ltd; 2012. Available: https://ieer.org/wp/wp-content/uploads/2012/03/DOE-2011-Buildings-Energy-DataBook-BEDB.pdf [Retrieved 18th August, 2018]

[6] Boyano A, Hernandez P, Wolf O. Energy demands and potential savings in European office buildings; case studies based on energy plus simulations. Energy and Buildings. 2013;**65**:19-28

[7] Zhu S, Chen J. A simulation study for a low carbon consumption HVAC project using energy plus. International Journal of Low Carbon Technologies. 2012;**7**(3):248-254

[8] Baniyounes AM, Ghadi YY, Rasul MG, Khan MM. An overview of solar assisted air conditioning in Queensland's subtropical regions, Australia. Renewable and Sustainable Energy Reviews. 2013;**26**:781-804

[9] EU Commission. Communication from the Commission to the European Parliament: The Council, the European Economic and Social Committee and the Committee of the Regions—An EU Strategy on Heating and Cooling. Brussels; 2016;**2**:2016. Available: https://ec.europa.eu/transparency/regdoc/rep/1/2016/EN/1-2016-51-EN-F1-1.PDF [Retrieved 18th August, 2018]

[10] Clausse M, Alam KC, Meunier F. Residential air conditioning and heating by means of enhanced solar collectors coupled to an adsorption system. Solar Energy. 2008;**82**(10):885-892

[11] Balaras CA, Grossman G, Henning HM, Ferreira CA, Podesser E, Wang L, Wiemken E. Solar air conditioning in Europe—An overview. Renewable and Sustainable Energy Reviews. 2007;**11**(2):299-314

[12] Hamdeh NH, Mu'Taz A. Optimization of solar adsorption refrigeration system using experimental and statistical techniques. Energy Conversion and Management. 2010;**51**(8):1610

[13] Ajib S, Günther W. Solar thermally driven cooling systems; some investigation results and perspectives. Energy Conversion and Management. 2013;**65**:663-669

[14] Kohlenbach P, Jakob U. Solar Cooling: The Earthscan Expert Guide to Solar Cooling Systems. 1st ed. Routledge; 12 August 2014

[15] Daniel Mugnier D, Neyer D, White S. The Solar Cooling Design Guide—Case Studies of Successful Solar Air Conditioning Design. Wilhelm Ernst & Sohn, Verlag für Architektur und Technische Wissenschaften GmbH & Co. KG; 2017. DOI: 10.1002/9783433606841

[16] Desideri U, Proietti S, Sdringola P. Solar-powered cooling systems; technical and economic analysis on industrial refrigeration and air-conditioning applications. Applied Energy. 2009;**86**(9):1376-1386

[17] Riffat SB, Qiu G. Comparative investigation of thermoelectric air-conditioners versus vapour compression and absorption air-conditioners. Applied Thermal Engineering. 2004;**24**(14-15):1979-1993

[18] Wang J, Shang S, Li X, Wang B, Wu W, Shi W. Dynamic performance analysis for an absorption chiller under different working conditions. Applied Sciences. 2017;**7**(8):797. DOI: 10.3390/app7080797

[19] Al-Rbaihat R, Sakhrieh A, Al-Asfar J, Alahmer A, Ayadi O, Al-Salaymeh A, Al_hamamre Z, Al-bawwab A, Hamdan M. Performance assessment and theoretical simulation of adsorption refrigeration system driven by flat plate solar collector. Jordan Journal of Mechanical and Industrial Engineering. 2017;**11**(1):1-11

[20] Behbahani-nia A, Sayfikar M. Study of the performance of a solar adsorption cooling system. Energy Equipment and Systems. 2013;**1**(1):75-90

[21] Alsaqoor S, Alahmer A, Chorowski M, Pyrka P, Rogala Z. Performance evaluation for a low temperature heat powered for 3-beds with dual evaporators silica gel water adsorption chillers. In: 2017 8th International Renewable Energy Congress (IREC); IEEE; 2017. pp. 1-6

[22] Fasfous A, Asfar J, Al-Salaymeh A, Sakhrieh A, Al_hamamre Z, Al-Bawwab A, Hamdan M. Potential of utilizing solar cooling in the University of Jordan. Energy Conversion and Management. 2013;**65**:729-735

[23] Alahmer A. Thermal analysis of a direct evaporative cooling system enhancement with desiccant dehumidification for vehicular air conditioning. Applied Thermal Engineering. 2016;**98**:1273-1285

[24] Varga S, Oliveira AC, Diaconu B. Analysis of a solar-assisted ejector cooling system for air conditioning. International Journal of Low Carbon Technologies. 2009;**4**(1):2-8

[25] Zhang B, Lv JS, Zuo JX. Theoretical and experimental study on solar ejector cooling system using R236fa. International Journal of Low Carbon Technologies. 2013;**9**(4):245-249

[26] Zeyghami M, Goswami DY, Stefanakos E. A review of solar thermo-mechanical refrigeration and cooling methods. Renewable and Sustainable Energy Reviews. 2015;**51**:1428-1445

Chapter 4

State-of-the-Art Technologies on Low-Grade Heat Recovery and Utilization in Industry

Janie Ling-Chin, Huashan Bao, Zhiwei Ma,
Wendy Taylor and Anthony Paul Roskilly

Additional information is available at the end of the chapter

http://dx.doi.org/10.5772/intechopen.78701

Abstract

To improve energy efficiency in industry, low-grade heat recovery technologies have been advanced continuously. This chapter aims to provide a basic understanding of state-of-the-art technologies for low-grade heat recovery and utilization in industry, which are developed based on the concept of thermodynamic cycles. The technologies include adsorption, absorption, liquid desiccant, organic Rankine cycles (ORC), and Kalina cycles. The definition of low-grade heat sources, the working principle, recent advances in research and development (R&D), and commercial applications of the technologies (if any) will be discussed, followed by concluding remarks on advantages and disadvantages, future outlook, barriers, and opportunities.

Keywords: industrial low-grade heat, adsorption, absorption, liquid desiccant, organic Rankine cycle, Kalina cycle

1. Introduction

Energy-related issues including energy resources, prices, demand, supply, and use always attract global attention. In particular, international governments from developed nations such as the US and UK have constantly allocated substantial budgets to carry out contemporary evaluations on relevant issues either on national or international levels. Two recent examples include the International Energy Outlook 2018 [1] by the US Energy Information Administration and the independent assessment delivered by the UK Committee on Climate Change [2] as requested by the UK Government. To indicate the seriousness of energy issues, [1] projected that world energy consumption in 2040 would reach up to 736 quadrillion British

thermal units (Btu) where industry sector (which would show an 18% increase from 2015 to 2040) would attribute to more than 50% of the total world energy consumption. In the UK context, the Government has set a national target to achieve more than 20% of improvement in industrial energy efficiency by 2030 [2]. To support long-term energy efficiency improvement, action plans are also established, for instance, enabling innovation and dialog for finance access improvement opportunities.

Exploiting the utilization of industrial waste heat and adopting more thermally efficient practices are examples of possible ways to improve industrial energy efficiency [3]. During industrial processes e.g. drying, heating and combustion, waste heat presents in the forms of vapor, fume, exhaust, waste water and heat; and is discharged from furnaces, motors, refrigeration systems, boilers etc. on without further utilization. The temperature of waste heat varies with industrial processes and the range is very broad, from as low as 30°C to more than 1000°C. Accordingly, waste heat is generally distinguished as high-, medium- and low-grade heat. Compared to medium- and high-grade heat, utilizing and recovering low-grade heat is far more challenging, less feasible and not commonly applied in practice. It is worth noting that low-grade heat has the potential to be utilized in producing (i) electrical power; (ii) heating; (iii) cooling; (iv) heating, cooling, and electricity simultaneously; (v) fresh water; and (vi) hydrogen [4], with the deployment of advanced technologies.

This chapter aims to provide a basic understanding of the state-of-the-art technologies including adsorption, absorption, liquid desiccant, organic Rankine cycles (ORC), and Kalina cycles, which are developed based on the concept of thermodynamic cycles for low-grade heat recovery and utilization in industry. Following the definition of low-grade heat sources in Section 2, the working principle, recent advances in research and development (R&D) and commercial applications of each technology are presented in Section 3. This chapter is closed with concluding remarks on advantages and disadvantages, future outlook, barriers, and opportunities. By providing insights and strengthening knowledge in the subject, this chapter will be beneficial to engineering students, researchers and industrial practitioners.

2. Definition and potential sources of industrial low-grade waste heat

During industrial processes, heat is transferred between heat sources and heat sinks. Low-grade waste heat and low-grade heat sources have been defined in literature where the definition applied in this chapter is adopted from [4]. In brief, low-grade waste heat is the (process) heat that is discharged to the environment as its recovery and utilization within the processes is not viable. Meanwhile, low-grade heat sources are the waste heat sources, which have a temperature ($T_{\text{low-grade heat source}}$) higher than the sum of the temperature of the heat sink (T_{sink}) and the minimum allowable temperature difference in the system (ΔT_{min}) but not high enough to break through the minimum temperature required for viable heat recovery ($T_{\text{viable min}}$, which is 250°C). In other words, low-grade heat sources are the waste heat sources with a temperature

ranging between $T_{viable\ min} + \Delta T_{min}$ and $T_{viable\ min}$, that is, $T_{viable\ min} + \Delta T_{min} < T_{low\text{-}grade\ heat\ source} < T_{viable\ min}$. **Table 1** presents the temperature ranges of numerous industrial low-grade waste heat sources. Among all, flue gas from boilers, waste heat from compressor cooling systems and condensate from both steam heating and spent cooling water are common waste heat sources across all industrial sectors. Other waste heat sources are industrial sector specific. Most industrial waste heat sources have temperatures below 175°C rather than approaching $T_{viable\ min}$, i.e. 250°C.

	Low-grade waste heat source	Temperature (°C)
Generic unit/process		
1. Boilers [5, 6]	• Flue gases	110–260
2. Air compressors [7]	• Waste heat from compressor cooling system	30–60
3. Heating/cooling network [7]	• Condensate from steam heating and spent cooling water from cooling systems	60–90
Industrial sector		
1. Petrochemical [5]	• Stack gas from crude distillation	156
	• Stack gas from vacuum distillation	216
	• Exhaust from ethylene furnace	149
2. Iron/steel making [5]	• Waste gas from coke oven	200
	• Blast furnace gas	93
	• Blast stove exhaust	250
3. Aluminum [5]	• Exhaust from aluminum casting with a stack melter	121
4. Food and drink [7]	• Extracted air from cooking with fryers or ovens	150–200
	• Exhaust from drying with spray/rotary dryers	110–160
	• Water vapor from evaporation and distillation	100
5. Textile [6]	• Dyed waste water from drying	90–94
	• Stenter exhaust for fabric drying and finishing	180
	• Waste water rejected from heat exchangers	58–66
6. Paper [8]	• Waste steam from slag flushing in furnace	95–100
	• Waste water from slag flushing in furnace	65–85
	• Cooling water from furnace wall cooling	35–45
7. Cement [9]	• Exhaust from cement kilns using 5- or 6-stage preheaters	204–300
	• Hot air discharged from clinker coolers	100

Table 1. Low-grade waste heat sources and temperatures.

3. State-of-the-art technologies for low-grade heat utilization

3.1. Vapor compression

Generally, vapor compression systems [10], which are also referred to as mechanical or refrigerative compressors have been established as the most mature machines for cooling, heat pumping and/or dehumidification purposes. As illustrated in **Figure 1**, a typical vapor compression system consists of a refrigeration circuit (which is made up of an evaporator, a condenser, a compressor, and an expansion valve) and an air circulation fan. Water, R407c and R134a are the refrigerants, which are commonly used as the working fluids of commercial vapor compression systems. When air is drawn to the evaporator by the fan, the low-pressure, low-temperature liquid-vapor refrigerant mixture coming from the expansion valve extracts heat from the air; the liquid refrigerant evaporates and the air is cooled. Leaving the evaporator, the saturated refrigerant vapor is compressed to high-pressure superheated state, which dumps condensation heat in the condenser. If in a dehumidifier, the high-temperature, high-pressure superheated refrigerant vapor is condensed by the cool but dry air from the evaporator, heat is rejected and the air becomes dryer and warmer. To run the fan and the compressor, electricity is consumed intensively. As vapor compression systems are conventional technology, they are not further discussed in this chapter. More details are available in [11].

3.2. Adsorption

Adsorption is the enrichment or depletion of one or more components in an interfacial layer between adsorbent and adsorbate, as defined by International Union of Pure and Applied

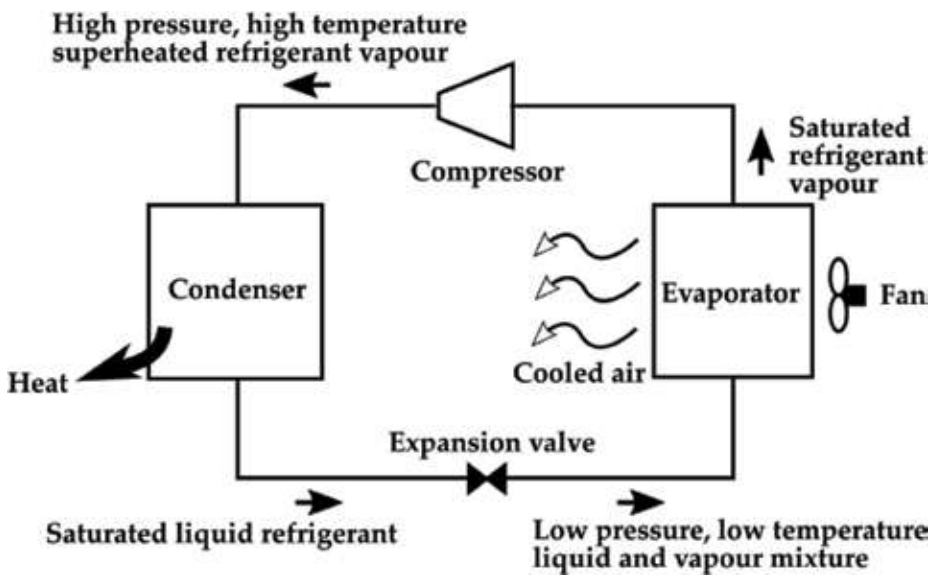

Figure 1. A schematic diagram of a traditional vapor compression system.

http://dx.doi.org/10.5772/intechopen.78701

Chemistry [12]. There are four types of adsorption depending on the interface: solid-gas, solid-liquid, liquid-liquid, and liquid-gas. The solid-gas adsorption has been extensively used and studied in recent decades and is often referred to adsorption or solid sorption [13]. If the solid-gas binding force involves intermolecular forces, i.e. Van der Waals forces, it is categorized as physical adsorption (physisorption) and the typical physisorption working pairs are silica gel-water [14], activated carbon-ammonia or methanol or ethanol [15], zeolite-water [16], etc. If the coordination reaction takes place on the exposed surface forms a strong ionic or covalent bond between the adsorbate and the adsorbent, it is recognized as chemical adsorption (chemisorption) that consists of mainly two types of working pairs for low-grade heat utilization: metal halides-ammonia [17] and salt hydrates-water [18]. In other words, multi-layers (in physisorption) or monolayer (chemisorption) of absorbate accumulates on the surface of an adsorbent during an adsorption.

The fundamental principle of an adsorption refrigeration cycle is schematically by a basic adsorption unit shown in **Figure 2**, where reversible sorption process operates or chemical reaction performs in an intermittent manner. Low-grade heat is supplied to the adsorbent bed to break the binding force between the adsorbent and the adsorbate (refrigerant) as the adsorbate (refrigerant) gas is desorbed from the adsorbent bed and heading for the refrigerant container that acts as a condenser. Such a process is referred to endothermic decomposition as shown in **Figure 2(a)**. When the decomposition is finished, two vessels are isolated from each other for an internal prior to the exothermic synthesis. Once sufficient pressure difference has been built up between these two vessels and there is a need of refrigeration, as soon as two vessels are connected in **Figure 2(b)**, driven by the pressure difference the adsorbate inside the refrigerant container (becomes evaporator in this process) evaporates and is adsorbed inside the adsorbent bed. The evaporation of the refrigerant provides the refrigeration power, and the adsorption heat of the adsorbent bed is to be released to the proper heat sink. For heating purpose in two types of heat pump applications, (1) adsorption unit can perform as a heat multiplier to produce a large quantity of medium temperature heat through both the condensation and synthesis process at the cost of a small quantity of high-temperature heat input for the decomposition [19]; or (2) in a heat transformer it can deliver concentrated high-temperature heat through synthesis process if both decomposition and evaporation processes are provided with medium temperature heat [20].

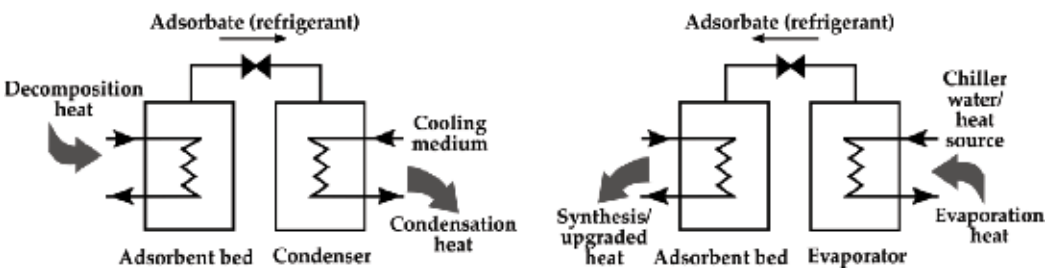

Figure 2. (a) Endothermic decomposition (left) and (b) exothermic synthesis (right).

Adsorption heating and cooling application have been widely developed in the past decade. Various advanced cycles have been developed for improvement in energy efficiency of thermal energy recovery and utilization in a wider temperature range e.g. cycles with heat and mass recovery, multi-stage, multi-sorbent, and cascaded cycles, etc. [21]. Considerable effort has been also focused on the development of composite adsorbent materials to enhance heat and mass transfer properties, improve adsorption capacity and enlarge specific power [13]. Especially, physisorption type air conditioning and heat pumping machines developed by some European and Japanese companies are on or near-market currently (SorTech, GBU mbH, Invensor, Mayekawa chillers; Vaillant and Viessmann heat pumps, etc.). Meanwhile, substantial R&D effort has been put on water-based adsorption systems for such as dehumidification/drying and desalination application. The first worldwide adsorption water desalination and cooling plant has been implemented in Riyadh, Saudi Arabia since 2016, and the process has a cooling capacity of up to 1 MW and desalinated water production up to 100 m^3/day. With the inherent nature of intermittency, adsorption cycle also presents itself as a promising solution for energy storage as the decomposition is charging energy and the synthesis is the energy discharging process. Such an adsorption energy storage system is superior to the methods of sensible and latent heat storage not just because of its high energy density but also its low energy loss during long-term storage [22] as the binding energy is stored independently of the time span between decomposition (charging process) and synthesis (discharging process). With ever increasing energy prices and greater environmental concerns it can be expected that adsorption refrigeration and heat pumping will soon join the mainstream technologies.

Adsorption power generation concept, especially ammonia-based adsorption cycle which has greater potential of productive power generation than water-based types due to the higher working pressure, has recently started to attract interest for more versatile application, as the adsorption unit integrated with turbine or expander can convert thermal energy to mechanical work, or produce electricity when a generator is attached [23]. Modeling, simulation, and experimental investigation have been conducted and demonstrated the feasibility of the adsorption cogeneration of cooling and electric power [24, 25]. Most recently, a new dual energy storage system through the integrated ammonia-based resorption cycle is being developed for simultaneous electric and thermal energy storage [26, 27] as illustrated in **Figure 3**. In the energy charging process, mechanical or electrical power is stored together with the ultra-low-grade thermal energy (~100°C) as the ammonia (refrigerant) is desorbed in the endothermal decomposition and further pressurized through vapor compression driven by mechanical energy or electricity. In the energy discharging process, the stored energy can be delivered as either heating or cooling power as the conventional adsorption cycle promises, or even mechanical energy if the transferred high-pressure ammonia passes through a turbine or expander. In fact, when the integrated system restores mechanical energy, it would also generate a considerable quantity of upgraded thermal energy, plus a small quantity of cold energy depending on heat source temperature and the refrigeration requirement, as so-called the Tri-generation Recovery and Efficient Energy Storage (TREES) concept [26]. In contrast with conventional chemisorption systems, the TREES cycle embraces broader application with higher penetration of renewable energy; not just utilizing thermal energy (waste heat, solar energy, or geothermal energy) but also potentially storing intermittent electric power from solar PV and wind power or off-peak cheap electricity.

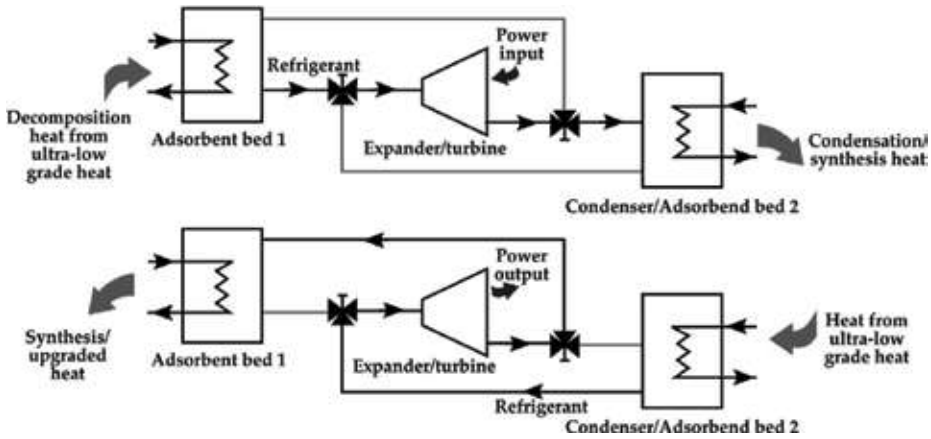

Figure 3. (a) Ultra low-grade heat input (top) and (b) power generation (bottom).

3.3. Absorption

Absorption is a process where a device (i.e. an absorber) is used to enable any substance (i.e. an absorbent, also referred to as an "absorption medium") to soak up or take in another substance e.g. liquid or gas (i.e. an absorbate). In other words, an absorber enables an absorbent to absorb an absorbate during absorption. To differentiate from adsorption, in absorption process the molecules of the adsorbate penetrate the surface layer and enter the structure of the bulk solid or liquid, causing the change of the composition of one or both bulk phases [28]. The absorption process using liquid absorbent and gas absorbate has been applied in refrigeration industry and also successfully adopted in commercial chillers and heat pumps for a long period. A liquid-gas absorption heat pump system (heat multiplier) is illustrated in **Figure 4**, consisting of a solution and refrigerant loops as the absorbate is also referred to as a refrigerant.

The key components of an absorption system include a generator, an absorber, a condenser and an evaporator whilst a heat exchanger, a solution pump, and expansion valves are commonly incorporated. The working fluid is made of an absorbent-refrigerant solution, which presents in the generator and the absorber. Lithium bromide-water (LiBr-H_2O) and water-ammonia (H_2O-NH_3) are two absorbent-refrigerant solutions commonly chosen for absorption systems. For an absorption cooling system, in the absorption loop, the solution weak in refrigerant leaves the generator as its temperature and pressure are lowered by the heat exchanger and the expansion valve respectively before entering the absorber where absorption takes place and the refrigerant is absorbed, which releases absorption heat to the surroundings. The solution strong in refrigerant from the absorber is then pumped and preheated before entering the generator. In the refrigerant loop, high-pressure refrigerant vapor from the generator condenses in the condenser and releases heat to the surroundings. The pressure of the refrigerant liquid is lowered by the expansion valve before it reaches the evaporator and evaporates. The low-pressure refrigerant vapor then enters the absorber where the vapor is absorbed. As the working fluid is regenerated in the generator and the absorption in the system repeats continuously, the quantity of the solution remains the same. In addition to utilizing waste heat for

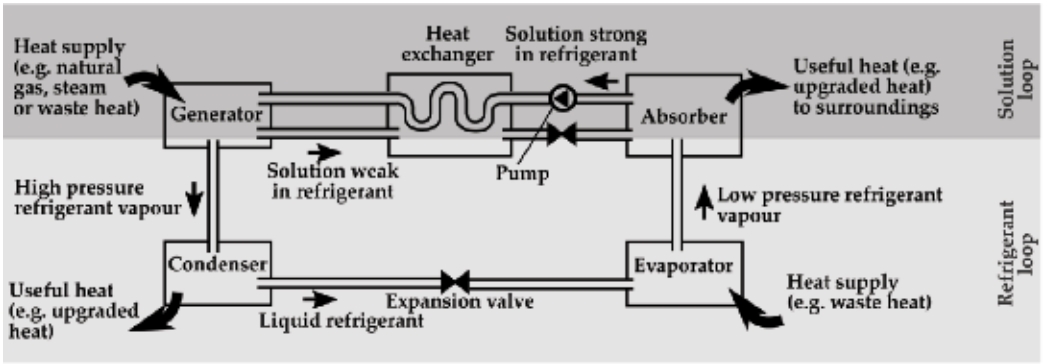

Figure 4. The schematic diagram of an absorption heat multiplier.

solution regeneration in the generator, industrial low-grade waste heat can be supplied to the evaporator to assist the evaporation processes of the refrigerant in a heat transformer so that the upgraded heat can be gained from the absorber; or in a heat multiplier, condensation and absorption processes in the condenser and absorber respectively can be collected for further utilization.

Various modifications have been proposed to advance absorption systems for enhanced capacity, improved coefficient of performance, and increased temperature lift for heating or temperature drop for cooling. For instance, the system can be simplified to form an open-cycle absorption heat pump by removing the evaporator and bringing the solution in the absorber in direct contact with the absorbate source (e.g. moist air, waste vapor, or exhaust flue, etc.) to release the absorption heat [29]. When solution and refrigerant tanks are additionally incorporated to absorption systems, the systems work as absorption heat storage systems [30]. Two or three absorption systems can be coupled with each other in series to form a two- or three-stage absorption heat transformer by recovering the absorption heat of one system for the generation and vaporization heat of the next system (and so on) [30]. Also, an absorption system can deploy high- and low-pressure absorbers, to form a double absorption heat transformer. The low-pressure absorber also acts as an additional evaporator where the adsorption heat is used to vaporize the refrigerant vapor that is to be absorbed by the high-pressure absorber [30, 31]. A double-effect absorption heat transformer employs two generators as the high-temperature refrigerant vapor generated from the high-pressure generator is recovered to provide the low-pressure generator with generation heat, thus two streams of refrigerant vapor from two generators converge in the condenser [31]. There are also researches on 1.X (or variable) effect cycles that can flexibly perform in larger working range with higher energy efficiency [32]. The combination of an absorption system and a traditional heat exchanger, as so-called absorption heat exchanger, can realize larger temperature drop through heat exchange, i.e. the outlet temperature of the cold fluid becomes higher than the outlet temperature of the hot fluid [29]. In relation to the working fluid of the systems, the use of alternative mixtures e.g. water-ternary hydroxides, water-lithium iodide, ammonia-sodium thyocianate, ammonia-ionic liquid etc. have been explored. More details are available in [29, 30].

3.4. Liquid desiccant systems (LDSs)

Solid or liquid desiccant materials can be used in industry for dehumidification and cooling purposes. Desirable characteristics required for desiccants include low vapor pressure, regeneration temperature, crystallization point, viscosity and cost with high density [33]. Whilst silica gel, zeolites, aluminas and polymers are solid desiccants, organic desiccant e.g. tri-ethylene glycol (TEG) and inorganic salt solutions such as LiBr, lithium chloride (LiCl), and calcium chloride ($CaCl_2$) are examples of liquid desiccants [33, 34]. LDSs involve liquid-gas absorption. They have the edge over solid desiccant systems as they can operate at regeneration temperatures, which are very low and they show higher thermodynamic coefficient of performance with lower pressure drops [35]. Compared to traditional vapor compression systems, apart from the advantages of being environmental friendly and heat driven LDSs are more flexible in temperature and humidity controls [34].

An LDS employs (i) a desiccant as a working fluid; (ii) two towers (also referred to as columns) which serve as a dehumidifier (i.e. an absorber, also referred to as a conditioner) and a regenerator respectively for air dehumidification and desiccant regeneration processes; (iii) devices e.g. pumps and fans for desiccant solution circulation; and (iv) a heat source and a heat sink (e.g. low-grade heat and a coolant) to heat up and cool down desiccant solution. **Figure 5** shows a typical LDS design. The strong desiccant solution is sprayed on top of the absorber whilst the wet, cool air used by industrial processes (referred to as "process air") is drawn into the absorber by a fan. The water vapor pressure of the strong solution is lower than that of process air. When the strong solution contacts with process air directly, the difference in the water vapor pressures results in mass transfer i.e. the strong solution absorbs moisture from the process air and becomes weak whilst it is chilled (by a coolant). The weak desiccant solution is heated (by a low-grade heat, hot water or renewable energy sources) and sprayed into the regenerator and heated (by a low-grade heat) whilst regeneration air is circulated by a fan. The water vapor pressure of the weak solution is higher than that of regeneration air. When the weak solution makes contact with regeneration air directly, the

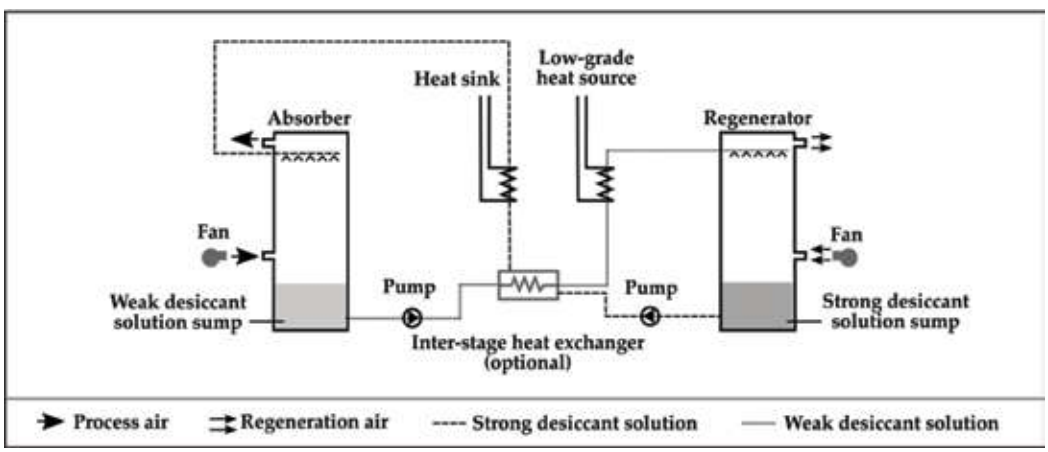

Figure 5. A schematic diagram of a LDS.

difference in the water vapor pressures results in mass transfer i.e. the weak solution releases moisture to regeneration air and becomes strong. An inter-stage heat exchanger may be used to chill or preheat the desiccant solution before entering the absorber and the regenerator.

R&D has been advanced in connection to the design of the towers, flow directions, liquid desiccant materials and system design. Following the introduction of membrane-based LDSs, towers applied for LDSs can be classified as randomly or structured packed, spray, wetted wall (also referred to as failing-film), and hollow fiber or parallel-plate membrane based (also referred to as membrane modules or membrane contactors), as illustrated in **Figure 6**. The directions in which the solution and the air enter and leave the towers distinguish the flow i.e. counter flow if both are in opposite directions and cross/parallel flow if both are in the same direction. To improve performance and cost-effectiveness, composite desiccant materials such as silica gel or SiO_2 impregnated with an inorganic salt (including $CaCl_2$, LiCl, LiBr, $SrCl_2$, and $NaSO_4$) have also been explored [36]. To enhance heat and mass transfer between desiccant solution and air, multi-stage LDSs have been proposed by [37], which operates in a cascade way to cool the solution in multiple stages when it flows through more than one absorber. Moreover, a pilot study has been carried out in power plants to investigate an LDS application, which integrates with a CO_2 capture system for moisture recovery [38]. Recently, vertical and horizontal discharge dehumidifiers, fiberglass packed regenerators and small packaged dehumidifier-regenerator commercial LDSs have been made available by Alfa Laval Kathabar [39].

3.5. Organic Rankine cycles (ORC)

An ORC is an emerging prime mover technology, which recovers low-grade heat for power generation. As a derivative of the conventional steam Rankine cycle, a basic ORC consists of four main components, as shown in **Figure 7**, including an evaporator, an expander, a condenser, and a feed pump. In the system, the working fluid at its lowest temperature and

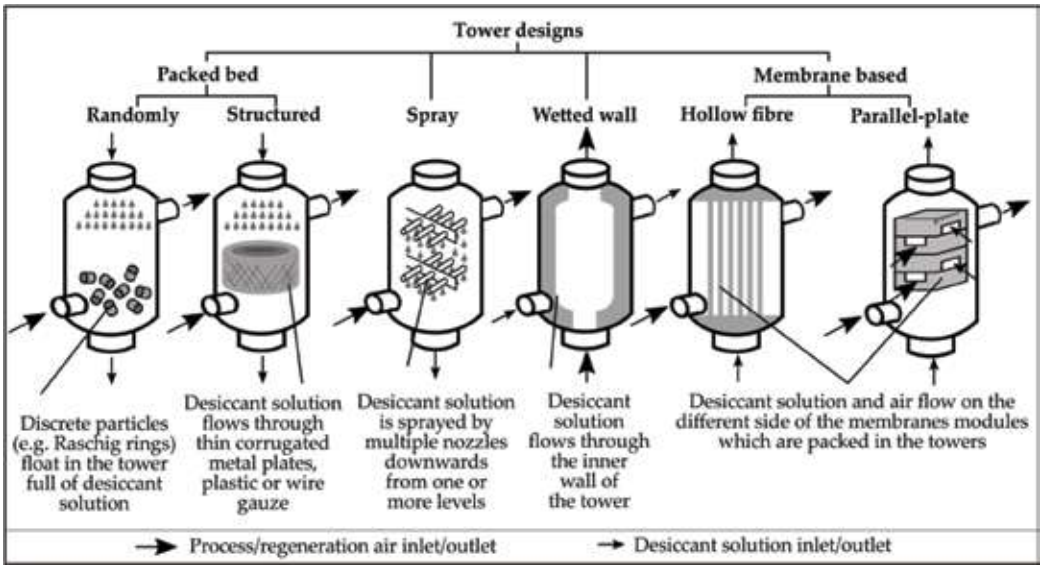

Figure 6. Various tower designs for absorbers and regenerators to enable heat and mass transfer between desiccant solution and process or regeneration air.

pressure is pumped by a feed pump to achieve the required pressure (maximum pressure in the cycle) before it goes into an evaporator where the working fluid is isobarically heated to form dry vapor. The dry vapor enters an expander where expansion takes place to generate mechanical work. The expander is connected to a generator where the resulting work is converted into electric power. Leaving the expander, the working fluid, which is now a mixture of vapor and liquid at minimum pressure, cools down in a condenser. The saturated liquid from the condenser flows into the feed pump and the cycle repeats.

The working fluids of ORCs are organic compounds, which have lower boiling points, critical points, specific volumes, and viscosity values than water. They can be classified as organic refrigerants, hydrocarbons, and siloxanes. Each works well for different heat source temperatures i.e. organic refrigerants are suitable for temperatures between 100 and 175°C; hydrocarbons for 175–250°C; and silozanes for 250–400°C. As industrial waste heat sources are generally below 175°C, organic refrigerants are more ideal for applications. Some working fluids with low supercritical temperatures, such as CO_2 (the critical pressure and temperature at 73.8 bar and 31.1°C) and hydrocarbons, have been studied for ORC systems, as the cycles operate at supercritical condition, and therefore is known as the supercritical Rankine cycle (SRC). Because SRCs bypass a two-phase region during the heating process, they have a better thermal match with a heat source which results in less irreversibility. After expansion, the working fluid exiting the turbine can be purely superheated in vapor form or as a mixture of vapor and liquid [40].

Using pure fluids as the working fluid of ORCs involves isothermal condition in the boiler and the condenser, which creates a bad thermal match between the working fluid and the heat source or heat sink, leading to large irreversibilities. The issue can be diminished by adopting a mixture of working fluids (also referred to as "multi-component fluids," "fluid blends," or "binary mixtures"), such as zeotropic mixtures. This is because working fluid mixtures can offer a boiling temperature range rather than a boiling point at constant pressure. Likewise, SRCs using zeotropic mixtures potentially have further reduced exergy destruction during both boiling and condensation, leading to higher efficiency.

To safeguard the overall performance of ORCs in particular when the application scale is small and the temperature of heat sources is low, expanders play a key role, and therefore, have been researched for highly efficient design. To date, expanders proposed for ORCs can be classified as velocity- or volume-type [41], which show different characteristics. Velocity-type expanders e.g. axial turbine expanders possess higher flow rates but contain lower pressure ratios, rotational speeds, and tolerance of a two-phase condition at the outlet. Volume-type expanders e.g. screw expanders, scroll expanders, and reciprocal piston expanders are simpler with less moving parts, a wider power output range, and require less maintenance. The selection should be made by taking account of cost, efficiency, operating conditions, noise level, safety and leaking issues.

Various configurations with the potential of higher energy efficiency have been explored in R&D. When a regenerator (also known as feed-water heater, preheater, recuperator, and internal heat exchanger) is deployed to achieve a better thermal match between the working fluids and the heat sources, the working fluid will be preheated before entering the evaporator using either the vapor exiting the turbine or via the turbine bleeding during expansion. Such ORC configuration is referred to as a regenerative ORC. Also, one or more flash evaporator

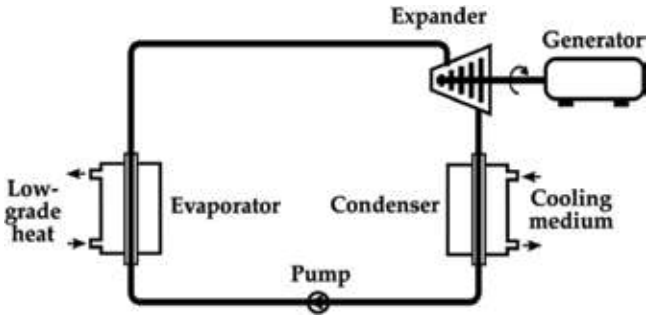

Figure 7. The schematic diagram of an ORC.

can be incorporated in an ORC to form single-, double-, or multiple-stage organic flash cycles, in which the working fluid of an ORC is flash evaporated before the gas vapor entering the expander. When more than two separate stages are incorporated in an ORC to enable the condenser of Stage 1 acting as the evaporator of Stage 2 (and so on), the configuration is known as a cascade ORC. More details can be found in [42].

To date, a number of ORC manufacturers (e.g., Turboden, Opcon Powerbox, and EXERGY) and commercial applications in industry sectors have been reported. To recover waste heat from furnace exhaust, the ORC units manufactured by Turboden have been operated by iron and steel foundries, including (i) Fonderia di Torbole in Italy since 1996; (ii) Toscelik Hot Strip Mill in Turkey with a 1000 kW net electric power output since 2011; (iii) NatSteel in Singapore with a 555 kW gross electric power output since 2013; (iv) Elbe-Stahlwerke Feralpi in Germany with a 2700 kW gross electric power output since 2013; and (v) ORI Martin in Italy with a 1900 kW gross electric power output since 2016 [43]. In Sweden, a NH_3 based, fully automated, remotely controlled ORC system supplied by Opcon Powerbox has been recovering low-grade heat from wastewater stream originated from the manufacturing processes in the Munksjö pulp mill since 2010, which produces electricity with a net output capacity of 750 kWel [44]. ORC systems manufactured by EXERGY have been operated in three glass manufacturing plants of Sisecamin in Italy, each with a capacity of 5 MWe electricity [45]. According to [46], recovering industrial waste heat using ORCs commercially is limited to 10 applications around the world with a total installed power of 29 MWel, and therefore, the market is still in its infancy.

3.6. Kalina cycles

Kalina cycles can recover industrial waste heat ranging between 80 and 400°C for power generation. In principle, Kalina cycles are absorption-based power generation cycle. Kalina cycles show superior performance over ORCs and supercritical cycles. Irresibility is scaled down as Kalina cycles reduce the heat transfer temperature difference between its working fluid i.e. ammonia-water (NH_3-H_2O) and heat source. Moreover, the Kalina cycle has one more degree of freedom than the Rankine cycles to be flexibly adopted to match with a certain heat source and heat sink, as the NH_3-H_2O composition can be adjusted as well as the system high- and low-pressure levels. Other benefits of using NH_3-H_2O as the working fluid include (i) enabling

efficient use of low-grade heat for vapor generation at higher pressure; (ii) less oxidation due to extremely low oxygen levels within the mixture, therefore, standard materials like carbon steel and standard high-temperature alloys can be used to handle ammonia [47].

To suit heat source characteristics and accommodate specific applications, more than 30 configurations, that is, Kalina Cycle Systems (KCSs) 1–34 have been introduced to date [45]. **Figure 8** depicts the system configuration developed for waste heat recovery in cement industry, which is based on KCSs 1–2 for power generation [48]. Low-grade heat is fed to the vapor generators respectively to boil and superheat the working fluid. The superheated vapor expands in the turbine to generate electrical power. The turbine exhaust is cooled down when passing through one of the recuperative heat exchangers, diluted by the working fluid from the vapor separator and condensed in the low-pressure condenser. Some saturated working fluid from the condenser passes through the other recuperative heat exchanger before reaching vapor separator while the remaining mixes with the vapor steam from the separator to form ammonia-rich working fluid. It is condensed in the high-pressure condenser by the cooling medium before being pumped back to the heat recovery vapor generators. As ammonia and water have close molecular weights, Kalina cycles do not require specific equipment design and piping system. Due to the lower boiling points of the mixture, a higher turbine inlet pressure and lower mass flow rate are permissible for Kalina cycles, which helps to minimize the running costs of the system. KCS-11 is the most suitable cycle for low-grade heat between about 121 and 204°C and KSC-34 or KSC-34 g are popular for application with heat source temperature below 121°C. More details can be found in [42].

System development, modeling, and experimental studies, which analyze the working fluid (including zeotropic mixtures), thermodynamic performance (i.e. entransy, entropy, and/or exergy), and parametric optimization of the cycles have been extensively researched over the years. Substituting an ejector for the absorber and the throttle valve has been proposed to reduce the pressure of the expander exhaust, which results in a larger difference in the working pressure of expansion [49]. As such, thermal efficiency and the power output of Kalina cycles are improved. Also aiming for greater power output, Kalina-Flash cycles have been introduced [50] where a flash vessel is incorporated into the cycles to produce secondary NH_3-rich vapor by depressurizing the NH_3-poor solution. Recently, Kalina cogeneration cycles [51] integrating an ejector have been developed to improve system performance and produce power and refrigeration simultaneously.

Focusing on industrial waste heat recovery, recent R&D direction has steered toward comparing ORCs and Kalina cycles. For instance, recovery of multiple heat streams in the process industry has been compared based on three waste heat patterns [52], which shows that the Kalina cycles are more superior when the temperatures of the heat streams form a linear relationship or increase slowly with enthalpy but become inferior if the temperatures increase rapidly. R&D has also advanced to integrate an ORC and a Kalina cycle to recover waste heat from the exhaust of a natural gas power generation system using the combination of solid oxide fuel cells and a gas turbine while the cryogenic energy of liquefied natural gas (LNG) is used as the heat sink, which shows an acceptable thermal efficiency with reduced exergy loss through temperature matches between heat sources and heat sinks [53].

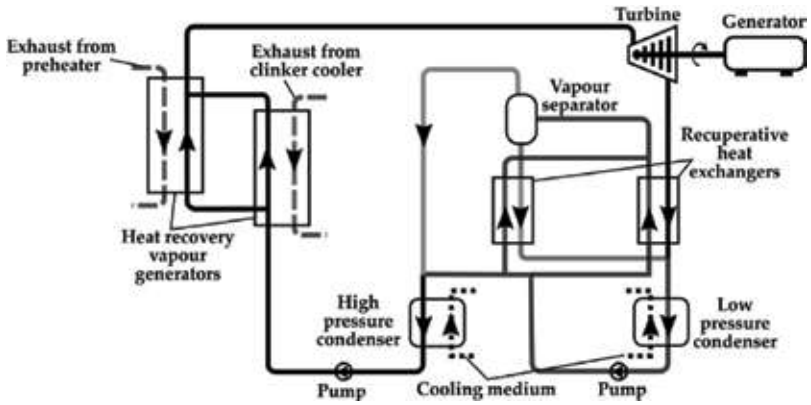

Figure 8. The schematic diagram of KCSs 1–2 developed for cement industry application.

Existing industrial waste heat recovery applications include [54] (i) 3.5 MW Sumitomo plant in Japan from 98°C hot water since 1999; (ii) 2.0 MW Kalina plant in Husavik, Iceland using geothermal brine at 124°C since 2000; (iii) 4.0 MW Fuji Oil plant in Japan from 116°C condensing vapors since 2005; (iv) 8.6 MW DG KHAN plant in Pakistan from the gas and air rejected from the kiln since 2013; and (v) 4.75 MW Star Cement plant in Dubai from hot air from kiln since 2013. Still, commercial application of Kalina cycles are limited due to a few practical issues (on top of expensive capital investment), including (i) the requirement of an accurate evaporation ratio in the boiler; (ii) the tendency of NH_3-H_2O mixture to prematurely condense during expansion; (iii) requirement of low condensation temperature for productive generation; and (iv) the patents of Kalina cycles.

4. Concluding remarks

The technologies discussed in this chapter bring both advantages and disadvantages, as summarized in **Table 2**.

R&D has been ongoing to resolve technical constraints and enhance coefficient of performance of the state-of-the-art technologies. To achieve a low-carbon future, it is envisaged that R&D for these low-grade heat utilization and recovery technologies will continue to carry out more experimental studies, investigate working fluids and materials, examine thermodynamic properties (including energetic, exergy and entransy analyzes), cover performance analysis and optimization, develop and verify modeling with experimental results, propose new system design, integrate technologies with renewable sources and compare alternative systems or technologies. As evidenced by the examples of worldwide commercial applications, utilizing, or recovering industrial low-grade heat (which is otherwise discharged to the environment) for useful work is possible by taking advantage of the state-of-the-art technologies discussed in this chapter. Inevitably, the number of commercial applications is still very limited, even though industrial waste heat is abundantly available and the concept of utilization or recovery is not new. This is because of resource constraints and lack of motivation due to the technical, regulatory, business, and organizational barriers as illustrated in **Figure 9**.

Technology	Advantage	Disadvantage
Adsorption [13]	• Simple configuration without moving parts; eco-friendly refrigerants; and suitable for ultra-lowgrade heat recovery and utilization; high energy density of chemisorption	• Bulky; solid material related issues, e.g. poor heat and mass transfer within solid sorbent in the fixed bed; modest COP; temperature swing in the fixed bed and the sensible heat load of solid sorbent and metallic reactor; potential performance degradation; intermittency of the basic configuration; and lack of industrialization
Absorption [29]	• Eco-friendly working fluid; reduce peak power demand; and mitigate greenhouse gas emission issues	• Large initial cost; and operational constraints; crystallization and corrosion issue of the working fluid
LDS [34, 36]	• Effective air quality control; high density energy storage; can be driven by ultra-low grade heat	• Desiccant solution carryover leads to corrosion and high maintenance cost; and high thermal energy requirements for desiccant regeneration; low system efficiency; bulk system; system performance depends on atmospheric condition
ORC [41, 55]	• Higher efficiency at low temperature and pressure; no blade erosion; and reduced maintenance	• Low efficiency and high cost for small scale application; and not environmental–friendly working fluid
Kalina cycle [47]	• Improved heat transfer process and recuperation; common, bio-degradable and environmentally benign working fluid; and mature safety standards	• Complex circuit; unsuitable to be used with copper and copper alloys; and corrosive to mild steel and aluminum; and bulk system

Table 2. Advantages and disadvantages of the state-of-the-art technologies.

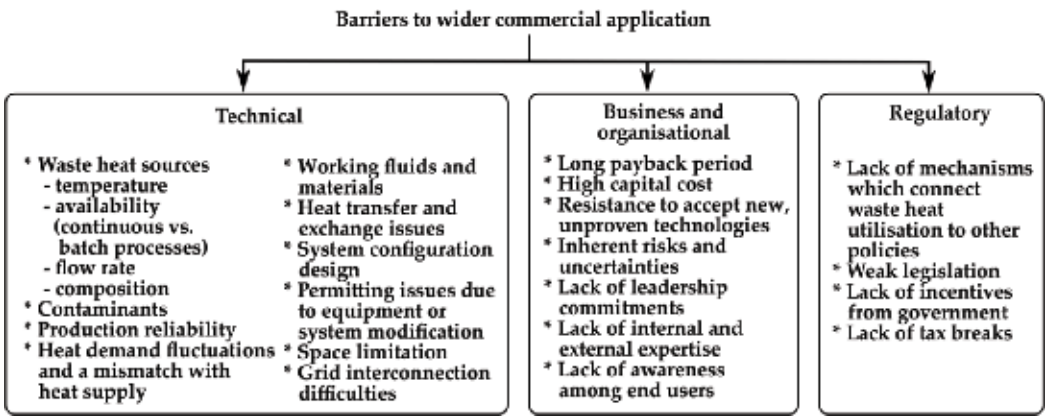

Figure 9. Technical, regulatory, business and organizational barriers to commercially deploying low-grade heat utilization and recovery technologies.

From a technical perspective, the varied nature of the low-grade heat sources including temperature, availability, flow rate, composition, contaminating content and working fluids affect the application significantly. From a business and organizational perspective, capital cost and payback period are the key factors considered by the management boards of industrial organizations. Currently, commercial applications are also hindered by the regulatory barriers such as the absence of financial incentives, tax breaks, strong policies and legislation.

Nevertheless, the successful stories of the existing commercial applications indicate more possibilities and opportunities in future. Indeed, they have set important precedents for feasible uptake of the technologies in various industry sectors. Opportunities present for wider commercial applications in future as a result of the following drives:

a. Technical—R&D has been ongoing to (i) identify more working fluids from a wider range of fluid types and mixtures for different heat source temperatures; (ii) enhance heat transfer and exchange; and (iii) achieve optimal system performance.

b. Economic—Significant energy cost savings are realized from the commercial applications in particular when energy prices soar.

c. Business—The deployment of the state-of-the-art technologies is (i) justifiable on the grounds of improved corporate images when organizations endeavor in energy efficiency and sustainability; and (ii) possible for upcoming facility expansion and renovation while existing infrastructure can be used as a backup.

d. Policy—Industrial willingness to go beyond business as usual can be stimulated by tax breaks or exemption and new feed-in tariffs for low-grade heat utilization and recovery.

e. Information, training and knowledge transfer—More commercial applications can be realized provided manufacturers, dealers and technicians are informed about R&D advance on a regular basis.

f. Social—The deployment brings along some advantages to the society, for instance, local/national economic development, new job opportunities, energy security, and indirect health benefits from reduced green house gas (GHG) emission.

Prior to commercial applications, the system must be designed with precautions and assessed thoroughly using a whole-system approach by taking account of technical, economic, legislative, social and environmental consideration. Life cycle assessment, which is a methodology widely applied for environmental assessment, is not further discussed but can be found in [56].

Acknowledgements

With support from the Research Councils UK Energy Program (EP/P005667/1), the chapter was delivered as a research outcome of the Thermal Energy Challenge Network.

Author details

Janie Ling-Chin*, Huashan Bao, Zhiwei Ma, Wendy Taylor and Anthony Paul Roskilly

*Address all correspondence to: j.l.chin@ncl.ac.uk

Sir Joseph Swan Centre for Energy Research, Newcastle University, UK

References

[1] International Energy Outlook 2017. U.S. Energy Information Administration; 2017. pp. 1-151. [cited 2018 27 April]. Available from: https://www.eia.gov/outlooks/ieo/pdf/0484(2017).pdf

[2] An independent assessment of the clean growth strategy—From ambition to action. Committee on Climate Change; 2018. [cited 2018 27 April]. Available from: https://www.theccc.org.uk/wp-content/uploads/2018/01/CCC-Independent-Assessment-of-UKs-Clean-Growth-Strategy-2018.pdf

[3] Rajendran K, Ling-Chin J, Roskilly AP. Thermal energy efficiency in industrial processes. In: Handbook of Clean Energy Systems. UK: John Wiley & Sons; 2015

[4] Ammar Y et al. Low grade thermal energy sources and uses from the process industry in the UK. Applied Energy. 2012;**89**(1):3-20

[5] Elson A, Tidball R, Hampson A. Waste Heat to Power Market Assessment. Oak Ridge, TN, United States: Building Technologies Research and Integration Center (BTRIC), Oak Ridge National Laboratory (ORNL); 2015

[6] Rakib MI et al. Waste-heat utilization—The sustainable technologies to minimize energy consumption in Bangladesh textile sector. Journal of Cleaner Production. 2017; **142**:1867-1876

[7] Law R, Harvey A, Reay D. Opportunities for low-grade heat recovery in the UK food processing industry. Applied Thermal Engineering. 2013;**53**(2):188-196

[8] Luo A et al. Mapping potentials of low-grade industrial waste heat in northern China. Resources, Conservation and Recycling. 2017;**125**:335-348

[9] Johnson I, Choate WT, Davidson A. Waste heat recovery. Technology and Opportunities in US Industry. Laurel, MD, United States: BCS, Inc.; 2008

[10] Bao H et al. Emerging technologies for improved energy efficiency and heat recovery in industry. In: Baking Europe. UK: Graham Pendred; 2017

[11] Park C et al. Recent advances in vapor compression cycle technologies. International Journal of Refrigeration. 2015;**60**:118-134

[12] Sing KSW. Reporting physisorption data for gas/solid systems with special reference to the determination of surface area and porosity (recommendations 1984). Pure and Applied Chemistry. 1985;**57**(4):603-619

[13] Wang R, Wang L, Wu J. Adsorption Refrigeration Technology: Theory and Application. Singapore: John Wiley & Sons; 2014

[14] Sah RP, Choudhury B, Das RK. A review on adsorption cooling systems with silica gel and carbon as adsorbents. Renewable and Sustainable Energy Reviews. 2015;**45**:123-134

[15] Wang LW et al. Study of the performance of activated carbon–methanol adsorption systems concerning heat and mass transfer. Applied Thermal Engineering. 2003;**23**(13): 1605-1617

[16] Kayal S, Baichuan S, Saha BB. Adsorption characteristics of AQSOA zeolites and water for adsorption chillers. International Journal of Heat and Mass Transfer. 2016;**92**:1120-1127

[17] Bao HS et al. Choice of low temperature salt for a resorption refrigerator. Industrial & Engineering Chemistry Research. 2010;**49**(10):4897-4903

[18] N'Tsoukpoe KE et al. A systematic multi-step screening of numerous salt hydrates for low temperature thermochemical energy storage. Applied Energy. 2014;**124**:1-16

[19] Miles DJ, Shelton SV. Design and testing of a solid-sorption heat-pump system. Applied Thermal Engineering. 1996;**16**(5):389-394

[20] Glaznev IS, Ovoshchnikov DS, Aristov YI. Kinetics of water adsorption/desorption under isobaric stages of adsorption heat transformers: The effect of isobar shape. International Journal of Heat and Mass Transfer. 2009;**52**(7):1774-1777

[21] Li TX, Wang RZ, Li H. Progress in the development of solid–gas sorption refrigeration thermodynamic cycle driven by low-grade thermal energy. Progress in Energy and Combustion Science. 2014;**40**:1-58

[22] Yu N, Wang RZ, Wang LW. Sorption thermal storage for solar energy. Progress in Energy and Combustion Science. 2013;**39**(5):489-514

[23] Wang L et al. A resorption cycle for the cogeneration of electricity and refrigeration. Applied Energy. 2013;**106**:56-64

[24] Bao H, Wang Y, Roskilly AP. Modelling of a chemisorption refrigeration and power cogeneration system. Applied Energy. 2014;**119**:351-362

[25] Bao H et al. Chemisorption cooling and electric power cogeneration system driven by low grade heat. Energy. 2014;**72**:590-598

[26] Bao H, Ma Z, Roskilly AP. Integrated chemisorption cycles for ultra-low grade heat recovery and thermo-electric energy storage and exploitation. Applied Energy. 2016; **164**:228-236

[27] HS B, AP R. GB Patent: Energy Storage Device. UK: University of Newcastle; 2014. [cited 2018 27 April]. Available from: https://patents.google.com/patent/EP3102892A1/pt

[28] Iup A. Manual of symbols and terminology for physico-chemical quantities and units, appendix II; part I: Definitions, terminology and symbols in colloid and surface chemistry. Pure and Applied Chemistry. 1972;**31**:579-638

[29] Wu W et al. Absorption heating technologies: A review and perspective. Applied Energy. 2014;**130**:51-71

[30] Rivera W et al. A review of absorption heat transformers. Applied Thermal Engineering. 2015;**91**:654-670

[31] Ma Z, Bao H, Roskilly AP. Principle investigation on advanced absorption power generation cycles. Energy Conversion and Management. 2017;**150**:800-813

[32] Xu ZY, Wang RZ, Xia ZZ. A novel variable effect LiBr-water absorption refrigeration cycle. Energy. 2013;**60**:457-463

[33] Mohammad AT et al. Survey of liquid desiccant dehumidification system based on integrated vapor compression technology for building applications. Energy and Buildings. 2013;**62**:1-14

[34] Fu H-X, Liu X-H. Review of the impact of liquid desiccant dehumidification on indoor air quality. Building and Environment. 2017;**116**:158-172

[35] Das RS, Jain S. Simulation of potential standalone liquid desiccant cooling cycles. Energy. 2015;**81**:652-661

[36] Rafique MM, Gandhidasan P, Bahaidarah HMS. Liquid desiccant materials and dehumidifiers – A review. Renewable and Sustainable Energy Reviews. 2016;**56**:179-195

[37] Su B et al. A two-stage liquid desiccant dehumidification system by the cascade utilization of low-temperature heat for industrial applications. Applied Energy. 2017;**207**:643-653

[38] Martin CL et al. Application of liquid desiccant dehumidification to amine-based carbon capture systems. International Journal of Greenhouse Gas Control. 2016;**54**:557-565

[39] Liquid desiccant dehumidification systems [cited 2018 3 April]. Available from: http://www.kathabar.com/wp-content/uploads/2010/12/Kathabar-liquid-desiccant-product-guide-digital.pdf

[40] Chan CW, Ling-Chin J, Roskilly AP. Reprint of "a review of chemical heat pumps, thermodynamic cycles and thermal energy storage technologies for low grade heat utilisation". Applied Thermal Engineering. 2013;**53**(2):160-176

[41] Qiu G, Liu H, Riffat S. Expanders for micro-CHP systems with organic Rankine cycle. Applied Thermal Engineering. 2011;**31**(16):3301-3307

[42] Iglesias Garcia S et al. A review of thermodynamic cycles used in low temperature recovery systems over the last two years. Renewable and Sustainable Energy Reviews. 2018;**81**:760-767

[43] Foresti A, Archetti D. Waste heat recovery valorization with ORC technology [cited 2018 3 May]. Available from: http://www.tasio-h2020.eu/wp-content/uploads/2018/02/Waste-Heat-Recovery-Valorization-With-ORC-Technology.pdf

[44] Öhman H. Implementation and evaluation of a low temperature waste heat recovery power cycle using NH_3 in an organic Rankine cycle. Energy. 2012;**48**(1):227-232

[45] Green power through innovation. Available from: http://exergy-orc.com/references/case-studies

[46] Tartière T. ORC market: A world overview. Analysis of the Organic Rankine Cycle Market; 2016. [cited 2018 27 April]. Available from: http://orc-world-map.org/analysis.html

[47] Zhang X, He M, Zhang Y. A review of research on the Kalina cycle. Renewable and Sustainable Energy Reviews. 2012;**16**(7):5309-5318

[48] Mirolli MD. The Kalina cycle for cement kiln waste heat recovery power plants. In: Cement Industry Technical Conference, 2005. Conference Record. IEEE

[49] Li X, Zhang Q, Li X. A Kalina cycle with ejector. Energy. 2013;**54**:212-219

[50] Cao L et al. Comprehensive analysis and optimization of Kalina-flash cycles for low-grade heat source. Applied Thermal Engineering. 2018;**131**:540-552

[51] Ghaebi H et al. Thermodynamic and thermoeconomic analysis and optimization of a novel combined cooling and power (CCP) cycle by integrating of ejector refrigeration and Kalina cycles. Energy. 2017;**139**:262-276

[52] Wang Y et al. Thermodynamic performance comparison between ORC and Kalina cycles for multi-stream waste heat recovery. Energy Conversion and Management. 2017;**143**:482-492

[53] Pan Z et al. Thermodynamic analysis of KCS/ORC integrated power generation system with LNG cold energy exploitation and CO_2 capture. Journal of Natural Gas Science and Engineering. 2017;**46**:188-198

[54] THE KALINA CYCLE®–A major breakthrough in efficient heat to power generation [cited 2018 4 May]. Available from: http://www.heatispower.org/wp-content/uploads/2013/11/Recurrent-Eng-macwan_chp-whp2013.pdf

[55] Ahmed A et al. Design methodology of organic Rankine cycle for waste heat recovery in cement plants. Applied Thermal Engineering. 2018;**129**:421-430

[56] Ling-Chin J, Heidrich O, Roskilly AP. Life cycle assessment (LCA)—From analysing methodology development to introducing an LCA framework for marine photovoltaic (PV) systems. Renewable and Sustainable Energy Reviews. 2016;**59**:352-378

Chapter 5

The Role of Material Selection and Microfluidics for Optimized Energy Conversion in Microbial Fuel Cells

Giulia Massaglia and Marzia Quaglio

Additional information is available at the end of the chapter

http://dx.doi.org/10.5772/intechopen.78641

Abstract

This chapter book aims to present some key aspects, which play a crucial role to optimize the energy conversion process occurring in microbial fuel cells (MFCs): fluid dynamics and the materials selected as anodic electrodes. MFCs are (bio)-electrochemical devices that directly convert chemical energy into electrical energy, thanks to the metabolic activity of some bacteria. In the anodic compartment, these bacteria, named exoelectrogens, are able to oxidize the organic matter, directly releasing the electrons to the anode surface. The conversion process can be deeply influenced by how the electrolyte solution, containing the carbon-energy source, moves inside the device. For this reason, fluid dynamic modeling is an important tool to explain the correlation between the fluid flow and power output production, optimizing also the overall MFC performance. Moreover, the morphology of anode electrodes results to be essential to guarantee and enhance the bacteria proliferation on them, improving the energy conversion.

Keywords: microbial fuel cells, bioelectrochemical devices, exoelectrogenic bacteria, fluid dynamic, modeling

1. Introduction

Since in the next years, the high level of greenhouse gas emissions (GHG) must be reduced as confirmed by Kyoto protocol [1, 2], the development and investigation of renewable energy sources are of ever increasing importance, since they are expected to play a leading role to further improve the life quality all over the world [3].

As represented in **Figure 1**, the conventional energy sources, based on oil, coal and natural gas, are widely used comparing with the renewable energy ones that is only 10% of U.S energy

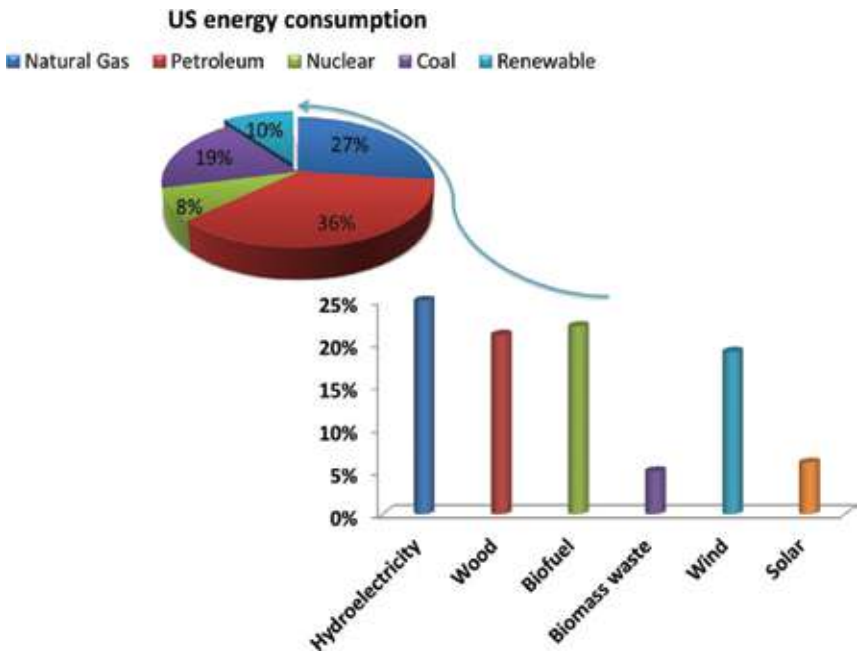

Figure 1. US energy consumption by energy sources in 2015.

consumption in 2015 [4]. The main targets of EU's Renewable Energy Directive are focused on two important aspects: (1) the renewable energy sources must represent the 20% of final/total energy consumption by 2020; (2) all EU countries must adopt national energy action plans, leading to carry out their renewable targets. Among all renewable energy sources, such as hydroelectricity, wood, geothermal, wind and solar, biofuel is produced/obtained/carried out/achieved through the biological processes, such as agriculture and anaerobic digestion, rather than a fuel obtained by geological processes, which are achieved in fossil fuels formation like coal and petroleum. Biofuels can be obtained directly from plants or derived indirectly by agricultural, commercial, domestic and/or industrial wastes. Furthermore, a biofuel cell is a device that realizes the conversion of chemical energy into electrical energy toward biochemical reactions. The electrons are produced by the oxidation reaction of a specific fuel. Among all different biofuel cells, microbial fuel cell (MFC) represents a promising technology as renewable energy sources.

In this chapter, MFC devices are proposed as bio-electrochemical devices that convert the chemical energy, embedded in organic compounds (fuel), into electrical energy by the action of exoelectrogenic microorganisms [5]. These electrochemical cells are based on a bio-anode, whose surfaces are colonized by microorganisms, which proliferate and drive/catalyse the oxidation reaction, occurring in the anodic compartment. In the past few decades, in order to validate the application of MFCs as energy production devices, different works in the literature focused their attention on different carbon energy sources as fuel [6–8]. Moreover, as highlighted by different works in the literature, both device architecture, which influence on the fluid dynamic distribution inside MFCs, and morphological properties of electrode materials play a crucial role to optimize/enhance overall performance/power output production. In this

chapter, we also explained/described a growing interest in miniaturized these devices at the milliliter to microliter size [9–12]. In particular, the design of milliliter-size MFCs induced an optimization of carbon sources transport and the reduction of internal resistance of device, improving thus the power output production. The authors of several works in the literature demonstrate how the reduction/diminution of MFCs volume guarantees a small distance between electrodes, fast response time, a low Reynolds number and the possibility to investigate the electron transfer process due to the interaction between bacteria and anodic electrode.

2. MFCs technical aspects principle

The MFC is a bio-electrochemical device, where the microorganisms are used to convert chemical energy, trapped in an organic matter, into the electrical energy. The process is based on the concept that particular kind of microorganisms, named exoelectrogens, are able to oxidize the organic matter (also known as carbon energy sources) [13] and to directly transfer the produced electrons outside their cells exogenously [5]. Indeed, these microorganisms are capable to directly release the electrons to a chemical or materials that are not immediately the electron acceptor. Successively, the produced electrons flow from anodic electrode to terminal electron acceptor (TEA) through an external applied load. TEA acquires the electrons and becomes reduced in the cathode compartment (see **Figure 2**). Therefore, MFCs are characterized by three main compartments, as shown in **Figure 2**:

1. Anode chamber, where the organic matter oxidation reaction occurred, catalyzed by exoelectrogenic bacteria;
2. Cathode chamber, where the reduction reaction is carried out. The released electrons flow into cathode chamber through an external load applied, leading thus to reduce the terminal electron acceptor. Regarding the electrolyte in MFCs cathode compartment, many different chemical species accept the electron and then are reduced. One of them is the

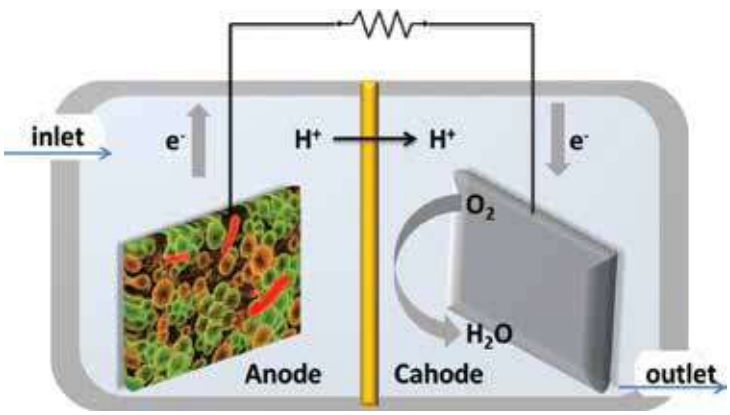

Figure 2. Scheme of working principle of microbial fuel cells (MFCs).

oxygen, dissolved into the electrolyte (normally electrolyte is based on water). The oxygen is reduced through a catalysed reaction of the electron with the protons, named oxygen reduction reaction (ORR). Many TEAs, such as oxygen, nitrate, sulphate and others, accept the electrons making some products that can diffuse outside the devices.

3. Proton exchange membrane (PEM), which is an anionic or cationic membrane that separates the anode and cathode chambers and ensure the protonic flow into the electrolyte.

3. Anode compartment

In the anode chamber bacteria grow on the electrode surface, generating a biofilm. According to IUPAC definition, the biofilm is an "Aggregate of microorganisms in which cells that are frequently embedded within a self-produced matrix of extracellular polymeric substance (EPS) adhere to each other and/or to a surface" [14]. The main difference between biofilm and planktonic microorganisms (bacteria that float in the liquid electrolyte) is represented by ability of bacteria to self-produce all the connections between among them and with anodic electrode surface. The adhesion of bacteria to the electrode surface is ensured by weak and reversible van der Waals forces. If the microorganisms are not immediately separated from the electrode surface, their anchorage became more effective and stronger by direct cell-adhesion by pili, and by a self-produced matrix of extracellular polymeric substances. The resulting biofilm in MFC's anode is formed by electrochemically active bacteria that oxidize the organic matter dissolved in the electrolyte, and acting as the carbon energy source in MFCs. In the last years, different works in the literature investigated the different electron transfer processes, carried out by bacteria in MFCs [15–20]. These processes can be divided into two mainly different ways:

1. electron shuttling via self-produced mediators [17, 18].
2. nanowires produced by some bacteria which are used as endogenous mediators [19, 20].

Direct electron transfer can be obtained by physical contact of redox active bacterial membrane organelle, such as cytochromes, with the anode electrode [21], as represented in **Figure 3a**. Otherwise, Gorbi et al. [19] investigated the conductive bacterial nanowires (or pili), produced

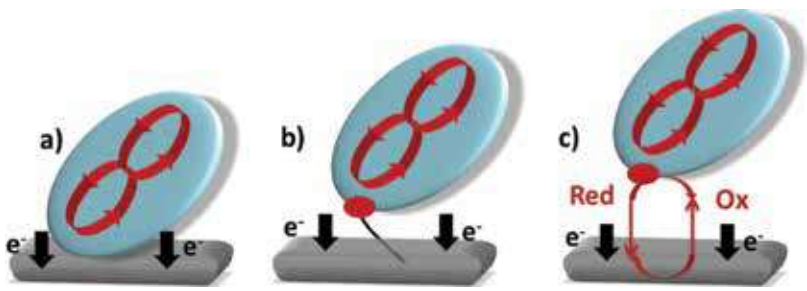

Figure 3. Scheme of the direct electron transfer pathway through (a) the membrane bound cytochromes, (b) nanowires self- produced by bacteria and (c) self-produced redox mediators.

by bacteria (Geobacter and Shewanella) as the pathway to direct transfer the electrons to anodic electrode, as shown in **Figure 3b**. Rabaey et al. [17, 18] defined the ability of certain bacteria to self-produce redox mediators, which then ensure the direct electron transfer to the anodic surface (see **Figure 3c**). He demonstrated that bacteria exist, which are able to generate exogenous redox mediators, which not have to be added to a culture. These self-produced mediators permit to shuttle the electrons to an electrode, inducing the power generation in a MFC.

4. Microbial fuel cells power output production

The theoretical concept, based on the power output production from MFCs, defined a direct correlation between power production and the measured voltage across the external applied load [22], as represented in Eq. (1):

$$P = I \cdot E_{MFC} \tag{1}$$

where I is the current produced from MFCs, E_{MFC} is voltage drop across the external applied resistor. One of the main parameters, that can affect produced current and consequently power production, is the surface area of anode electrode available for the microorganisms growth. For this reason, it is common to introduce the concept of power density, defined normalizing power production with anodic surface area (A_{anode}) [22]. Furthermore, since the measured current is defined as a function of the potential across the external resistance and it is needed to take into account the accessible surface area for bacteria proliferation, the power density output can be determined by Eq. (2):

$$P = \frac{E_{MFC}^2}{A_{anode} R_{external}} \tag{2}$$

As widely investigated by several works in the literature [22–24], the generated voltage by MFCs depends on both the microorganisms proliferation on anode electrode surface and anode and cathode voltages, as explained by Eq. (3):

$$E_{MFC} = E_{cathode} - E_{anode} \tag{3}$$

where $E_{cathode}$ and E_{anode} are respectively the cathode and anode voltages [22].

In particular, the anodic voltage is strictly correlated with the organic matter used as carbon energy source inside MFCs, the metabolic activity of the microorganisms and their adhesion on electrode surface, on which charge transfer depends. Different organic compounds are used as carbon energy sources inside MFCs [25, 26] to produce electricity. The most commonly used is sodium acetate, which can release a maximum of eight electrons when bacteria oxidized it [27, 28].

Chae et al. [28] investigated the single chamber microbial fuel cells (SCMFCs) performances with different substrates, such as acetate, butyrate, propionate and glucose. They demonstrated that the highest power output is associated with acetate feeding, followed by butyrate,

propionate and glucose. Despite of all kinds of organic matters, anodic open circuit voltage (a-OCV), defined as the highest potential reached by MFC when no external load is applied, is close to −0.3 V. At the cathode, the standard reduction potentials of all electrolytes, which must be reduced, influence the cathode voltage. Among all oxidants used in the cathode, such as metallic oxidants [29–35] (like U, Cd, Cr, Cu), the most commonly applied is oxygen, whose standard reduction potential is equal to 0.805 V. Nevertheless, direct oxygen reduction reaction (ORR) results to be thermodynamically disadvantageous due to its high reduction potential, low kinetics and high activation losses induced [22]. In order to evaluate the MFC voltage, it is mandatory to take into account the voltage losses caused by electrode overpotentials and ohmic losses, as represented by Eq. (4):

$$E_{MFC} = \sum V_{anode} + \left|\sum V_{cathode}\right| + IR_{\Omega} \tag{4}$$

where $\sum V_{anode}$ and $\left|\sum V_{cathode}\right|$ represent electrodes overpotentials and IR_{Ω} is the ohmic losses that are directly proportional to the generated current and internal resistance of MFCs. Theoretically, overpotentials consider all voltage drops required to favor, respectively, the electrons and protons transport inside the device. The electrode overpotentials are induced by three losses, as represented in **Figure 4** [5].

i. **Activation polarization losses** are due to the energy lost needed/necessary to start the oxidation or reduction reactions and to ensure electron transfer from the bacterial cells to the anode surface. The presence of catalyst at the cathode, the different bacteria in the anode compartment and the optimized electron transfer between bacteria and anode surface can minimize these losses. Furthermore, since the current density tends to be reduced when the anode surface increase, one of the strategies to overcome activation losses is related to use anode electrodes characterized by an high porosity and/or high roughness [36]. Another way can be represented by an improvement of interaction between bacteria and anodic electrodes, enhancing thus the electron transfer outside the microbe cells to anode surface. As shown in **Figure 4**, it is possible to appreciate that the activation losses result to be more evident at low current values.

ii. **Ohmic losses** are strictly correlated with internal resistance (R_{Ω}) of MFCs. Ohmic losses are due to all parameters that can increase the internal device resistance. The internal resistance is defined as the resistance to the electrons flow in electrodes and connections, and the resistance to ionic transport in the electrolyte and through PEM, if is present. They can be defined by Ohm's Law, as explained in Eq. (5):

$$\eta_{\Omega} = IR_{\Omega} \tag{5}$$

The distance between anode and cathode electrodes, the biofilm formation on anode surface, the fluid dynamic distribution of electrolyte inside the device and consequently the designed architecture of MFCs can influence the ohmic losses. In order to improve overall device performance, ohmic losses must be overcome. In particular, increasing of electrical conductivity of anode materials, minimizing the distance between anode and cathode leading to favor electrons flow and optimizing the contact between electrodes and electron collectors can

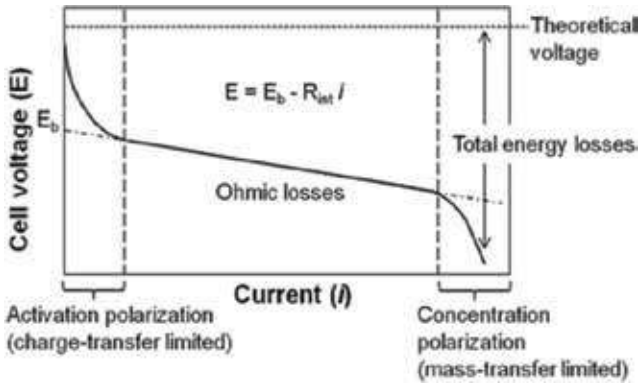

Figure 4. The polarization curve for typical MFCs. Reprinted with the permission from (chemical society reviews, 2012, 41, 7228–7246) copyright (2012) Royal Society of Chemistry.

avoid ohmic losses, as much as possible. Xie et al. [37] demonstrated how three-dimensional structure of anode electrode increases the surface area to volume ratio, improving thus the interaction between microorganisms and electrodes and consequently ensuring a higher electron transport. Another important parameter is the distance between anode and cathode electrodes, lower is this distance, lower is the internal resistance since the electron and protonic pathway is reduced. Liu et al. [38] compared the power outputs obtained by MFCs when two different spacing, equal to 4 cm ad 2 cm, between two electrodes are used, highlighting that power density, when the distance is of 2 cm, is double than the one reached when distance is 4 cm. Different works in the literature also underlined how the proton exchange membrane (PEM) increases the internal resistance of MFCs [39]. Indeed, the removal of PEM not only simplifies the design of device, but it can also reduce ohmic losses and consequently increases the power output production.

iii. Mass transports losses carry out when the amount of reactants to the electrodes or products from electrodes is insufficient, leading thus to minimize the reaction rate. These losses, moreover, can be modified the metabolic activities of microorganisms. These losses not only limit the power generation of MFCs, but they increase the pH, hindering/minimizing the proton diffusion and consequently reducing significantly the current density production. Mass transport losses achieved at high current densities.

Moreover, among all voltage losses, it is needed to consider the bacterial metabolism, which induces a voltage drop due to the energy suitable for bacteria sustainability.

5. Anodic materials and their influence on power output production

Among all parameters that influence the overall device performance, the materials used at the anode, the electrochemical active biofilm at the electrode, and the device configuration play an important active role to establish the MFCs power output production. In particular, anodic electrodes must satisfy several properties [22] in order to enhance bacteria proliferation on them

and consequently to improve the overall device performance: (1) biocompatibility for microorganisms proliferation; (2) high electrical conductivity and high chemical resistance; (3) high specific area to volume ratio, with pores size of order of some micrometers to enhance bacteria proliferation on electrode surface and to facilitate the diffusion of carbon energy source inside the electrode; (4) cheap production cost. Among all these properties, the electrical conductivity, the morphology and the porosity of anodic material can mainly influence the device performance, especially in terms of the power output production. In recent years, some works in the literatures investigate some metals and their alloys as anodic materials, thanks to their high electrical conductivity, combined with good mechanical properties [40, 41]. One of the main limit of metals and their alloys, designed as anodes in MFCs, is related to their chemical resistance. Since these materials do not satisfy the no corrosive requirements, different surface treatment are provided to overcome the corrosive limit and at the same time to induce a certain roughness on the surface, ensuring thus the bacteria adhesion on it. As proposed in the literature, only stainless steel and titanium are suitable to be applied as anodes in MFCs. Dumas et al. [42] tested stainless steel plates as both anodic and cathode electrodes inside device, demonstrating that the power density (close to 23 mW/m^2) result to be limited by anode. As reported in other work of literature, Dumas et al. [43] confirm worst performance of MFCs, when a stainless steel plate is used as anode, than the one reached when graphite anode. Titanium wires are commonly used as current collector in MFCs. Heijne et al. demonstrate the lowest performance reached when untreated titanium is employed as anodes in the cells [44]. Few works in the literature [6, 45] focused their attention on gold anodes, which enhance the growth of Geobacter on its surface, generating a current density close to the one obtained by MFCs with graphite anodes. Since carbon-based materials show a high biocompatibility for bacterial proliferation, good chemical resistance, good electrical conductivity and low cost production, they result to be the most promising anodes in MFCs [46]. Generally, carbon-based materials conjugate the best chemical surface and morphological properties, able to enhance the biofilm formation [47]. It is possible to divide these kinds of materials in three different groups, according to their structure [46]: (1) plane organization, (2) packed organization and (3) brush organization.

5.1. Planar structure of anode electrodes

Among all carbon materials with a planar structure, carbon paper, carbon cloth, graphite plates or sheets are widely applied as anodes in MFCs [48, 49]. Both carbon paper and carbon cloth are cheaper than graphite based electrodes. Nevertheless, these samples are characterized by a low thickness and an enough dense structure, able to reduce the porosity of electrodes, minimizing the surface area and the bacteria growth [46]. Graphite sheets show a higher mechanical resistance than the one offered by carbon cloth or carbon paper. In particular, Heijne et al. [44] highlighted that the anodes, based on graphite sheets with a certain roughness degree, show a higher power output than smooth graphite sheets. In order to overcome the high production cost of all these carbon materials, Wang et al. [50] investigated a carbon mesh electrodes, treated with ammonia gas and compared to a carbon cloth, on which the same treatment was employed. They demonstrated that treated carbon mesh reached a power output greater than the one obtained by carbon cloth. In particular, many works in the literature demonstrated how the ammonia gas treatment enhances the positive charge of carbon surfaces, maximizing the bacterial proliferation and increasing the

overall device performance [51]. Furthermore, surface treatments of carbon-based materials, especially nitrogen-based functionalization, demonstrated to significantly improve microbial proliferation on anode and thus the overall device performances [50, 51].

Since high porosity is an important property that anode electrode must satisfy, two classes of materials can be considered: graphite or carbon felt and graphite foam. Generally, the structure of felt samples are made of fibres, with a total thickness greater than the one of previously described carbon materials [30]. These materials showed pores size distribution of some micrometers, able to increase the bacterial growth, which, however, is restricted by diffusion of carbon energy sources inside the electrodes [30]. Another porous carbon material that is not commonly used as anodes in MFCs is graphite foam [52]. Chaudhuri et al. [52] confirmed that the current density obtained with graphite foam results to be 2.4 times higher than the one reached with graphite rod.

5.2. Packed structure of anode electrodes

Different arrangement of above described carbon-based materials has been investigated in order to obtain the packed structure of anode electrodes, able to increase the surface area of electrodes, available for microorganisms proliferation [53–56]. One of these kinds of structures is granular graphite. Rabey et al. designed granular graphite as anode in MFCs. Li et al. [55] reported a power density of 557 mW/m^2 achieved with granular activated carbon anode, which is double than the one reached with carbon cloth. This good result confirmed how the enhanced surface area of anode guarantees a better bacterial proliferation and then an improved electron transfer from bacteria to anode surface. Aelterman et al. [53] analyzed overall device performance when different anodes, as carbon felt, graphite felt and granular graphite, are applied. They defined a large/great power density, close to 386 W/m^3, carried out by graphite felt as anode electrode.

5.3. Brushed structure of anode electrodes

The graphite brush materials are classified as an ideal electrode, able to conjugate high surface area, high porosity and great electrical conductivity. Logan et al. [22] designed brushes anodes made of carbon fibres that covered two titanium wires. In particular, they developed two brush anodes characterized by different dimensions: the smaller one (2.5 cm in diameter and 2.5 in long) and a greater one (5 cm in diameter and 7 cm in long). The MFCs with the smaller anodes achieve a power density of 2.4 W/m^2, higher than the one reached with greater brush anode (1.43 W/m^2). Both achieved power densities result to be higher than the one obtained with plain carbon paper, used as anode. The worst performance of large brush anodes can be explained by the fact that an excessive amount of fibres can hinder bacterial proliferation and consequently the diffusion of organic matter inside the anode.

5.4. Composite carbon-based anodes

The anodic surface plays a crucial role to influence the microorganisms adhesion on it, the electrical connections, self-produced by bacteria, with the electrode and consequently the overall MFCs performance [40, 57, 58]. One of the several strategies, which can be carried

out to properly modify the electrode surfaces, is based on the coating materials deposition on the electrode. This coating layer must be able to improve the biofilm formation, while the electrical conductive backbone part ensures the charge transfer [40, 57]. Many works in the literature developed composite anodes, made of metals as backbone electrode part and carbon-based materials as interface layer between all electrode and bacteria. These anodic configurations improve not only the bacterial growth on the electrode surface but simultaneously the power output production [50, 59, 60].

6. Device configurations

Two main configurations of MFCs are widely used in the literature [22]: (1) dual chamber microbial fuel cells (DC-MFCs), characterized by two different chambers, respectively anode and cathode, normally divided by proton exchange membrane (PEM) and (2) single chamber microbial fuel cells (SC-MFCs), where anode and cathode compartments constitute only one chamber. Typically, SCMFCs are membrane-less device and the electrolyte result to be in common between anode and cathode. **Figure 5a** shows DC-MFCs, where the electrolyte inside the cathode is based on chemical solutions, like hexacyanoferrate of potassium. This architecture requires the presence of a cationic membrane, which allows the protons transfer between the anode and cathode and create two different and separate compartments: the anode and the cathode chamber. In this way, the produced electrons, which flow into the cathode, can be recombined with protons. **Figure 5b** represents SC-MFCs configuration, characterized by only one chamber. The electrolyte is unique and common with anode and cathode. Different works in the literature developed this configuration in order to use oxygen, dissolved into the electrolyte, as the final electron acceptor.

As confirmed by some works in the literature [14], the main advantage of DC-MFCs is strictly due to the presence of water-soluble electrolyte as a terminal electron acceptor. Indeed, if the electrolyte contains potassium hexacyanoferrate, its standard reduction potential is very low, close to 0.361 V, leading thus to favor the reduction reaction. On the contrary, the presence of a chemical compound as TEA in the cathode chamber minimizes/limits the application of these devices in the environment. In order to overcome this limitation, SC-MFCs are designed.

In the latter configuration, oxygen is usually used as unique terminal electron acceptor, without the presence of other chemical compounds, ensuring then the environmental-friendly application of MFCs. Nevertheless, the direct oxygen reduction reaction (ORR) shows low kinetics and requires a high reduction potential (close to 0.805 V) to carry out, causing several overpotentials in the devices. Indeed, the development of catalyst layer, to accelerate and favor direct ORR, is required [61]. Logan et al. [61] designed/investigated/proposed the development of a catalyst layer (CL) and a diffusion layer (DL) in order to overcome/avoid all disadvantage of SC-MFCs. The diffusion layer is made of several polytetrafluorethylene (PTFE) layers, able to enhance the diffusion of oxygen from outside to inside the devices, while the catalyst layer is typically based on platinum, which is considered the ideal catalyst for ORR.

http://dx.doi.org/10.5772/intechopen.78641

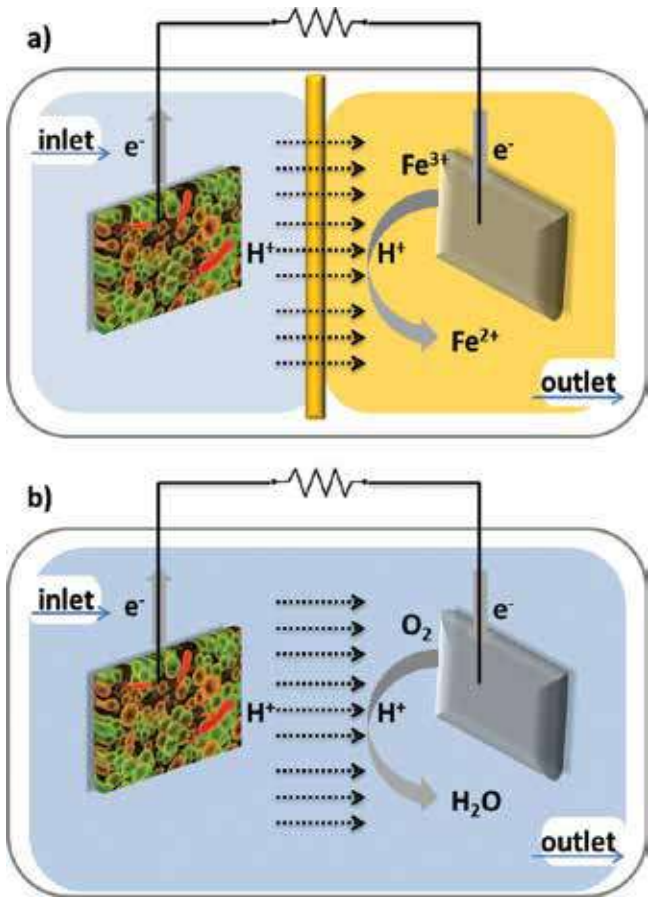

Figure 5. Two different electrochemical schemes describing two different architectures of MFCs: (a) shows the dual chamber MFCs where the reduced species in the cathode is hexacyanoferrate of potassium; (b) represents the single chamber MFCs where on the contrary, the oxygen in the cathode is reduced into the water.

7. Role of fluid dynamics inside the device

The necessity to improve the power output produced by MFCs demanded different strategies, focused on scaling-up MFCs [62], using different kinds of microbial communities and exploring several substrates (i.e., derived from wastes) [25]. However, during the last decades, different works in the literature considered these devices in terms of small dimensions and optimized fluid dynamic distribution, in order to minimize the internal ohmic resistance, leading thus to improve the overall MFCs performance [63]. Fluid dynamic modeling can be implemented to define the correlation between the fluid distribution inside the device and its overall performance [64, 65]. Furthermore, this kind of simulation can have a predictive role of fundamental importance in driving the design of the reactors toward the optimal MFC configuration.

Massaglia et al. [65] analyzed two different architectures of open air cathode MFCs, (drop-MFCs and square-MFCs), with an inner volume of few milliliters. They demonstrated a direct correlation between the fluid distribution inside MFCs and the power output production. In this work, Drop-MFCs, indeed, represented the best architecture design, maximizing the fluid dynamic distribution and consequently the power density output. **Figure 6** shows the fluid dynamic distribution inside both drop-MFCs and square-MFCs, obtained implementing two different flow rate values. The presented results confirm the better fluid distribution inside drop-MFCs for both flow rates.

Qian et al. reported the advantages of design MFCs with smaller volumes of the order of milliliter. They demonstrated how this configuration results to be effective for reducing internal electrical resistance device and enhancing mass transport. Ringeisen et al. [66] achieved great power densities of 500 W/m^3 with a MFCs with an internal volume of 1.2 mL.

Fan et al. [67] investigated the power density production, close to 1 W/m^3, obtained with an open air cathode configuration MFCs, characterized by a volume of 2.5 mL. Both the interaction between biofilm and anode electrode and consequently the metabolic activity of microorganisms that drive the oxidation reaction in anodic chamber show a pivotal role to define the power output production. Nevertheless macro-size MFCs and milliliter-size MFCs show higher output performance, the miniaturization of MFCs to microliter-size (μL-MFCs)

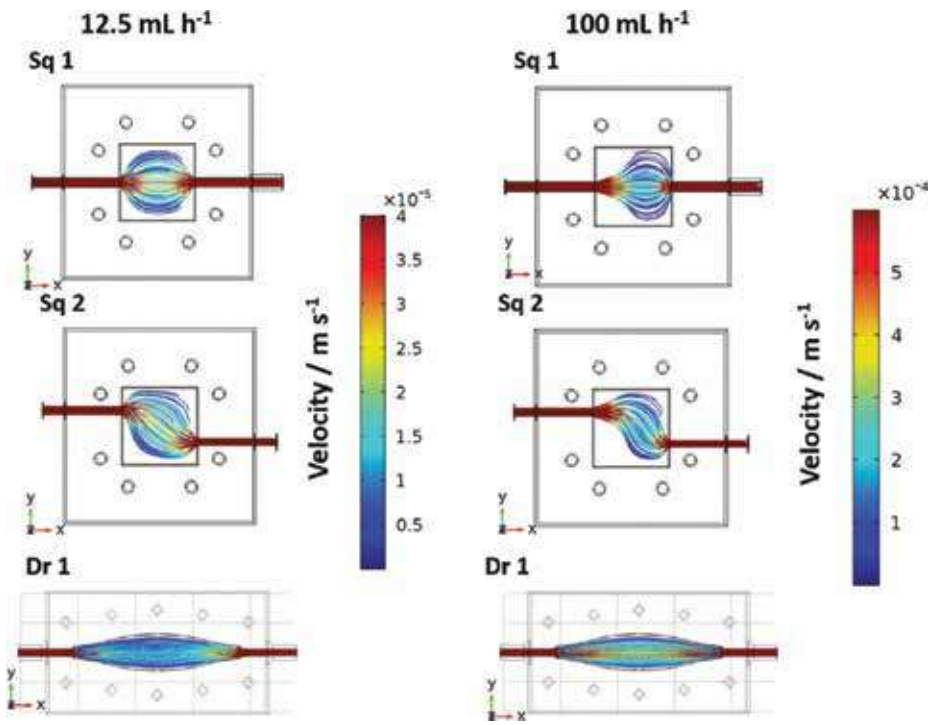

Figure 6. Results of simulations of fluid distribution inside drop-MFCs and square-MFCs, implemented two different values of flow rate, 25 mL h^{-1} and 100 mL h^{-1}. Reprinted with the permission from (Fuel Cell, 2017, 17, 627–634) Copyright (2017) Wiley online library.

resulted to be needed to deeply understand/investigate the relationship and the interconnection between all the biological, chemical and electrical parameters. Since some parameters, such as mass transport, reaction kinetics and ohmic resistance deeply influence overall MFC performance, the design of microliter-size MFCs (μL-MFCs) is required to better investigate electrochemically active bacteria and electrode performance. μL-MFCs, in particular, employ important and pivotal features:

1. Lower electrode distance for reducing the ohmic internal resistance and optimizing the mass transport;
2. Laminar fluid dynamic inside the device for ensuring a better distribution of organic matter to be oxidized;
3. Device fast response time.

Several works underline/confirm advantageous characteristics of these devices, as high surface area to volume ratio, lower electrode distance and fast response time [11]. The designed micro-channels ensures a laminar flow of electrolyte, containing the organic matter to be oxidized, minimizing the mixing with the oxidant species and consequently avoiding the use of PEM, decreasing then the ohmic resistance [39]. Some works in the literature focused their attention on the critical role of the relationship between the size and electrode distance, demonstrating that μL-MFCs equipped with small electrodes could maximize the performances and minimize the amount of residual fuel [9, 68]. Furthermore, the selection of the most promising anode materials, together with the reduction of device impedance, plays a crucial role to improve the performance of these microscale devices. Qian and Morse [68] studied a carbon cloth anode applied in μL-MFCs with a volume of 4 μL, achieving a power density of 62.5 W/m^3. Lee et al. [9] demonstrates from a fluid dynamic point of view that nano-sized anodes electrodes ensure the best performance of microfluidic devices.

8. Conclusion

The proper selection of anode electrodes and deep study of fluidic distribution inside MFCs play a pivotal role to define the overall devices performance. In particular, several works in the literature demonstrated how the morphology of anode electrodes must be optimized in order to improve the bacteria proliferation on their surface, maximizing then the energy conversion. For this reason, all anode electrodes must satisfy key properties: (1) biocompatibility for microorganisms proliferation; (2) high electrical conductivity and high chemical resistance; (3) high specific area to volume ratio, with pores size of order of some micrometers to enhance bacteria proliferation on electrode surface and to facilitate the diffusion of carbon energy source inside the electrode and (4) cheap production cost. Among all possible materials, carbon-based results to be the most promising ones to be applied as anode in this bioelectrochemical devices. It has also been evidenced that fluid management inside the reactor is of critical importance, since an optimal chemical energy to electrical energy conversion is possible only if proper interactions of fluids (i.e. the electrolyte) and the bioanode are possible.

In this perspective, fluid dynamic modeling is a key tool to design systems with optimized electrolyte/bioanode interfaces. During the last few years, different strategies were implemented to enhance the power output production. Among all them, the optimization of fluid distribution and the reduction of MFC dimensions were employed. Nevertheless, macro-sized MFCs and milliliter-size MFCs show higher output performance, the miniaturization of MFCs to microliter-size (μL-MFCs) resulted to be needed to deeply understand/investigate the relationship and the interconnection among all the biological, chemical and electrical parameters.

Author details

Giulia Massaglia[1,2]* and Marzia Quaglio[1]

*Address all correspondence to: giulia.massaglia@polito.it

1 Center For Sustainable Future Technologies@Polito, Istituto Italiano Di Tecnologia, Torino, Italy

2 Department of Applied Science and Technology (DISAT), Politecnico di Torino, Torino, Italy

References

[1] Akella A, Saini R, Sharma M. Social, economical and environmental impacts for renewable energy systems. Renewable Energy. 2009;**34**:390-396

[2] Kyoto Protocol to the United Nations Framework Convention on Climate Change; 2005. https://unfccc.int

[3] Luther W, Eickensbuch H, Kaiser O, Brand L. Application of Nanotechnologies in the Energy Sector. Wiesbaden, Germany: Hessen Trade and Invest GmbH. 2008

[4] US energy Information Administration (EIA); April 2016

[5] Logan BE, Hamelers B, Reozendal R, Schroeder U, Keller J, Freguia S, Aelterman P, Verstraete W, Rabaey K. Microbial fuel cells: Methodology and technology. Energy and Environmental Science. 2006;**40**:5181-5192

[6] Richter H, McCarthy K, Nevin KP, Johnson JP, Rotello VM, Lovley DR. Electricity generation by *Geobacter sulfurreducens* attached to gold electrodes. Langmuir. 2008;**24**:4376-4379

[7] Bretschger O, Obraztsova A, Sturm CA, Chang IS, Gorby YA, Reed SB, Culley DE, Reardon CL, Barua S, Romine MF, Zhou J, Beliaev AS, Bouhenni R, Saffarini D, Mansfeld F, Kim B-H, Fredrickson JK, Nealson KH. Current production and metal oxide reduction by *Shewanella oneidensis* MR-1 wild type and mutants. Applied and Environmental Microbiology. 2007;**73**:7003-7012

[8] Kim BH, Chang IS, Gadd GM. Challenges in microbial fuel cell development and operation. Applied Microbiology and Biotechnology. 2007;**76**:485-494

[9] Lee J, Lim KG, Tayhas G, Palmore R, Triphati A. Optimization of microfluidic fuel cells using transport principles. Analytical Chemistry. 2007;**79**:7301-7307

[10] Qian F, Morse DE. Miniaturizing microbial fuel cells. Trends in Biotechnology. 2011;**29**: 62-70

[11] Wang HY, Bernarda A, Huang CY, Lee DJ, Chang JS. Micro-sized microbial fuel cell: A mini-review. Bioresource Technology. 2011;**102**:235-243

[12] Qian F, Baum M, Gu Q, Morse DE. A 1.5 mL microbial fuel cell for on-chip bioelectricity generation. Lab on a Chip. 2009;**9**:3076-3081

[13] Larminie J, Dicks A. Fuel Cell Systems Explained. Chichester, West Sussex UK: John Wiley& Sons Ltd; 2013

[14] W. t. f. encyclopedia. https://en.wikipedia.org/wiki/Biofilm [Online]

[15] Babuata J, Renslow R, Lewandowski Z, Beyenal H. Electrochemically active biofilms: Facts and fiction. A review. Biofouling. 2012;**28**:789-812

[16] Hernandez M, Newman D. Extracellular electron transfer. Cellular and Molecular Life Sciences. 2001;**58**:1562-1571

[17] Rabaey K, Boon N, et al. Biofuel cells select for microbial consortia that self-mediate electron transfer. Applied and Environmental Microbiology. 2004;**70**:5373-5382

[18] Rabaey K, Boon N, Siciliano SD, Verhaege M, Verstraete W. Biofuel cells select for microbial consortia that self-mediate electron transfer. Applied and Environmental Microbiology. 2005;**70**:5373-5382

[19] Gorbi e al Y. Electrically conductive bacterial nanowires produced by *Shewanella oneidensis* strain MR-1 and other microorganisms. PNAS. 2006;**103**:11358-11363

[20] Reguera G, McCarthy K, Mehta T, Nicoli JS, Tuominen MT, Lovley DR. Extracellular electron transfer via microbial nanowires. Nature. 2005;**435**:1098-1101

[21] Harnisch F, Aulenta F, Shroeder U. Microbial Fuel Cells and Bioelectrochemical Systems: Industrial and Environmental Biotechnologies Based on Extracellular Electron Transfer. New York: Elsevier; 2011. pp. 644-659

[22] Logan BE. Microbial Fuel Cells. Pennsylvania USA: John Wiley & Sons Inc. Publication; 2008

[23] Rabaey K, Verstraete W. Microbial fuel cells: Novel biotechnology for energy generation. Trends in Biotechnology. 2005;**23**:291-298

[24] Logan BE. Exoelectrogenic bacteria that power microbial fuel cells. Nature Reviews Microbiology. 2009;**7**:375-381

[25] Pant D, Bogaert GV, Diels L, Vanbroekhoven K. A review of the substrates used in microbial fuel cells (MFCs) for sustainable energy production. Bioresource Technology. 2010;**101**:1533-1543

[26] Santoro C, Arbizzani C, Erable B, Ieropoulos I. Microbial fuel cells: From fundamentals to applications. Journal of Power Sources. 2017;**356**:225-244

[27] Bond DR, Holmes DE, Tender LM, Lovley DR. Electrode-reducing microorganisms harvesting energy from marine sediments. Science. 2002;**295**:483-485

[28] Chae KJ, Choi MJ, Lee JW, Kim KY, Kim IS. Effect of different substrates on teh perfromance. Bacterial diversity and bacterial viability in microbial fuel cells. Bioresource Technology. 2009;**100**:3518-3525

[29] Gregory KB, Lovley DR. Remediation and recovery of uranium from contaminated subsurface environments with electrodes. Environmental Science & Technology. 2005;**39**:8943-8947

[30] Wang H, Ren ZJ. Bioelectrochemical metal recovery from wastewater: A review. Water Research. 2014;**66**:219-232

[31] Wang H, Luo H, Fallgren PH, Jin S, Ren ZJ. Bioelectrochemical system platform for sustainable environmental remediation and energy generation. Biotechnology Advances. 2015;**33**:317-334

[32] Li Y, Wu Y, Liu B, Luan H, Vadas T, Guo W, Ding J, Li B. Self-sustained reduction of multiple metals in a microbial fuel cell–microbial electrolysis cell hybrid system. Bioresource Technology. 2015;**192**:238-246

[33] Nancharaiah YV, Venkata Mohan S, Lens PN. Metals removal and recovery in bioelectrochemical systems: A review. Bioresource Technology. 2015;**195**:102-114

[34] Heijne AT, Liu F, Weijden R, Weijma J, Buisman CJN, Hamelers HVM. Copper recovery combined with electricity production in a microbial fuel cell. Environmental Science & Technology. 2010;**44**:4376-4381

[35] Ntagia E, Rodenas P, Ter Heijne A, Buisman CJN, Sleutels T. Hydrogen as electron donor for copper removal in bioelectrochemical systems. International Journal of Hydrogen Energy. 2016;**41**:5758-5764

[36] Kadier A, Kalil MS, Abeshahian P, Chandrasekhar K, Mohamed A, Azman NF, Logrono W, Simayi Y, Hamid AA. Recent advances and emerging challenges in microbial electrolysis cells (MECs) for microbial production of hydrogen and value-added chemicals. Renewable and Sustainable Energy Reviews. 2016;**61**:501-525

[37] Xie X, Hu L, Pasta M, Wells GF, Kong D, Criddle CS, Cui Y. Three-dimensional carbon nanotube-textile anode for high-performance microbial fuel cells. Nano Letters. 2011;**11**:291-296

[38] Liu H, Cheng S, Logan BE. Power generation in fed-batch microbial fuel cells as a function of ionic strength, temperature, and reactor configuration. Environmental Science & Technology. 2005;**39**:5488-5493

[39] Liu H, Logan BE. Electricity generation using an air-cathode single chamber microbial fuel cell in the presence and absence of a proton exchange membrane. Environmental Science & Technology. 2004;**38**:4040-4046

[40] Guo K, Prevoteau A, Patil S, Rabaey K. Engineering electrodes for microbial electrocatalysis. Current Opinion in Biotechnology. 2015;**33**:149-156

[41] Baudler A, Schmidt I, Langner M, Greiner A, Schroder U. Does it have to be carbon? Metal anodes in microbial fuel cells and related bioelectrochemical systems. Energy and Environmental Science. 2015;**8**:2048-2055

[42] Dumas C, Mollica A, Feron D, Basseguy R, Etcheverry L, Bergel A. Marine microbial fuel cell: Use of stainless steel electrodes as anode and cathode materials. Electrochimica Acta. 2007;**53**:468-473

[43] Dumas C, Basseguy R, Bergel A. Electrochemical activity of *Geobacter sulfurreducens* biofilms on stainless steel anodes. Electrochimica Acta. 2008;**53**:5235-5241

[44] Ter Heijne A, Hamelers HVM, Saakes M, Buisman CJN. Performance of non-porous graphite and titanium-based anodes in microbial fuel cells. Electrochimica Acta. 2008;**53**:5697-5703

[45] Crittenden SR, Sund CJ, Sumner JJ. Mediating electron transfer from bacteria to a gold electrode via a self-assembled monolayer. Langmuir. 2006;**22**:9473-9476

[46] Wei J, Liang P, Huang J. Recent progress in electrodes for microbial fuel cells. 2011;**102**:9335-9344

[47] Santoro C, Gulizzoni M, Baena JPC, Pasaogullari U, Casalegno A, Li B, Babanova S, Artyushkova K, Atanassov P. The effects of carbon electrode surface properties on bacteria attachment and start up time of microbial fuel cells. Carbon. 2014;**67**:128-139

[48] Min B, Logan BE. Continuous electricity generation from domestic wastewater and organic substrates in a flat plate microbial fuel cell. Environmental Science & Technology. 2004;**38**:5809-5814

[49] Sun JJ, Zhao HZ, Yang QZ, Song J, Xue A. A novel layer-by-layer selfassembled carbon nanotube-based anode, preparation, characterization, and application in microbial fuel cell. Electrochimica Acta. 2010;**55**:3041-3047

[50] Wang X, Cheng SA, Feng YJ, Merril MD, Saito T, Logan BE. Use of carbon mesh anodes and the effect of different pretreatment methods on power production in microbial fuel cells. Environmental Science & Technology. 2009;**43**:6870-6874

[51] Cheng S, Logan BE. Ammonia treatment of carbon cloth anodes to enhance power generation of microbial fuel cells. Electrochemistry Communications. 2007;**9**:492-496

[52] Chaudhuri SK, Lovley DR. Electricity generation by direct oxidation of glucose in mediatorless microbial fuel cells. Nature Biotechnology. 2003;**21**:1229-1232

[53] Aelterman P, Versichele M, Marzorati M, Boon N, Verstraete W. Loading rate and external resistance control the electricity generation of microbial fuel cells with different three-dimensional anodes. Bioresource Technology. 2009;**99**:8895-8902

[54] Di Lorenzo M, Scott K, Curtis TP, Head IM. Effect of increasing anode surface area on the performance of a single chamber microbial fuel cell. Chemical Engineering Journal. 2010;**156**:40-48

[55] Li FX, Sharma Y, Lei Y, Li BK, Zhou QX. Microbial fuel cells: The effects of configurations, electrolyte solutions, and electrode materials on power generation. Applied Biochemistry and Biotechnology. 2010;**160**:168-181

[56] Rabaey K, Clauwaert P, Aelterman P, Verstraete W. Tubular microbial fuel cells for efficient electricity generation. Environmental Science & Technology. 2005;**39**:8077-8082

[57] Li S, Cheng C, Thomas A. Carbon-based microbial fuel cell electrodes: From conductive supports to active catalysts. Advanced Materials. 2017;**29**:1602547

[58] Santoro C, Babanova S, Artyushkova K, Cornejo JA, Ista L, Bretschger O, Marsili E, Atanassov P, Schuler AJ. Influence of anode surface chemistry on microbial fuel cell operation. Bioelectrochemistry. 2015;**106**:141-114

[59] Sonawane JM, Yadav A, Ghosh PC, Adeloju SB. Recent advances in the development and utilization of modern anode materials for high performance microbial fuel cells. Biosensors and Bioelectronics. 2017;**90**:558-576

[60] Liang Y, Feng H, Shen D, Li N, Guo K, Zhou Y, J X, Chen W, Jia Y, Huang B. Enhancement of anodic biofilm formation and current output in microbial fuel cells by composite modification of stainless steel electrodes. Journal of Power Sources. 2017;**342**:98-104

[61] Cheng S, Liu H, Logan BE. Increased performance of single-chamber microbial fuel cells using an improved cathode structure. Electrochemistry Communications. 2006;**8**:489-494

[62] Logan BE. Scaling up microbial fuel cells and other bioelectrochemical systems. Applied Microbiology and Biotechnology. 2010;**85**:1665-1671

[63] ElMekawy A, Hegab HM, Dominiguez-Benetton X, Pant D. Internal resistance of microfluidic microbial fuel cell: Challenges and potential opportunities. Bioresource Technology. 2013;**142**:672-682

[64] Kim JR, Bohani HC, Amini N, Zinsou K, Michie I, Dinsdale RM, Guwy A, Guo Z, Premier G. Porous anodes with helical flow pathways in bioelectrochemical systems: The effects of fluid dynamics and operating regimes. Journal of Power Sources. 2012;**213**:382-390

[65] Massaglia G, Gerosa M, Agostino V, Cingolani A, Sacco A, Saracco G, Margaria V, Quaglio M. Fluid dynamic modeling for microbial fuel cell based biosensor optimization. Fuel Cell. 2017;**17**:627-634

[66] Ringeisen BR, Henderson E, Wu PK, Pietron J, Ray R, Little B, Biffinger JC, Jones-Meehan JM. High power density from a miniature microbial fuel cell using *Shewanella oneidensis* DSP10. Environmental Science & Technology. 2006;**40**:2629-2634

[67] Fan YZ, Hu H, Liu H. Enhanced Coulombic efficiency and power density of air-cathode microbial fuel cells with an improved cell configuration. Journal of Power Sources. 2007;**171**:348-354

[68] Qian F, Morse DE. Miniaturizing Microbial Fuel Cells.Trends in Biotechnology. 2011;**29**:62-69

Chapter 6

The Bioenergy Potentials of Lignocelluloses

Olatunde Samuel Dahunsi and Munachi Enyinnaya

Additional information is available at the end of the chapter

http://dx.doi.org/10.5772/intechopen.79109

Abstract

Lignocellulosic biomass is abundant resources accrued from agricultural, municipal and other sources. Their high fermentable carbohydrate contents make them suitable candidates for bioenergy generation. The global increase in the generation of these resources is phenomenal, thus culminating in huge environmental disasters with its attendant global warming and climate change menace. Their improper management has equally been reported to cause several environmental challenges such as water, land and air pollution and the spread of pathogenic organisms which causes diverse diseases within the human and animal population. However, the proper and adequate management/utilization of these materials can improve human's living standards as well as ensuring environmental protecting via the production of environmental-friendly biofuels. In this regard, research on the use of lignocellulosic biomass as alternative energy feedstock to fossil fuels has gained considerable attention over the last few decades majorly because of their abundance and significant roles in greenhouse gas emissions reduction.

Keywords: agriculture, bioenergy, biomass, environment, pollution, resources

1. Introduction

Man has continued to exploit different sources of energy such as energy stored in plant either by burning as fuel or consuming plants for nutritional purposes. There is no doubt that energy can be converted from one form to the other and it is essential to life. However, the transformation of biomass to fossil fuel takes a long period of time and is non-renewable within the period man can utilize it. Several sources have been exploited for renewable and sustainable energy production for a short period of time [1, 2]. The hazard of fossil fuel on the environment especially in terms of greenhouse gas emission has led to the increase in demand for clean and sustainable energy. The utilization of renewable sources of energy for

bioenergy production is a possible option in order to meet this demand. A vital point to take cognizance of is the possibility of using multiple streams of raw materials. Plant biomass is one renewable source of energy as they contain the most abundant organic material which is lignocellulose and can be considered as a credible source for bioenergy production [3]. Sadly, energy from most biomass residue is harnessed directly through combustion which is not an efficient and sustainable means. The conversion of lignocellulosic raw material to bioenergy should involve advance technologies rather than combustion in order to avoid environmental degradation [4]. The most valuable biomass sources for energy production are agricultural crops and their residues, woody plants, waste from food processing and aquatic plants [5].

Lignocellulosic biomass is structurally composed of hemicellulose, cellulose and lignin, however the complex and recalcitrant nature of lignin limits degradability by hindering enzymatic actions for energy production [6–11]. Although, lignocellulosic structure can be altered using various methods of pretreatment to break the bonds between polysaccharides and lignin which in turn aid the degradable cellulose and hemicellulose accessible for enzymatic action. Lignin which is the third most abundant polymer in nature can be removed from lignocellulosic materials using chemical pretreatment leading to an increased internal surface area, biomass enlargement and increased actions of cellulases. Although not all pretreatment brings about an ample amount of delignification, sometimes modification may occur in the structure of lignin without pretreatment which may be due to alteration in the chemical properties [12].

The yearly worldwide primary production of biomass is around 220 billion tones on the basis of dry mass which is equal to 4500EJ of energy derived from the sun annually [13]. An estimated amount of energy which is about 30EJ per year is obtained from forest and agricultural wastes in contrast to a yearly global energy requirement of more than 400EJ. Hence, the cultivation of energy crops for energy production has to be considered and encouraged in large scale. Several factors are considered when selecting good energy yielding plants and these include atmospheric and soil condition, drought resistance, minimal nutrient requirements, high production rate of biomass per hectare, minimal energy input etc. [14]. Bioenergy production can improve income rate of farmers by utilizing the byproducts from processing or storage and also contribute to rural development as energy independence, climate change and rural development are the principal drivers for promotion and application of bioenergy [15].

This focus of this paper is to address the terrestrial sources of lignocellulosic materials that can be utilized for bioenergy production, evaluate the various biofuels that can be produced from lignocellulosic feedstock and to further examine the vice and virtue of biofuel commercialization, utilization and production.

2. Terrestrial sources of lignocellulosic materials for bioenergy production

The major sources of lignocellulosic raw materials that can be exclusively utilized as feedstock for bioenergy are as follow:

1. Agricultural residue

2. Municipal solid waste
3. Woodland trees
4. Dry energy grasses

2.1. Agricultural residue

Agricultural residues are the most economic and abundant organic waste which can biologically converted to biofuels and they provides about 5% of the average amount of biomass energy [16]. They include by-products of agricultural processes such as straw, stover, bagasse, cobs, stalks, husks, etc. all of which are basically lignocellulosic in nature [17]. Although a large amount of these materials are annually produced globally but not adequately utilized [18]. Usage of these materials has been on the increase in the last few decades majorly due to the "food versus energy" debate in which most research endeavors now seek ways of producing fuels from energy crops and wastes as against the earlier practice of producing energy from food crops. Agricultural waste also includes field and processing wastes which can be utilized for bioenergy production [19, 20]. A major problem involved with utilization of agricultural waste however is the efficiency and strategy of collection. Most methods of collection involve multiple transfer of equipment over fields during which about half of the biomass is lost [21]. Yusoff [22] reported that the biomass energy potentials from the processing of wood and palm oil were about 280 TJ and 250 TJ, respectively. In another study, Peterson [23] reported the potential bioethanol and biogas production from winter rye, oilseed rape and faba bean to be 66, 70 and 52%, respectively while methane production is 0.36, 0.42 and 0.44 l g^{-1} volatile solids, respectively. Among most agricultural materials, wheat straw has the highest potential as energy feedstock and is therefore being exploited in the industrial production of bioethanol. Similarly, rice straw has been largely used in global bioethanol production. It has been estimated that up to49.1 gallons $year^{-1}$ of global ethanol can be generated from73.9 Tg dry rice straw which is usually wasted during harvest. In total, lignocellulosic raw materials could generate up to 442 gallons $year^{-1}$ of bioethanol. Hence, the total potential generation of bioethanol from crop residues and wasted crops is higher than the world's current ethanol generation. Bagasse which is a by-product from sugarcane processing can potentially generate about 3.6% of world electricity and 2.6EJ of steam. In summary, the potential bioethanol generation agricultural resources could reduce about 32% of the global gasoline consumption when given priority [24].

2.2. Municipal solid waste

Municipal solid wastes also known as trash or garbage generally contains the usual items which includes food scraps, newspapers, furniture, grass clippings, clothing etc. These wastes can be in solid or semi-solid form and can be biodegradable, for example, food waste, green waste and paper [25]. Every person on the planet contributes about 250 kg of municipal solid waste annually [26]. In several nations, the waste is sorted into different components, which in turn enables the biodegradable portion of the waste stream also containing lignocellulosic products like papers, kitchen waste and garden trash be transformed into biofuels. The assorted variety in the municipal solid waste does not make it a perfect feedstock. In any case,

it might be valuable in districts where more ideal raw materials are absent or rare. For instance, with the advances in cellulosic ethanol technologies, the Mediterranean could utilize the cellulosic constituent of municipal solid waste as a transportation fuel feedstock and at the same time decrease externalities related with land filling [27]. Some conversion technologies like pyrolysis may involve combustion of municipal solid waste before conversion to energy [28].

2.3. Woodland trees

The capacity of forest as a source of energy is expanding globally. The utilization of woody biomass for power, heat and transportation can stimulate the area of forestry and make the bond closer to energy sector territorially and globally. However, the over-usage of forest ecosystems can put at risk the sustainable improvement of forest and communities dependent on forest. Thus, forest energy strategies must be founded on the guideline of sustainable development which guarantees economic stability, environmental cleanliness and durability in the utilization of the raw material [27]. The potential flow of woody raw materials for bioenergy from forests is not definitely known and should be checked before policy intervention can be effectively executed with regards to global concession on climate change [29].

A large amount of cellulose rich biomass for bioenergy and biopolymer generation can be obtained from fast growing, short-rotation forest trees like *Eucalyptus* and *Populus* [30]. Wood and wood wastes provides about three fifths of the average amount of biomass energy. Sawdust, board ends and barks which are wastes from wood processing and forest products industry are now widely employed for energy production. This sector is partially involved in electrical power generation by the combustion of waste [6]. Energy schemes are complicated and include various factors that must be stated, including socio-economic advantages, climate change mitigation, technological effectiveness the interaction among industries and policies [12]. Researchers have made different investigations for the purpose of assessing the chances of forest energy to mitigate climate change and concluded that the technical potential of primary biomass energy obtained from the forest sector would be 12–74 EJ while the economic potential would only be 1.2–14.8EJ. Woody biomass utilized for production of energy must have the capacity to contend with different utilizations like pulp and paper. In the meantime, the energy generated from biomass must be less expensive than that created from contending energy sources [27]. The theoretical potential of the global excess wood supply in 2050 has been estimated to be 6.1 Gm^3 (71 EJ) and the technical potential to be 5.5 Gm^3 (64 EJ) on the basis of a medium demand and plantation scheme. Based on medium scale scheme, the bioenergy potential from logging, processing residues and waste was assessed to be equal to 2.4 $Gm^3\ year^{-1}$ (28 EJ $year^{-1}$) wood [31]. Hypothetically, this shows that forests can be a considerable source of bioenergy and can be utilized without further deforestation and without jeopardizing the supply of wood.

2.4. Dry energy grasses

Perennial grasses have been broadly utilized as fodder crops for a considerable length of time, regularly contributing fundamentally to energy supply. The four most studied perennial rhizomatous grasses are *Panicum virgatum*, *Miscanthus* species, *Phalaris arundinacea* and

Arundodonax [32]. The use of *Miscanthus* as an energy grass has attracted attention among the perennial C4 grasses since it has been identified as a perfect energy grass and produces maximally when harvested dry. Yields of 3–10 years old plantations grown in two countries in Europe are 113–30 t/ha. This means that if a yield of 20 t/ha could be achieved; it would produce a total energy yield that is equal to 7 t/ha of oil over the life of each harvest. Switch grass has an energy value that is similar to wood yet with minimal water content [3]. After proper investigation of some crops which were perennial grasses, switch grass was observed to produce the highest potential [11]. Other than staying away from the competition between food and fuel crop usage, they are considered to have energy, financial, and ecological advantages over food crops for certain bioenergy products [10]. These grasses possess qualities and prospects as for their utilization and enhancement as lignocellulosic feedstock. In order to meet up to the large demand of biomass supply, an extensive environmental capacity is to be considered which marginal soils are included [33]. Another nutrient rich grass is Napier grass (*Pennisetum purpureum*), a grass that grows in the tropics and can withstand dry conditions. It has 30.9% total carbohydrates, 27% protein, 14.8% lipid 14.8%, and 9.1% fiber (dry weight). Thus, it is cultivated for livestock as energy crops and it is easy to cultivate with a high productivity rate of 87 ton/ha/year [32]. Sawasdee and Pisutpaisal [34] reported the feasibility of biogas production from Napier grass and observed that the methane content, yield and production rate were 53%, 122.4 mL CH 4/g TVS remove, 4.8 mL/hr. at the optimum condition.

3. Biofuels from lignocellulosic raw materials

3.1. Biobutanol

Due to the compelling need for alternatives to fossil fuel and increasing concern for environmental and health safety, biobutanol which is a second generation biofuel is now produced as a credible substitute for fossil fuel used as a blend with gasoline. Although butanol is still generated through petrochemical methods, the high demand, depletion rate and price of oil has driven the search for a sustainable source for butanol production. Biobutanol possess some better attributes which includes higher energy content, lower Reid vapor pressure, easy blending with gasoline at any ratio and ease in transportation when compared to bioethanol. Various challenges involved in lignocellulosic butanol production includes method of pretreatment, generation of unwanted solvents and the production cost, low butanol tolerance of microbes resulting in low yield, cost of raw materials. In order to enhance biobutanol production from lignocellulosic raw materials, methods in terms of inhibitors detoxification, strains improvement and process integration and optimization are be dealt with [35].

3.2. Bioethanol

Bioethanol is a first generation biofuel and is mainly produced by enzymatic fermentation using yeast to digest biodegradable raw materials with high energy content. Hydrolysis is employed when raw materials such as high energy yielding crops are utilized; this is done to breakdown the complex nature of the polymer into monomers such as simple sugar followed

by conversion of the sugar to alcohol after which distillation and dehydration are used to reach the desired amount that can be utilized directly as fuel [36]. Bioethanol contributed more than 30% of the total ethanol production globally in 2006 with a significant production rate from Asia [35]. Ethanol can be mixed with petrol if appropriately purified and when utilized in modified spark ignition engines, production of toxic environmental gases will be reduced. A liter of ethanol can yield about three fifths of the energy provided by a liter of gasoline [37]. The large scale production of sugar cane in Brazil is dedicated for alcohol and sugar production. Utilization of alcohol as fuel for vehicular engines has been in existence in Brazil since 1973. The increasing demand for alcohol in Brazil led to an increase in sugar cane production in the last 5 years in Brazil [38].

3.3. Biodiesel

In 1900 during the world exhibition in Paris, a diesel engine created by the first inventor of its kind ran on 100% peanut oil and years later the inventor stated that "the diesel engine can be fed with vegetable oils and would help considerably in the development of agriculture of the countries which use it". In 1912 Dr. Rudolf Diesel who is the actual inventor of the diesel engine stated that "The use of vegetable oils for engine fuels may seem insignificant today, but such oils may become in course of time as important as petroleum and the coal tar products of the present time". This hypothesis is gradually becoming significant in recent days because there is a global need for sustainability and energy security. The possibility of biodiesel replacing fossil fuels as main source for power is one reason for the global research of biodiesel [39]. Biodiesel is another example of a first generation biofuel and can be produced directly from vegetable oils and other oleo chemicals via trans-esterification methods or cracking. The Trans-esterification procedure may utilize acid, enzymes and alcohol to yield the biodiesel and glycerin as by-product [40]. Oleo chemicals are chemical substances produced from fats and natural oils, they are basically fatty acids and glycerol. Hypothetically, oleo chemicals are better substitute for petrochemicals in terms of sustainability and economic viability [41]. The high price rate of biodiesel is a major constraint to its commercialization in contrast with petroleum, thus the utilization of waste oil should be considered since it is relatively available and cheap [42]. Utilization of biodiesel as a fuel is considered to have a minimal or no release of carbon dioxide since any carbon dioxide released from its combustion was beforehand caught from the atmosphere during the development of the crop used as feedstock for the generation of biodiesel. Biodiesel is considered to have a minimal flash point than gasoline derived diesel, thus its transport is more secure and efficient [43, 44]. Operationally biodiesel blends performs similarly to the conventional diesel without causing any noticeable change in the engine due to the similarity in properties of biodiesel and conventional diesel [45]. This makes biodiesel an efficient replacement for conventional diesel.

3.4. Biogas

Biogas is produced from the anaerobic digestion of biodegradable organic materials which includes lignocellulosic biomass, animal dung, carcass etc. Biogas contains methane, carbon dioxide which occupy a significant amount in terms of volume and other gases which include hydrogen sulfide and nitrogen gas [46]. Sweden is one of the pioneers of biogas production

considering waste-based biogas technology [47]. The total potential for biogas production in Sweden is around 15 TWh per year and more than half comes from agricultural residues. About 5.8 TWh of the potential from agriculture is derived from straw as a feedstock [48]. Recently, this technology has gained so much attention and several researches are conducted regarding this technology. The multi-functional nature of this technology is one reason for its rapid expansion [48–50]. Methane which is the main energy product is generated in the final process of anaerobic digestion called methanogenesis. Naturally, methane is produced in environs such as peats, marshland, sediments and rumen [51]. Methane which is the most useful component of biogas can be utilized for the production of heat and electricity or through purification and enhancement to be utilized as vehicle fuel. Lignocellulosic materials are the most promising substrate for biogas production due to their relative abundance. Several assays have been made to ensure increase in the efficiency of biogas production using lignocellulosic feedstocks including different pretreatment techniques and codigestion with nutrient rich feedstock. However, little is known about the microbes responsible for the digestion of cellulose during biogas production. In 2014, 158 TWh biogas per year was generated from more than 14,500 biogas plants actively utilized within the European Union (EU). Germany, United Kingdom and Italy are known to have the highest primary production of biogas, which are 79.5, 21.6 and 21.5 TWh per year, respectively. In Germany, biogas production from maize, other energy crops, slurry and miscellaneous organic waste are 60, 16, 12 and 8%, respectively [48]. Even with the advancement in this technology thus far, generation and utilization of biogas is still not adequate. The industry is still young and going through challenges of low profit margins and slow return on investment [47].

3.5. The virtue and vice of biofuel commercialization, utilization and production

Recently, biofuels and gasoline have become equals in terms of cost but the total cost of benefit using biofuel is higher. Energy independence and economic stability is a major concern for any developing country and crude oil is scarcely deposited globally and developing countries without this "liquid gold" may experience a huge dent in economy if the crude oil is imported. If the use of biofuel is encouraged, countries will reduce their dependence on fossil fuel hereby creating control on monopoly of fossil rich states and also new jobs will be created with a growing biofuel industry, thus creating economic security and a less toxic environment. However some challenges associated with biofuel commercialization, utilization and production includes "food vs. fuel "crisis, future increase in price due to high demand, policies such as tax credit on production of biofuels and land use change and high cost of production which includes technology cost [8, 37, 46].

4. Conclusion

Lignocellulosic materials are viable sources of bioenergy and their usage as energy sources can play a vital role in helping the industrialized regions of the world reduce the environmental hazards of burning fossil fuel. Therefore, utilization of lignocellulosic materials as sources of energy should be promoted as one of the major routes for bioenergy production.

Acknowledgements

The authors appreciate the support of our technical staff.

Conflicts of interest

Authors declare no conflict of interest.

Funding

This work received funding from Ton DucThang University, Ho Chi Minh City, Vietnam.

Author details

Olatunde Samuel Dahunsi[1,2]* and Munachi Enyinnaya[2]

*Address all correspondence to: dahunsi.olatunde.samuel@tdt.edu.vn

1 Faculty of Environment and Labour Safety, Ton DucThang University, Ho Chi Minh City, Vietnam

2 Biomass and Bioenergy Group, Environment and Technology Research Cluster, Landmark University, Nigeria

References

[1] Sambusiti C, Ficara E, Rollini M, Manzoni M, Malpei F. Sodium hydroxide pretreatment of ensiled sorghum forage and wheat straw to increase methane production. Water Science and Technology. 2012;**66**:2447-2452

[2] Dahunsi SO, Oranusi US. Co-digestion of food waste and human excreta for biogas production. British Biotechnology Journal. 2013;**3**(4):485-499

[3] Petersson A, Thomsen MH, Hauggaard-Nielsen H, Thomsen AB. Potential bioethanol and biogas production using lignocellulosic biomass from winter rye, oilseed rape and faba bean. Biomass and Bioenergy. 2007;**31**:812-819

[4] Montingelli ME, Benyounis KY, Quilty B, Stokes J, Olabi AG. Optimisation of biogas production from the macroalgae*Laminaria sp*. at different periods of harvesting in Ireland. Applied Energy. 2016;**177**:671-682

[5] Ghasimi DSM, Zandvoort MH, Adriaanse M, van Lier JB, de Kreuk M. Comparative analysis of the digestibility of sewage fine sieved fraction and hygiene paper produced from virgin fibers and recycled fibers. Waste Management. 2016;**53**:156-164

[6] Dahunsi SO, Oranusi S, Owolabi JB, Efeovbokhan VE. Mesophilic anaerobic co-digestion of poultry droppings and *Carica papaya* peels: Modelling and process parameter optimization study. Bioresource Technology. 2016;**216**:587-600

[7] Dahunsi SO, Oranusi S, Owolabi JB, Efeovbokhan VE. Comparative biogas generation from fruit peels of fluted pumpkin (*Telfairiaoccidentalis*) and its optimization. Bioresource Technology. 2016;**221**:517-525

[8] Dahunsi SO, Oranusi S, Owolabi JB, Efeovbokhan VE. Synergy of Siam weed (*Chromolaenaodorata*) and poultry manure for energy generation: Effects of pretreatment methods, modeling and process optimization. Bioresource Technology. 2017;**225**:409-417

[9] Dahunsi SO, Oranusi S, Efeovbokhan VE. Optimization of pretreatment, process performance, mass and energy balance in the anaerobic digestion of *Arachishypogaea* (peanut) hull. Energy Conversion and Management. 2017;**139**:260-275

[10] Dahunsi SO, Oranusi S, Efeovbokhan VE. Cleaner energy for cleaner production: Modeling and optimization of biogas generation from *Carica papayas* (pawpaw) fruit peels. Journal of Cleaner Production. 2017;**156**:19-29

[11] Dahunsi SO, Oranusi S, Efeovbokhan VE. Bioconversion of *Tithoniadiversifolia* (Mexican sunflower) and poultry droppings for energy generation: Optimization, mass and energy balances, and economic benefits. Energy and Fuels. 2017;**31**:5145-5157

[12] Agbor VB, Cicek N, Sparling R, Berlin A, Levin DB. Biomass pretreatment: Fundamentals toward application. Biotechnology Advances. 2011;**29**:675-685

[13] Hall DO, Rosillo-Calle F. Biomass - Other than Wood. In Survey of Energy Resources. 18th ed. London; World Energy Council; 1998. pp. 227-241

[14] McKendry P. Energy production from biomass (part 1): Overview of biomass. BioresourceTechnology. 2002;**83**:37-43

[15] Luque R, Herrero-Davila L, Campelo JM, Clark JH, Hidalgo JM, Luna D, Romero AA. Biofuels: A technological perspective. High Energy Density Physics. 2008;**1**(5):542-564

[16] Demirbas A, Ozturk T, Demirbas MF. Recovery of energy and chemicals from carbonaceous materials. Energy Sources, Part A: Recovery, Utilization, and Environmental Effects. 2006;**28**:1473-1482

[17] Mtui GYS. Recent advances in pretreatment of lignocellulosic wastes and production of value added products. Africa Journal of Biotechnology. 2009;**8**(8):1398-1415

[18] Kim S, Dale BE. Global potential bioethanol production from wasted crops and crop residues. Biomass and Bioenergy. 2014;**26**:361-375

[19] Sasaki N, Knorr W, Foster DR, Etoh H, Ninomiya H, Chay S. Woody biomass and bioenergy potentials in Southeast Asia between 1990 and 2020. Applied Energy. 2009;**86**:S140-S150

[20] Mizrachi E, Mansfield SD, Myburg AA. Cellulose factories: Advancing bioenergy production from forest trees. New Phytology. 2012;**194**:54-62

[21] Smeets E, Faaij A. Bioenergy production potentials from forestry to 2050. Climatic Change; in press. 2006

[22] Yusoff S. Renewable energy from palm oil -innovation on effective utilization of waste. Journal of Cleaner Production. 2004;**14**:87-93

[23] Domac J, Richards T, Risovic S. Socioeconomic drivers in implementing bioenergy projects. Biomass and Bioenergy. 2005;**28**(2):97-106

[24] Barker T, Bashmakov I, Bernstein L, Bogner J, Bosch P, Dave R, Zhou D. Technical summary. In *Climate change 2007: Mitigation*. In: Metz B, Davidson OR, Bosch PR, Dave R, Meyer LA, editors. Contribution of Working Group III to the Fourth Assessment Report of the Intergovernmental Panel on Climate Change. Cambridge, UK and New York, NY, USA: Cambridge University Press; 2007. pp. 541-584

[25] Kwon E, Westby KJ, Castaldi MJ. Transforming municipal waste (MSW) into fuel via gasification/pyrolysis process. In: Proceedings of the 18th Annual North American Waste-To-Energy Conference, NAWTEC18, Orlando, Florida, USA. 2010

[26] Li A, Antizar-Ladislao B, Kharisheh M. Bioconversion of municipal solid waste to glucose for bioethanol production. Bioprocess and Biosystems Engineering. 2007;**30**:189-196

[27] Al-Salem S, Lettieri P, Baeyens J. Recycling and recovery routes of plastic solid waste (PSW): A review. Waste Management. 2009;**29**:2625-2643

[28] Seltenrich N. Emerging waste-to-energy technologies: Solid waste solution or DeadEnd. Environmental Health Perspectives. **124**(6)

[29] Lewandowski I, Scurlock JMO, Lindvall E, Christou M. The development and current status of perennial rhizomatous grasses as energy crops in the US and Europe. Biomass and Bioenergy. 2003;**25**:335-361

[30] Cherney JH, Johnson KD, Volenec JJ, Kladivko EJ, Greene DK. Evaluation of Potential Hebaceous Biomass Crops on Marginal Crop Lands: (1) Agronomic Potential. Oak Ridge, TN: Oak Ridge National Laboratory; 1990. pp. 37831, 43-36285

[31] van der Weijde T, Kamei CLA, Torres AF, Vermerris W, Dolstra O, Visser RGF, Trindade LM. The potential of C4 grasses for cellulosic biofuel production. Frontiers in Plant Science. 2013;**4**:107

[32] Sawasdee V, Pisutpaisal N. Feasibility of biogas production from Napier grass. Energy Procedia. 2014;**61**:1229

[33] Morone A, Pandey RA. Lignocellulosicbiobutanol production: Gridlocks and potential remedies. Renewable and Sustainable Energy Reviews. 2014;**37**:21-35

[34] Dahunsi SO, Oranusi S, Efeovbokhan VE. Anaerobic mono-digestion of *Tithoniadiversifolia* (wild Mexican sunflower). Energy Conversion and Management. 2017;**148**:128-145

[35] Larson ED. Biofuel production technologies: status, prospects and implications for trade and development. Report No. UNCTAD/DITC/TED/2007/10. United Nations Conference on Trade and Development, New York and Geneva; 2008

[36] IEA. Biofuels for transport e an international perspective. International Energy Agency (IEA), http://www.iea.org/textbase/nppdf/free/2004/biofuels2004.pdf; 2004

[37] Barakat A, Monlau F, Solhy A, Carrere H. Mechanical dissociation and fragmentation of lignocellulosic biomass: Effect of initial moisture, biochemical and structural proprieties on energy requirement. Applied Energy. 2015;**142**:240-246

[38] Samuel NM, Santos RF, Fracaro GPM. Potential for the production of biogas in alcohol and sugar cane plants for use in urban buses in the Brazil, World renewable energy congress 2011, Sweden. pp. 418-424

[39] Owolabi RU, Adejumo AL, Aderibigbe AF. Biodiesel: Fuel for the future (a brief review). International Journal of Energy Engineering. 2012;**2**:223-231

[40] Nigram PS, Singh A. Production of liquid biofuels from renewable resources. Progress in Energy and Combustion Science. 2011;**37**:52-68

[41] Naik SN, Goud VV, Rout PK, Dalai AK. Production of first and second generation biofuels: A comprehensive review. Renewable and Sustainable Energy Reviews. 2010;**14**:578-597

[42] Zhang Y, Dube MA, McLean DD, Kates M. Biodiesel production from waste cooking oil: Economic assessment and sensitivity analysis. Bioresource Technology. 2003;**90**:229-240

[43] Demirbas A. Progress and recent trends in biodiesel fuels. Energy Conversion and Management. 2009;**50**:14-34

[44] Bajpai D, Tyagi VK. Biodiesel: Source, production, composition, properties and its benefits. Journal of Oleo Science. 2006;**55**:487-502

[45] Saravanan SV, Suresh L, Shankar KP, Veeramani R, Malarvannan S. Evaluate & analysis of single cylinder diesel engine by using sesame oil blend's with diesel. Journal of Engineering. 2014;**4**(3):38-42

[46] Ošlaj M, Muršec B. Biogas as a renewable energy source. Tech Gaz. 2010;**17**:109-114

[47] Li C. Biogas Production from Lignocellulosic Biomass: Impact of Pre-Treatment, Co-Digestion, Harvest Time and Inoculation. Lund: Lund University; 2017

[48] Sun L. Biogas Production from Lignocellulosic Biomass Materials. Uppsala, Sweden: Swedish University of Agricultural Sciences; 2015

[49] Weiland P. Biogas production: Current state and perspective. Applied Microbiology and Biotechnology. 2010;**85**(4):849-860

[50] Holm-Neilsen JB, Al Seadi T, Oleskwowicz-Popiel P. The future of anaerobic digestion and biogas utilization. Bioresource Technology. 2009;**100**(22):544785484

[51] Lowe DC. Global change: A green source of surprise. Nature. 2006;**439**(7073):148-149

Chapter 7

Free-Piston Stirling Engine Generators

Songgang Qiu and Laura Solomon

Additional information is available at the end of the chapter

http://dx.doi.org/10.5772/intechopen.79413

Abstract

Free-Piston Stirling Engines (FPSEs) have recently attracted attention as a promising energy conversion technology because of their desirable characteristics such as high efficiency, high reliability, and easy and quiet operation. FPSE are truly a closed cycle system that works using variations in the internal pressure to drive the power piston that is connected to the reciprocating magnets in a linear alternator for energy conversion. The lack of manual linages and the use of clearance seals in a FPSE increase both the system's reliability and lifespan, as there is no contact or wear on the seals. These desirable attributes coupled with the fuel independence of FPSE makes them ideal candidates for use in remote power generation applications, particularly where maintenance is a high concern such as in NASA deep space missions, solar power generator, and combined heat and power systems. This chapter presents an introduction to FPSE along with a brief review of the underlying thermodynamics and Stirling cycle analysis. The general engineering analysis and numerical modeling approaches of Stirling engines will be discussed, followed by a section of engine design and efficiency calculations.

Keywords: free-piston Stirling engine, additive manufacturing, energy conversion, regenerator, heater head, CFD, thermal conduction losses, design optimization

1. Introduction

The continuing depletion of fossil fuel resources has led to the increase of global research into sustainable energy. This has resulted in the resurrection of the forgotten Stirling engine which is an external combustion engine unlike the more widely known Otto and Diesel engines which are internal combustion engines. One application where FPSE are gaining interest is in combined heat and power (CHP) because of its operation on a closed cycle, FPSE can be run on a variety of fuels such as solar [1], biogas [2], natural gas [3], waste gas [4] etc. Although

patented in 1816 by Robert Stirling, it would take the better part of a century for scientist to fully understand its complex physics [1]. The key to the high efficiency of the Stirling engine is what Stirling called an economizer but it more commonly referred to today as a regenerator [2]. The regenerator acts as a solid storage medium between the hot and cold heat exchangers. This allows for a reduction in the total amount of thermal energy input to the engine leading to an increase in the cycle efficiency. However, despite its numerous attractive qualities, historically the Stirling engine was replaced by theoretically inferior engines due to performance limitations resulting from the available materials of the time. The limitation on operating temperature is highly detrimental to the performance of a Stirling engine because the cycle efficiency is dependent on the temperature ratio and not the pressure ratio like in the Otto or Diesel cycles. However, the development of modern high-temperature superalloys has drastically increased the operational temperature of Stirling engines to nearly 1200 K. Research is ongoing to use cutting-edge manufacturing techniques such as additive manufacturing of metals to further increase the efficiency, improve the reliability, and reduce the manufacturing cost of the next generation of Stirling engines.

2. Thermodynamic cycle

An ideal Stirling cycle consists of four stages: (1) the working fluid, typically air, helium, or hydrogen, undergoes an isothermal expansion; (2) a constant-volume heat; (3) isothermal compression; and (4) constant volume heat addition. Regenerators play an important role in the cycle, as the heat stored in the regenerator during the early stage is recovered by the gas in the fourth stage. The efficiency of an ideal Stirling cycle approaches that of a Carnot cycle which depends only on the hot and cold temperatures. However, it is impossible to achieve an ideal cycle in a real system, and the actual efficiency of a Stirling engine is lower than the theoretical Carnot efficiency. State of the art Stirling engines have efficiencies near 40%.

3. Types of Stirling engines

The mechanical configurations of Stirling engines are generally divided into three groups: alpha, beta, and gamma [2]. In the alpha configuration the engine consists of two pistons that are housed in separate cylinders which are connected by the hot heat exchanger, regenerator, and cold heat exchanger. For alpha engines the pistons also act as the displacers. Both the beta and gamma engines have separate power pistons and fluid displacers. For the beta configuration the displacer and power piston are housed in the same cylinder. In gamma engines however, the power piston and displacer are in separate cylinders which leads to gamma type engines being physically larger than beta engines. Because of their compact multi-cylinder configuration, alpha type engines were explored by the automotive industry as high specific power outputs are possible [2].

In addition to different physical configurations, Stirling engines can further be divided into two groups based on their drive methods. In kinematic Stirling engines, manual linkages like cranks, connecting rods, or flywheels are used to move the working fluid through the

engine's cycle like that of a reciprocating engine. These engines use temperature-resistant seals around the piston which is exposed to high temperatures. This imposes strict requirements on the materials that can be used to make the seals to ensure high reliability. Unlike kinematic Stirling engines, free-piston engines use pressure variations in the working fluid to generate motion in the reciprocating components. In FPSE work is generally removed via the use of a linear alternator. Because FPSE have no manual linkages and they use clearance seals both the reliability and life expectancy of the engine are increased as there is no wear in the system. In a FPSE the mechanical dynamics and the thermodynamics are highly coupled while in kinematic engines, only the behavior of the working fluid is required to determine the performance of the engine as the dynamic phases are fixed by the mechanical linkages. This makes designing a FPSE more complicated as the performance of each individual component is tied to the other parts of the engine.

4. Free-piston Stirling engine design concepts

A schematic of a Stirling converter is shown in **Figure 1**. The key components are the hot heat exchanger, regenerator, cold heat exchanger, displacer, flexures, piston, and linear alternator. The first step in the design process is to use a one-dimensional thermodynamic modeling tool such as the Sage modeling software produced by Geodon Associates [5]. This model can be used to predict dimension of the Stirling engine components as well as the estimated performance of the engine. An example of the predicted performance variable from Sage is listed in **Table 1**. The estimated Stirling cycle efficiency (heat to work) is about 45%. The system efficiency (fuel to electricity) is around 38.3%.

After the initial sizes of the components are determined based on the power output of the engine being designed, a detailed examination of each component is conducted to ensure that the manufactured parts will meets the required operational life and to minimize conversion losses. There are various ways in which conversion losses occur in a Stirling engine [6] including flow separation, insufficient fluid travel distance, dead volumes, poor regenerator performance, thermal conduction losses, and shuttle and pumping losses. Many of these

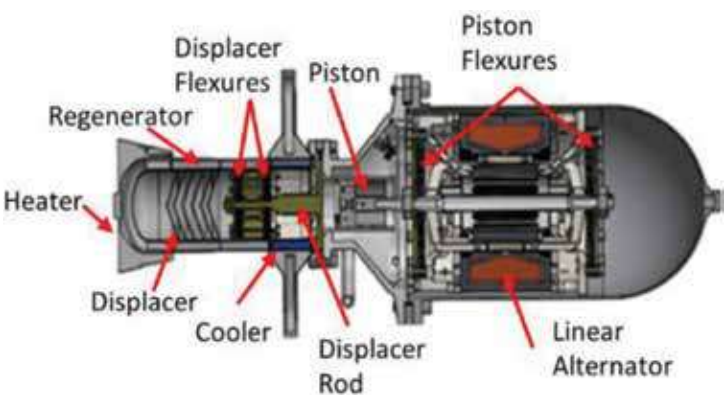

Figure 1. Stirling converter schematic.

Item	Value
Electrical power (W)	1215
Total thermal input (W)	3017
Parasitic loss/wall loss (W)	184
Heat rejection (W)	1493
Net cycle power (W)	1350
Stirling cycle efficiency (%)	44.74
Carnot efficiency (%)	71.01
Fraction of carnot (%)	63.00
Assumed alternator efficiency (%)	95.00
Burner efficiency (%)	90.00
System efficiency (%)	38.25

Table 1. Results of Stirling engine design analysis model.

losses are related to limitations in traditional manufacturing and can be alleviated by using additive manufacturing to produce a continuous heater head assembly. For example, thermal losses can be reduced by controlling the size of the gaps between components. As the size of the gaps is reduced the thermal losses decrease however if they become to small it leads to unwanted wear on both the moving and non-moving components resulting in a reduction in the expected lifespan of the convertor. The tolerance needed to achieve the optimal gap size requires high precision machining and often additional finish machining is required to obtain the desired fit. With traditional manufacturing, the components of the heater head assembly are joined using brazing or welding leading to added design change as their tolerance is hard to control. If an integrated design is produced via additive manufacturing, not only can the gap size between components be controlled but a smooth flow path between the heat exchangers and regenerator can be ensured while further reducing dead volumes.

4.1. Heater head assembly

A crucial component of a FPSE is the heater head assembly which consist of the hot heat exchanger, regenerator, pressure vessel, and cold heat exchanger. Historically the performance of Stirling engines was limited by the materials available. To achieve a long operational life of a FPSE, the hot end of the heater head assembly must withstand high temperatures and pressure over extended periods of time. Under these operating conditions, the reliability of the heater head assembly is influenced by the ultimate creep behavior of the material used. For operation at 810°C with an internal pressure of 3.3 MPa, the expected lifespan of the heater head would be limited if common metals are used because of their low tensile strength and creep resistance at high temperatures. Decreasing the operating temperature while increasing the life expectancy of the engine would vastly reduce the efficiency. Similarly, increasing the thickness of the heater head wall would also increase the life of the unit but it would lead to

an increase in axial conduction losses which also decreases the system's performance. Thus, the choice of an appropriate material with excellent creep resistance at high temperatures is critical to achieving both the desired performance and life expectancy of the designed FPSE. An evaluation of the use of various superalloys for the manufacturing of heater heads is presented in Ref. [7]. Finding a material that has all of the desired qualities is difficult. Alloys such as Udimet 720, IN 738LC, MA754, MarM-247, Inconel 718, and Inconel 625 are excellent candidates for use in high-temperature FPSE heater heads as they have high creep resistance and tensile strengths at high temperatures. However, they also have potential drawbacks such as post-weld cracking, welding difficulties, coarse grain recrystallization structures, and maximum temperature limitations.

In addition to the type of material used the type of heater head configuration used also is important. There are three types of heater heads commonly used in Stirling engines, monolithic, flat tubular, and vertical tubular heater heads, **Figure 2**. While monolithic heater heads are cheap and easy to manufacture, they have a limited heat flux and often used for small convertors. Both the flat tubular and vertical tubular configurations can have significantly higher heat fluxes. The flat tubular heater head design was used in solar Stirling engine applications. The high surface area and efficiency of the vertical U-shaped tubular heater head makes it ideal for use in larger Stirling convertors. The vertical tubes allow for easy integration with gas burners, however, using traditional manufacturing means, the reliability of the welded tube joints is low, and the associated manufacturing cost is high. The continued development of additive manufacturing would not only decrease the cost of a tubular heater head it would also increase the reliability as there would be no weld joints that are likely to fail.

4.1.1. Flow separation

A design drawback of a tubular heat exchanger design is the likelihood of jetting occurring at the outlet of the tubes. Flow separation between components is one of the major sources of conversion losses in a FPSE. Jetting at the exit of the hot heat exchanger not only increases

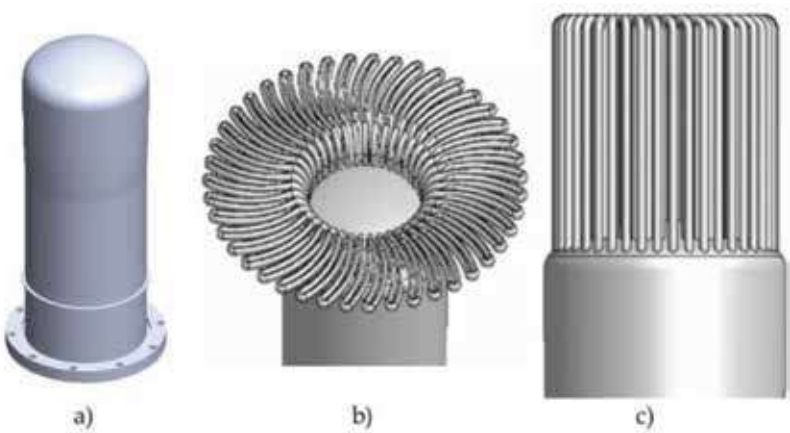

Figure 2. Different types of Stirling engine heater head configurations. (a) Monolithic, (b) flat tubular, (c) vertical tubular.

flow losses, it results in a reduction of the regenerator's performance. While the effects of jetting into the regenerator may be small for a random fiber regenerator where the flow can radially distribute within the regenerator, it is highly detrimental to the performance of a foil type regenerator where the flow in between foils cannot spread radially. Using computational fluid dynamics (CFD), the flow distribution between components can be analyzed and modification to the geometry can be suggested to ensure a smooth flow transition between components. For example, an internal diffuser was designed to eliminate the effects of jetting for a 1 kW tubular heater head along with a comparison of the flow distribution, **Figure 3**. The addition of the diffuser in the plenum space between the hot heat exchanger and the regenerator increases the Stirling convertors efficiency although there are added flow losses across the diffuser. This simulation verifies the idea that the integrated design will minimize the flow losses and maximize the thermal efficiency.

4.1.2. Dead volume analysis

Using additive manufacturing to reduce the thermal losses are possible by reducing the dead volumes between the heat exchangers and regenerator through controlling the size and shape of these plenum spaces. Dead volumes are areas that are un-swept by either the power piston or displacer and occur in the generator, cooler, heater and all clearance spaces. Passive dead volumes are areas that do not take part in the volumetric expansion-compression cycle, which decrease the overall cycle efficiency. A detailed analysis of the impact of dead volumes in an entire Stirling engine is presented by Ref. [8]. In the heater head assembly, dead volumes occur in the hot space and expansion space. In the hot space area, the dead volume occurs in the knuckle section, **Figure 4a**. In traditional Stirling engine design when using a tubular type heat exchanger, the heater tubes penetrate through the pressure vessel wall and extend to the top of the regenerator. The portion of the heat exchanger tubes inside the pressure vessel do not act as part of the heat exchanger and only function to reduce the dead volume of the working gas. However, the volume inside the extended heater tube section still acts as dead volume. The size of this dead space is related to the length of the extended heater tubes inside of the pressure vessel which depends on the knuckle (R_k) and dome (R_D) radii, **Figure 4a**. As

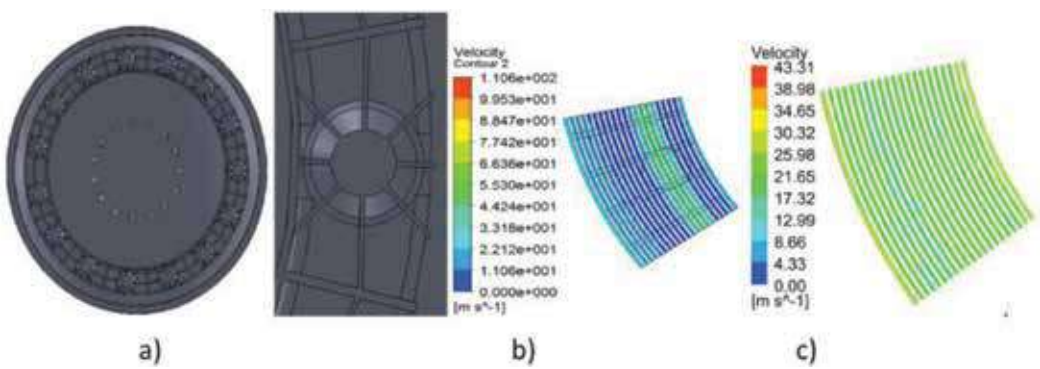

Figure 3. a) Designed diffuser plate and velocity distribution in a foil regenerator b) without and c) with the diffuser.

http://dx.doi.org/10.5772/intechopen.79413

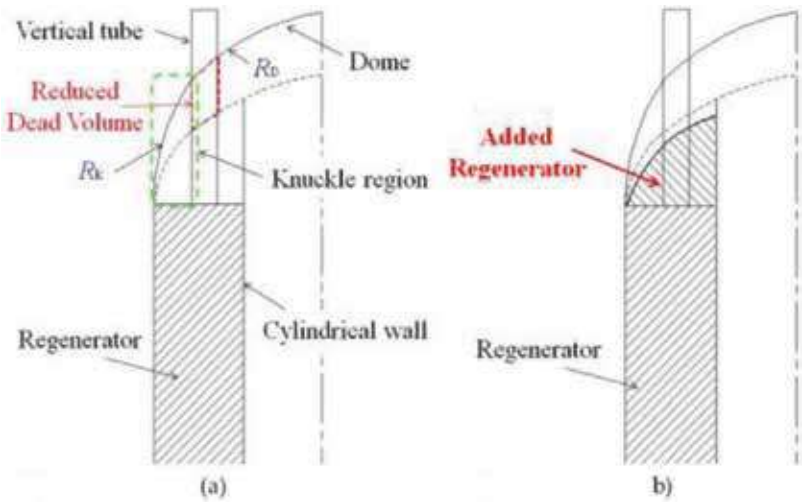

Figure 4. Dead volume in the hot space of heater head. (a) Knuckle and dome sections, (b) curved section of regenerator.

the dome radius is increased and the knuckle radius decreased the dome or cap of the heater head flattens. This reduces the length of the extended heater tubes, thus decreasing the dead volume. Ideally, the dome radius would be increased and the knuckle radius decreased until the dead volume was eliminated, however this leads to a stress concentration in the knuckle region from the high temperatures and pressures. A potential solution to reduce the stress is to increase the thickness of the wall in the knuckle region, but this results in an increase in axial conduction losses. Thus, the geometry of the knuckle and dome region must be optimized to balance axial conduction loses, localized stress, and dead volume. An alternative means of reducing the dead volume in the knuckle region is to add a curved section to the top of the regenerator to fill the knuckle region, **Figure 4b**. This method of dead volume reduction has never been employed before as manufacturing of the complex geometry was difficult and costly with traditional manufacturing methods. However, additive manufacturing can be employed to effectively create a complex regenerator geometry.

4.1.3. Stress analysis

Another major design challenge is the thickness of the pressure vessel wall. The heater head assembly not only experiences high pressures, but also a large thermal gradient. Therefore, the design is always a balance between minimizing thermal losses while maintaining structural integrity. Finite element analysis (FEA) is a useful tool to evaluate the stress within the heater head pressure vessel to ensure the parts will not fail. The pressure vessel of a FPSE heater head is generally designed using Section VIII Division 2 of the ASME Boiler and pressure vessel design code [9]. A coupled thermal and structural analysis out to be conducted to evaluate both the primary and secondary stresses in the heater head. An example of the resulting pressure distribution of a tubular heater head for a 1 kW FPSE is shown in **Figures 5** and **6** along with the employed boundary conditions. A zero-displacement boundary condition is applied

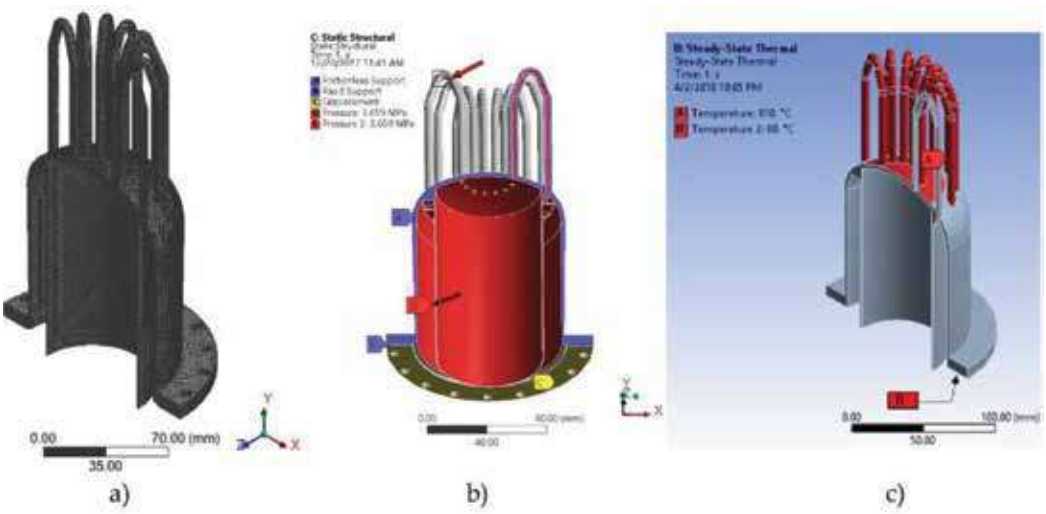

Figure 5. Heater head thermal and structural boundary conditions.

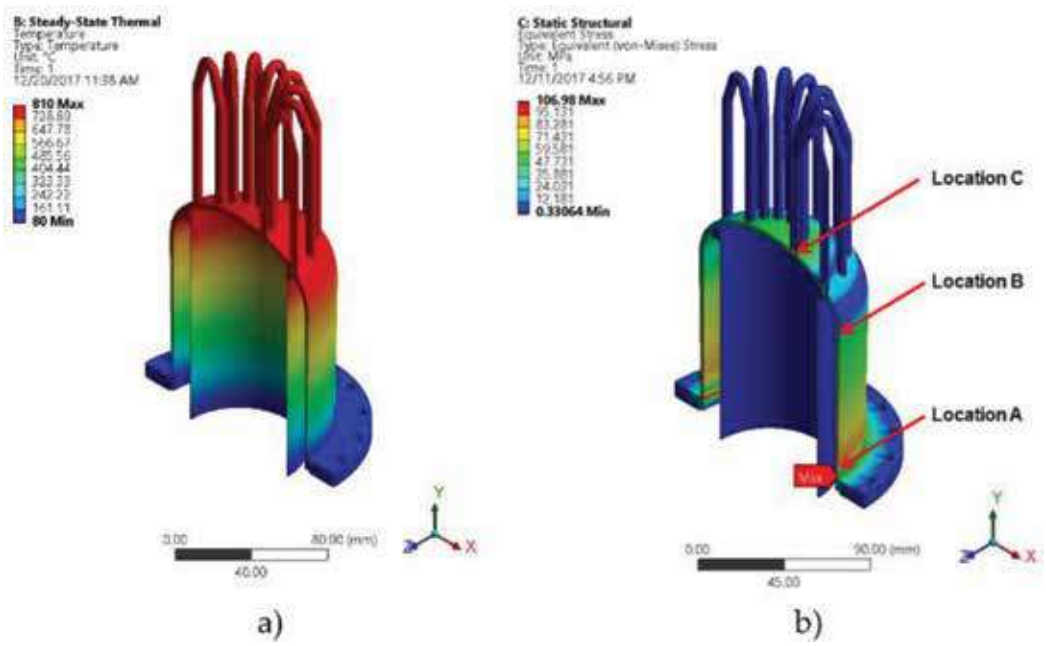

Figure 6. Temperature distribution and stress contours of heater head.

to the bottom surface of the heater head to prevent translation. Frictionless supports are used to mimic the symmetry in the system. A pressure of 3.66 MPa is applied to the internal surfaces of both the pressure vessel and tubular hot heat exchanger. For the thermal model, the bottom portion of the heater head assembly is set to 80°C and the outer surface of the hot heat exchanger tubes has an applied temperature of 810°C. The largest stress occurs at the bottom

flange and is 106.9 MPa at a temperature of 115°C. This is below the 238 MPa allowable stress of the material. Additionally, the membrane stresses at Location B & C are 36.6 and 32.8 MPa. The temperatures at these locations are 716 and 810°C respectively with allowable stresses of 198 and 84 MPa. Therefore, the stresses in the heater head assembly under peak operating pressure and temperature are acceptable based on ASME boiler codes as positive safety margins are obtained. Based on the creep and rupture life properties of Inconel 625, for the designed presented at locations C it would take over 6000 hours to reach an estimated 2% creep. The estimated rupture-life at location C is over 200,000 hours. For location B both the estimated creep and rupture-life are significantly higher in comparison to location C because of the lower temperature at location B.

4.1.4. Conduction losses

Axial conduction losses also contribute to conversion losses in a FPSE. As previously mentioned the axial conduction losses must be balanced with the allowable stress distribution and dead volumes. The conduction losses in the heater head assembly wall can be significant as it experiences a large thermal gradient. Minimizing the thickness of the displacer cylinder wall is only limited by the capabilities of additive manufacturing as there is equal pressure on both sides of the wall. Minimizing the thickness reduces axial conduction losses, therefore a thickness of 0.5 mm can be used based on the limitations of the state of the art in additive manufacturing. The outer wall of the heater head however does experience a large difference in pressure between the inner and outer surfaces. This wall is significantly thicker. As the axial conduction losses are a significant source of parasitic losses in a FPSE, every effort should be made to minimize the wall thickness. **Figure 7** shows four types of wall profiles often used. Steady state thermal models of the heater head can be used to estimate the conduction losses. The same boundary conditions used in the coupled thermal-structural model were used, **Figure 7**. In all the cases the thickness of the heater head dome and cap are kept the same as it is decided based on the allowable creep stress at the operating temperature. The thickness at the cold end can also be decided based on the local allowable stresses at the rejection temperature. Since this temperature is significantly lower the allowable stress is higher and this wall thickness is much smaller. In the single taper case, the thickness of the wall varies

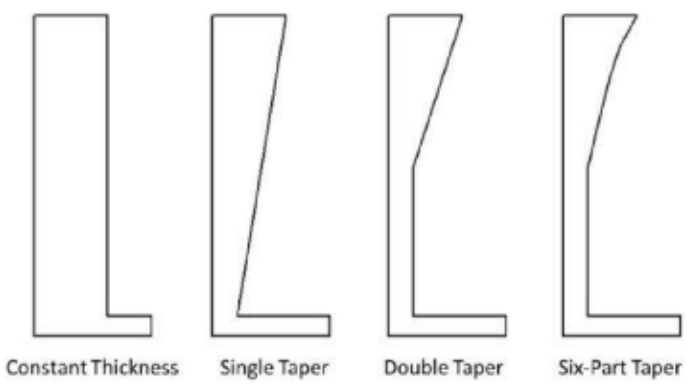

Figure 7. Heater Head Wall configurations.

linearly from the hot end (top) to the cold end (bottom). For the double taper, the thickness still linearly decreases however it reaches the minimum thickness at the midpoint of the wall and then remains constant. The six-part taper has five concave curves that decrease the thickness from the top to the middle.

The temperature distribution along the heater head wall varies based on the geometry examined (**Figure 8**). A nearly linear profile occurs for the constant wall thickness case. For the other cases considered a non-linear profiles forms. The non-linearity of the curve increases from the single to double to 6-part taper. The estimated axial conductions losses for the cases shown are listed in **Table 2**. The constant wall thickness case has the highest conduction losses, 83 W. Using a single taper results in a 23% reduction in the axial conduction losses compared to the constant wall thickness. If the cross-sectional area of the heater head wall is further reduced by using a double taper the conduction losses decrease an additional 4%. The 6-part tapper has the lowest conduction losses of the four cases shown.

4.2. Regenerator

The regenerator is crucial to the efficiency of a FPSE [10]. The regenerator acts as a means of temporary energy storage and is located between the hot and cold heat exchangers. When the working fluid travels from the hot heat exchanger to the cold heat exchanger, it transfers a portion of its energy to the solid regenerator medium. When the flow travels back from the cold to hot heat exchanger, it retrieves the energy from the regenerator. Various types of regenerators have been investigated to improve the heat transfer and achieve a high storage capacity. The types of regenerators investigated include woven screens, random fibers,

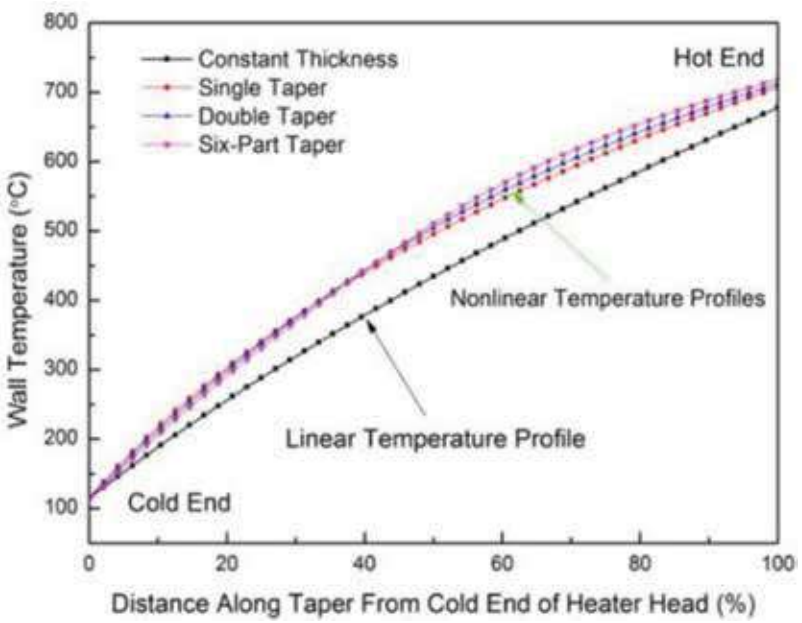

Figure 8. Temperature profile in the heater head wall.

Taper profile	Conduction loss (W)
Constant thickness	82.9
Single taper	63.7
Double taper	60.3
Six taper	54.7

Table 2. Conduction loss results for heater head taper configurations.

wrapped-foils, and segmented-involute foils [11]. Theoretically, a foil regenerator would have the best performance as it has the highest possible figure of merit which is the ratio of the heat transfer coefficient to the friction coefficient. However, because it is nearly impossible to manufacture a robust foil regenerator they are seldom used in FPSE. Using traditional manufacturing techniques, foil regenerators are made by wrapping the foils layer by layer using pre-formed dimples on the foils for spacing, **Figure 9a**. Because the performance of a foil regenerator is directly dependent on the spatial structure of the foils. If the foil spacing changes, the performance dramatically reduces. Unfortunately, due to thermal expansion during thermal cycles, the foil spacing changes within a short period because foils are not well connected and supported. This change leads to flow redistribution and a severe decrease in regenerator effectiveness. Therefore, FPSE manufactures use a less efficient albeit more reliable regenerator to ensure consistent operation. Although woven screen regenerators can be manufactured with high reliability there is a limit on their porosity which limits the maximum engine performance possible [12]. Random fiber regenerators are not limited by porosity, but their effectiveness is lower as they have a smaller area to volume ratio and significantly higher flow losses compared to foil regenerators. **Figure 9b** shows a random fiber regenerator.

Using additive manufacturing methods, a robust foil regenerator can be fabricated that has the same high reliability as a mesh screen regenerator while having superior heat transfer characteristics and minimal flow losses. The thin foils of the regenerator are ingeniously interconnected to increase the rigidity of the regenerator and maintain uniform foil spacing at high temperatures. The current state of the art in additive manufacturing has a limit on the minimum thickness based on the nominal diameter of the powder metals used. Currently the minimum foil thickness is 0.3 mm. Webs are designed to strengthen the regenerator and to keep the foil spacing unchanged. The designed regenerator is shown in **Figure 10**. There is a curved section at the top of the regenerator that is designed to fit into the space between the knuckle wall and displacer cylinder wall of the heater head to reduce the detrimental dead volumes. A ring is also added to the bottom of the regenerator to both add extra support and to fix the regenerator's axial location in the heater head assembly.

Using FEA, the robustness of the regenerator is investigated. A temperature of 810°C is applied to the top of the regenerator foils and a temperature of 80°C is applied to the bottom surface, **Figure 11**. For the structural model, the bottom edge of the outer ring is fixed to prevent the regenerator from translating, additionally, frictionless supports are applied to the symmetry planes. Because of the novel design of the regenerator, the only stress that occurs are thermally induced. The maximum stress, axial deformation, and radial deformation of

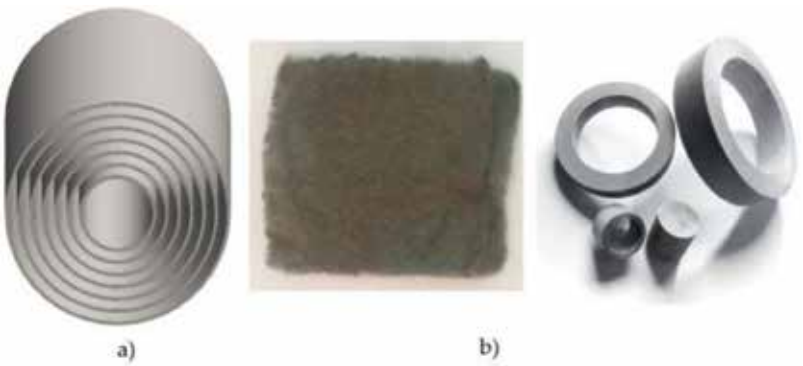

Figure 9. Wrapped foil and random fiber regenerators.

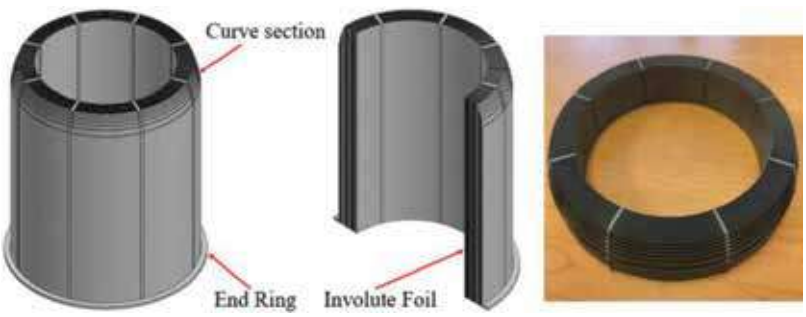

Figure 10. Involute foil regenerator.

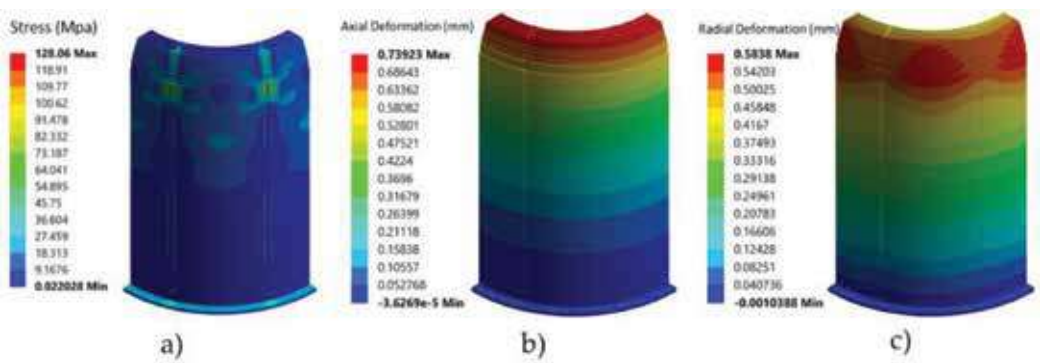

Figure 11. Stress distribution, axial and radial deformation of the involute regenerator.

the regenerator are shown in **Figure 11**. The maximum stress occurs in the outer foils near the regenerator ribs. This stress is well below the yield stress of Inconel 718 even at high temperatures leading to large margins of safety. The foils radially deform a maximum of 0.6 mm although this level of deformation may seem detrimental, there is only a 0.01 mm maximum deformation between foils. Therefore, the spacing between the foils remains constant even

at high temperatures. Thus, additive manufacturing can be used to produce a robust foil regenerator that can achieve the theoretically high figure of merit and vastly improve the performance of modern FPSE.

4.3. Heat exchangers

The hot heat exchanger in this study is a tubular type heat exchanger which has high heat transfer effectiveness while also exhibiting good fuel source integration capabilities. Using traditional manufacturing techniques, the heat exchanger tubes are bent and then welded to the pressure vessel. This can lead to numerous potential areas where leaks can form, thus the reliably of tubular heat exchangers are low. However, using additive manufacturing, the tubular heat exchanger and pressure vessel can be printed as one continuous part eliminating potential leaks and greatly increase the reliability. Additionally, the geometry of the tubes can be manipulated to further improve heat transfer with the chosen fuel sources burner. **Figure 12b** shows a tubular heater head where one end of the tube is extended through the knuckle region of the heater head and the other is connected to the dome of the pressure vessel. The diameter and length of the tubes are dependent upon the desired FPSE power output and the fuel combustor used. The heat exchanger shown in **Figure 12** has 15 U-shaped tubes with an internal diameter of 2.5 mm. However, the shape of the tube can be manipulated based on the feedback from additive manufactures and to increase the heat transfer, **Figure 5**. Furthermore, novel flow guides were used to increase the convective heat transfer around the tubes to further improve the system efficiency. The design of the burner interface with the hot exchanger is critical to the performance of the engine. A detailed description and numerical simulation of the flow guides and burner interface for the enhancement of heat transfer is available in Ref. [13]. An example of the combustion gas distribution is also seen in **Figure 12c**.

A fin-type heat exchanger is commonly used for the cold heat exchanger because of its low-cost and manufacturability (**Figure 13**). Extrusion or casting can be employed for the manufacturing of the fin heat exchangers. The dead volume can be reduced as well as minimizing flow separation by adding a curved section to the bottom of the heat exchanger. Usually a

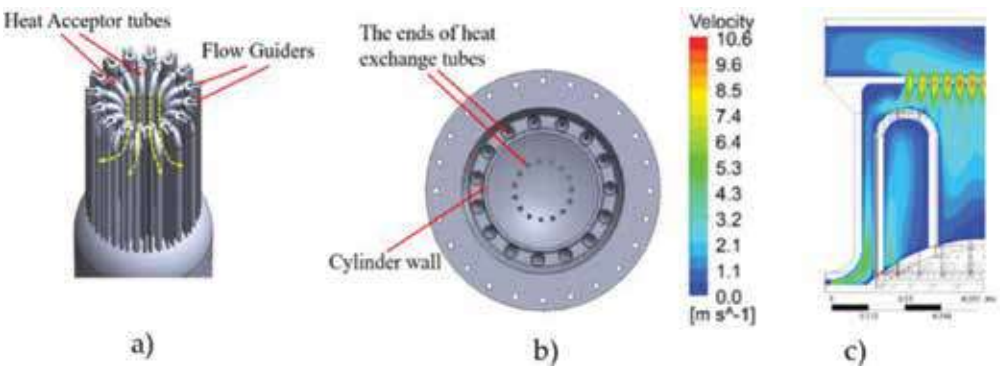

Figure 12. a) Tube bundle of tubular heat exchanger and (b) layout of tubular heat exchanger tubes and (c) combustion gas flow distribution.

highly conductive material such as copper is used for the cold heat exchanger to improve the heat transfer. The temperature difference between the coolant and the working gas in the cold heat exchanger is significantly smaller than that seen in the hot heat exchanger therefore the cold heat exchanger is typically larger compared to the hot heat exchanger.

4.4. Displacer assembly

The displacer assembly can also be evaluated using FEA to examine the resulting stress distribution. An example displacer assembly is shown in **Figure 14a**. Inconel 625 is used for the displacer cap while stainless steel 304 is used for the remaining parts. The thermal and structural boundary conditions are shown in **Figure 14b–d**. The top and bottom surface are set to 810 and 80°C, respectively. A 332.6 kPa pressure was applied to the outer surfaces of the displacer assembly. This is roughly 10% of the charge pressure. Additionally, a hydrostatic pressure load was applied to the displacer rod cylinder to mimic the pressure gradient from 332.6 kPa to 0 Pa. Again, frictionless supports are used to simulate the symmetry present in the system. Lastly,

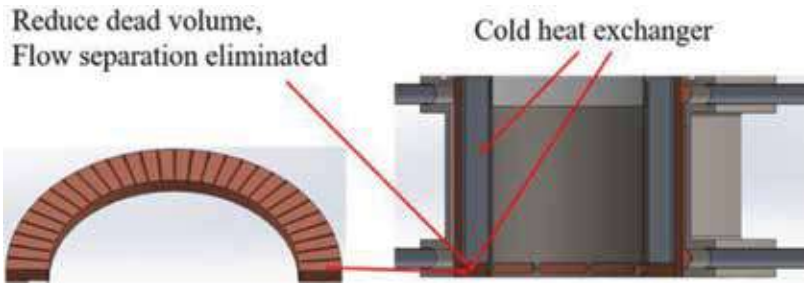

Figure 13. Cold heat exchanger.

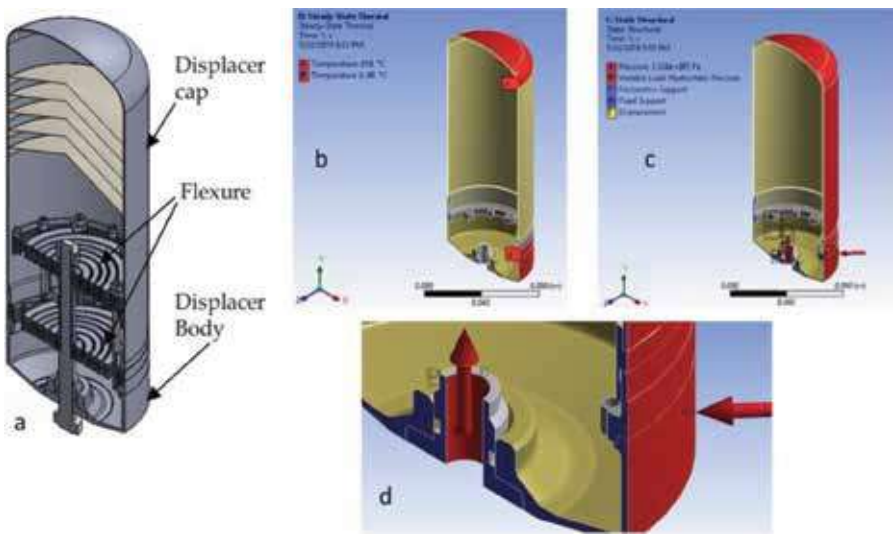

Figure 14. a) Displacer assembly, b) thermal, c) structural boundary and d) structural load at displacer body.

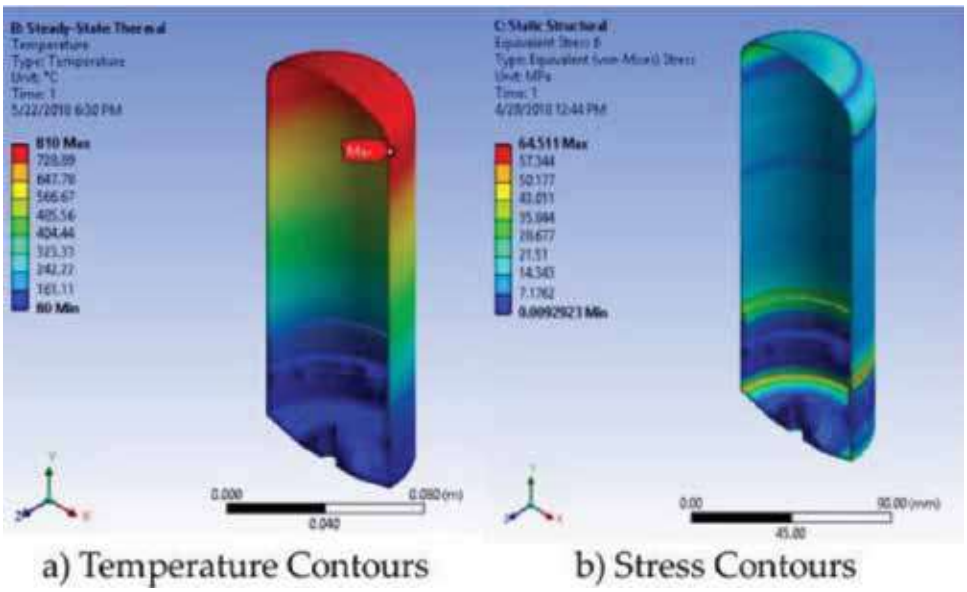

Figure 15. Temperature distribution and stress contours of displacer assembly.

fixed supports are applied to the faces where the flexures are connected to the displacer assembly. The predicted temperature and stress distributions are shown in **Figure 15**. The maximum stress of 64.5 MPa occurs at the interface between the displacer cap and the displacer body connector. The allowable stress for Inconel 625 at 90°C is 184 MPa. In addition to the maximum stress in the entire assembly, the maximum and membrane stresses for the individual displacer assembly parts has to be evaluated. In all cases both the maximum and membrane stresses shall stay below the allowable stresses at the corresponding part temperature with high margins of safety and to ensure that displacer design is acceptable and will have the desired operational life.

5. Dynamic analysis

5.1. Dynamic analysis of displacer assembly

In FPSE the cyclic motion of the working fluid is driven by the displacer. Both the displacer configuration and dynamics are critical to the performance of the engine, thus during the design of a FPSE, a dynamic analysis of the displacer assembly must be conducted. This analysis is used to figure out the required number of flexures to obtain the desired motion. A mass-spring diagram of the displacer is given in **Figure 16** along with a vector force polygon. An equation for the motion of the displacer is given in Eq. 1.

$$M_d \vec{\ddot{x}}_d = A_r \vec{P}_c + K_d \vec{x}_d + K_s \vec{x}_d + A_d\left(\vec{P}_c - \vec{P}_e\right) + D_d \vec{\dot{x}}_d \tag{1}$$

where x_d is the displacer motion, X_d is the amplitude of the displacer, X_p is the piston amplitude, Φ_m and Φ_p are the phase angle of the displacer and piston, A_r and A_d are the displacer

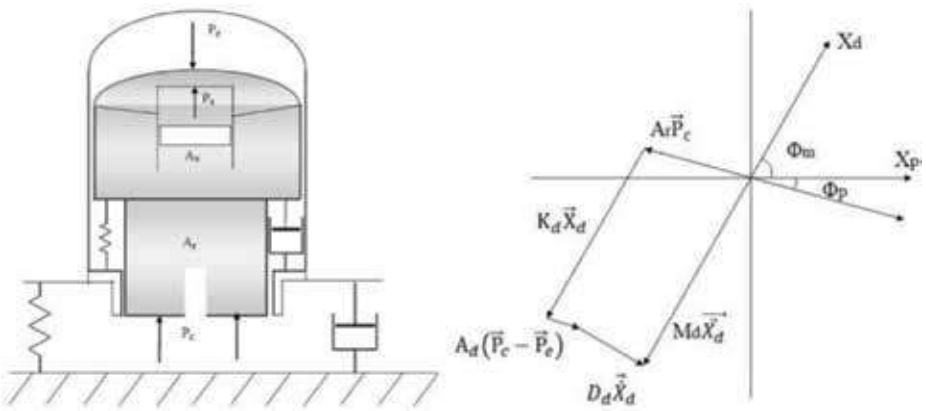

Figure 16. Dynamics of Stirling engine and displacer vector diagram.

road and frontal area, P_c and P_e are the pressure amplitude in the compression and expansion spaces, D_d is the displacer damping coefficient, M_d is the total moving mass, K_d is the total axial spring rate of the displacer flexures, $\vec{\dot{x}}_d$ is the displacer velocity, and $\vec{\ddot{x}}_d$ is the displacer acceleration. The velocity of the displacer assembly is calculated using Eq. 2.

$$\dot{x}_d = X_d \omega \cos(\omega t) = X_d \omega \sin\left(\omega t + \frac{\pi}{2}\right) \tag{2}$$

This is a harmonic function with the same frequency as the displacement and an amplitude ω times as large. The velocity is 90° out of phase with the displacement. The acceleration of the displacer assembly is given by Eq. 3:

$$\ddot{x}_d = -X_d \omega^2 \sin(\omega t) = X_d \omega^2 \sin(\omega t + \pi) \tag{3}$$

The acceleration is 180° ahead of the displacement with a ω^2 times larger amplitude. The remaining parameters listed in Eq. 1 are determined based on the one-dimensional thermodynamic model Sage. The main reason the dynamic analysis is conducted is to determine the number of flexures required. Based on the parameters for a 1 kW engine used as a case study here, a total of 8 flexures is needed. However, the natural frequency of the number of the system is considered as well. Thus, based on variations in fabrication and uncertainties a total of 10 flexures shall be chosen. A rocking mode analysis is used to determine the natural frequency of the system rocking mode to ensure that it is far from the operating frequency. In this system for 10 flexures, the frequency is 159 Hz this is far from the operating frequency of 60 Hz and its multiples. Therefore, the use of 10 flexures is acceptable.

5.2. Rocking mode analysis

The rocking mode of the displacer out to be analyzed to ensure that it is not close to the operating frequency or its harmonics. If it is, it can result in rubbing of the displacer on the pressure vessel inner wall leading to unwanted wear and a decrease in lifespan (**Table 3**). The rocking mode analysis is also used to determine the height between flexure stacks and verify the

Numbers of Flexure	Total Moving mass m (Kg)	*a* (m)	*b* (m)	K_r (N/m)	f_n(Hz)
10	0.931	0.01693	0.0093	2,225,346	158.6

a: the distance from spring to wheel base, b: the distance from spring to displacer center of gravity, K_r: flexure radial spring rate, f_n: rocking frequency

Table 3. Calculated model frequencies.

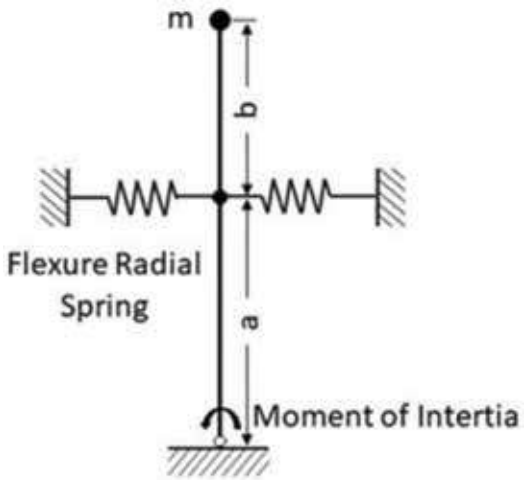

Figure 17. Displacer assembly rocking mode.

quantity from the dynamic analysis. As seen in **Figure 14a**, the flexures are separated into two stacks. Each stack consisted of five flexures. A schematic of the rocking mode analysis is depicted in **Figure 17**. The rocking or natural frequency is determined using Eq. 4.

$$f_n = \frac{1}{2\pi}\frac{\sqrt{a^2 k_r - mg(a+b)}}{m(a+b)^2} \tag{4}$$

where *a* is the distance between the flexure stacks centers and wheelbase, *b* is the distance between the center of gravity of displacer assembly and flexure stacks centers, K_r is the total radical spring rate of the flexures, *m* is the total moving mass of displacer assembly, and *g* is the gravity of earth. The predicted natural frequency of the displacer assembly using two stacks of 5 flexures is 159 Hz. This is not only far from the operating frequency of 60 Hz it is also far from its harmonics (120 and 180 Hz). Therefore, excess rocking of the displacer is unlikely to occur under the given operating conditions.

6. Performance specifications

The final step in the design of a FPSE is to map the performance of the engine over an operating frequency range. For example, if the design operation is at 60 Hz the performance should be mapped in the 50–70 Hz range. Examining the performance of the engine over

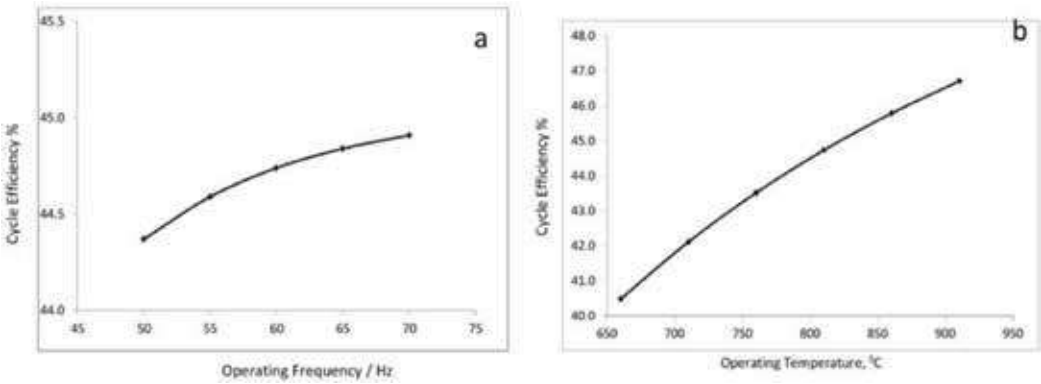

Figure 18. Frequency and temperature mapping of a FPSE.

a frequency range indicates that the efficiency of the system can be increased by increasing the operating frequency (**Figure 18a**). Generally speaking as the operating frequency increases both the efficiency and power density also increase [14]. For low power engines the frequency is limited to 80 Hz while for high power engines the operating frequency does not exceed 60 Hz. The limitations on operating frequency are due to the high velocities that can occur in the heat exchanges and regenerators with high frequencies, limited flexure spring forces for a given geometry, and the proximity to grid power of 60 Hz. In addition to performance mapping over the frequency, mapping over a range of temperatures should also be performed. The performance of a FPSE at various temperatures is shown in **Figure 18b**. As the operating temperature increases the efficiency of the system also increases. By increasing the temperature from 660–910°C an increase in system efficiency of 5.32% is possible. Note that these does not consider any potential conversion losses that can occur due to the potentially thicker walls required to counteract the allowable creep stress at high temperatures.

7. Conclusion(s)

The design analysis of a FPSE was presented. The key components including the heater head pressure vessel, regenerator, hot and cold heat exchangers, and displacer are discussed. FPSE are ideal for use in various power conversion applications. In addition to the design constraints and approaches of various components, dynamic and rocking mode analyses of the engine are also presented. Manufacturing of an integrated pressure vessel and heat exchanger assembly enables a new degree of control over conversion efficiency. Additionally, CFD and FEA can be used to further reduce axial conduction losses and flow separation to increase efficiency. Additive manufacturing is not just limited to the manufacturing of the heater head, it can be used to generator a robust foil regenerator that will have the highest figure of merit possible to further increase the systems efficiency. Therefore, the use of emerging manufacturing techniques can help to achieve higher system efficiency, better reliability, and enhanced robustness while reducing the cost.

Acknowledgements

This project was conducted under United State DOE ARPA-E contract, DE-AR0000864. Authors would like to express their appreciation to DOE ARPA-E for the financial support.

Conflict of interest

The authors declare no conflict of interest.

Nomenclature

X_d	displacer amplitude
Xp	piston amplitude
Ar	displacer rod area
A_d	displacer frontal area
D_d	displacer damping coefficient
K_d	$N*K_{axial}$, total axial spring rate of displacer flexure
$\ddot{x}_d$	acceleration of the displacer
K_r	radial spring rate of displacer flexure
S_y	yield stress
S_u	ultimate stress
CHP	combined heat and power
BPV	boiler and pressure vessel
Φ_m	phase angle of displacer motion
Φp	phase angle of dynamic pressure in compression space
P_c	dynamic pressure amplitude in compression space
P_e	dynamic pressure amplitude in expansion space
M_d	total moving mass of displacer assembly
N	quantity of displacer flexure
K_{axial}	axial spring rate of displacer flexure
f_n	displacer rocking mode frequency

S_m	allowable stress
S_{creep}	creep stress
FPSE	free-piston Stirling engine
FEA	finite element analysis

Author details

Songgang Qiu* and Laura Solomon

*Address all correspondence to: songgang.qiu@mail.wvu.edu

Department of Mechanical and Aerospace Engineering, West Virginia University, Morgantown, USA

References

[1] Abbas M, Boumeddane B, Said N, Chikouche A. Dish Stirling technology: A 100 MW solar power plant using hydrogen for Algeria. The International Journal of Hydrogen Energy [Internet]. 2011 Apr;**36**(7):4305-4314. Available from: http://linkinghub.elsevier.com/retrieve/pii/S0360319910024997

[2] Renzi M, Brandoni C. Study and application of a regenerative Stirling cogeneration device based on biomass combustion. Applied Thermal Engineering. 2014;**67**(1):341-351

[3] Magri G, Di Perna C, Serenelli G. Analysis of electric and thermal seasonal performances of a residential microCHP unit. Applied Thermal Engineering [Internet]. 2012 Apr;**36**(1):193-201. Available from: http://linkinghub.elsevier.com/retrieve/pii/S1359431-111006533

[4] Hsu ST, Lin FY, Chiou JS. Heat-transfer aspects of Stirling power generation using incinerator waste energy. Renewable Energy [Internet]. 2003 Jan;**28**(1):59-69. Available from: http://linkinghub.elsevier.com/retrieve/pii/S0960148102000186

[5] Gedeon D. Sage Stirling-Cycle Model-Class Reference Guide. 11th ed. Athens, OH: Gedeon Associates; 2016

[6] Tanaka M, Yamashia I, Chisaka F, Yamashita I, Chisaka F. Flow and heat transfer characteristics of the Sritling engine regenerator in an oscillating flow. JSME International Journal. 1990;**33**(2):283-289

[7] Bowman R, Ritzert F, Freedman M. Evaluation of candidate materials for a high-temperature Stirling convertor heater head. In: AIP Conference Proceedings. AIP; 2004. pp. 821-828

[8] Puech P, Tishkova V. Thermodynamic analysis of a Stirling engine including regenerator dead volume. Renewable Energy [Internet]. 2011 Feb 1 [cited 2018 May 21];**36**(2):872-878. Available from: https://www.sciencedirect.com/science/article/pii/S096014811000337X

[9] Boiler and Pressure Vessel Code–2010 Edition. New York, NY: ASME; Retrieved 9 November 2011

[10] Kongtragool B, Wongwises S. A review of solar-powered Stirling engines and low temperature differential Stirling engines. Renewable and Sustainable Energy Reviews [Internet]. 2003 Apr;**7**(2):131-154. Available from: http://www.sciencedirect.com/science/article/pii/S1364032102000539

[11] Ibrahim MB, Tew RC Jr. Stirling Convertor Regenerators. Boca Raton: CRC Press; 2012

[12] Zhao TS, Cheng P. Oscillatory pressure drops through a woven-screen packed column subjected to a cyclic flow. Cryogenics (Guildf). 1996;**36**(5):333-341

[13] Costa S-C, Tutar M, Barreno I, Esnaola J-A, Barrutia H, García D, et al. Experimental and numerical flow investigation of Stirling engine regenerator. Energy [Internet]. 2014 Aug [cited 2017 Jul 24];**72**:800-812. Available from: http://linkinghub.elsevier.com/retrieve/pii/S0360544214006975

[14] Urieli I, Berchowitz DM. Stirling Cycle Engine Analysis [Internet]. A. Hilger; 1984. 256 p. Available from: https://books.google.com/books?id=d9pSAAAAMAAJ

Chapter 8

Municipal Solid Waste Management and Energy Recovery

José Carlos Escobar Palacio,
José Joaquim Conceição Soares Santos,
Maria Luiza Grillo Renó,
Juarez Corrêa Furtado Júnior, Monica Carvalho,
Arnaldo Martín Martínez Reyes and
Dimas José Rúa Orozco

Additional information is available at the end of the chapter

http://dx.doi.org/10.5772/intechopen.79235

Abstract

The contribution of this chapter is to deepen and widen existing knowledge on municipal solid waste (MSW) management by analyzing different energy recovery routes for MSW. The main aspects related to the composition of waste are addressed, as well as the technological routes for thermochemical and biochemical energy usage. Within the thermochemical route, incineration is currently the most utilized technology for energy recovery of waste, with generation of electricity and heat and also a decrease in the volume of the produced waste. Gasification and pyrolysis are alternatives for the production of chemical products from wastes. The biological route is an interesting alternative for the utilization of the organic fraction of MSW, as aerobic or anaerobic processes enable the production of biogas and of a compound that can be utilized as a fertilizer. Depending on the size of the population, composition of waste, and products to be obtained (energy or chemical), more than one technology can be combined for a better energy usage of waste.

Keywords: municipal solid waste, waste to energy, thermochemical route, biochemical route

1. Introduction

With the growth of world population and progressive increase in living standards, the consumption of goods and energy has also increased, along with land use change and deforestation, intensified agricultural practices, industrialization and energy use from fossil fuel sources. All of these have contributed to ever-increasing concentrations of greenhouse gases in the atmosphere, since the industrial era.

Municipal solid waste (MSW) is a manifestation of the unsustainable consumption of natural resources by humankind, which has led to—and continues to—the depletion of natural capital and environmental degradation.

Current global MSW generation levels are approximately 1.3 billion tons/year, and by 2025, these are expected to increase to approximately 2.2 billion tons/year. This represents a significant increase in per capita waste generation rates, from 1.20 to 1.42 kg per person per day, in the next 15 years (2018–2033). However, global averages are broad estimates only, as rates vary considerably by region, country, and even within cities [1].

On a global scale, 70% of MSW is landfilled, 19% is recycled, and only 11% is utilized in Waste-to-Energy (WtE) schemes—this occurs due to logistical and economic issues—such as primary fossil energy scarcity and landfill volume restrictions [2].

The concept of circular economy (CE)—while not entirely new—has recently gained importance in the agendas of policymakers, to address the aforementioned and other sustainability issues [3]. The aim of CE is to maintain the value of products, materials and resources as long as possible, to minimize the use of resources; in other words, CE is based on a "win-win" philosophy that states that prosper economy and healthy environment can co-exist [4].

WtE plants have a dual objective: reduce the amount of waste sent to landfills and produce useful energy (heat and/or power). The WtE supply chain provides a method for simultaneously addressing issues related to energy demand, waste management and emission of greenhouse gases (GHG), achieving a circular economy system (CES) [5].

Traditionally, WtE has been associated with incineration. Yet, the term is much broader, embracing several waste treatment processes that generate energy (electricity and/or heat), such as pyrolysis, conventional or plasma arc gasification, as well as nonthermal processes such as anaerobic digestion and landfill-gas recovery.

2. Municipal solid waste: general aspects

2.1. Definition

Municipal solid waste (MSW), also referred to as trash or garbage, consists of several items that are discarded after use, such as grass clippings, furniture, clothing, food scraps, product packaging, bottles, newspapers, appliances, paint, and batteries [6]. Construction, industrial, and hazardous waste are not considered MSW.

http://dx.doi.org/10.5772/intechopen.79235

2.2. Waste hierarchy and MSW composition

In recent decades, there has been increasing pressure on developed countries to reduce their waste associated with single-use discarded materials. The objective is to conserve natural resources, including energy (which is utilized for the production of such materials), and reduce the amount of materials disposed in sanitary landfills. The philosophy of waste management aims at decreasing the amount of waste generated by society and incentivizing reutilization and recovery of its energy content, when reutilization or recycling is not possible through biochemical or thermochemical technological routes.

Figure 1 presents a scheme based on the pyramid proposed by the European Commission. Different management strategies are ranked from most to least environmentally preferred.

Most WtE transformation processes require pre-treatment of MSW. The characteristics of the raw materials within solid waste are affected by several factors, which range from the storage method (influence of humidity), maturity (wide variety of waste within an excavated landfill), classification policies (which vary depending on the country), to name a few. Successful implementation of WtE conversion technologies depends considerably on the efficiency of the process, which, in turn, depends on the quality of the waste considered. **Table 1** presents the global average composition of MSW.

The recovery of energy and materials from MSW through the production of a refuse derived fuel (RDF) is one of the alternatives advocated by waste management planners and government regulations [9]. RDF is the product of processing MSW to separate the noncombustible from the combustible portion, enabling better reuse of materials and recycling of MSW, with the possibility of achieving higher efficiencies in energy recovery treatments. RDF is an efficient fuel with several advantages in comparison with MSW, due to its high calorific value, more homogeneous chemical composition, more convenient storage and handling characteristics, and less carbon emissions.

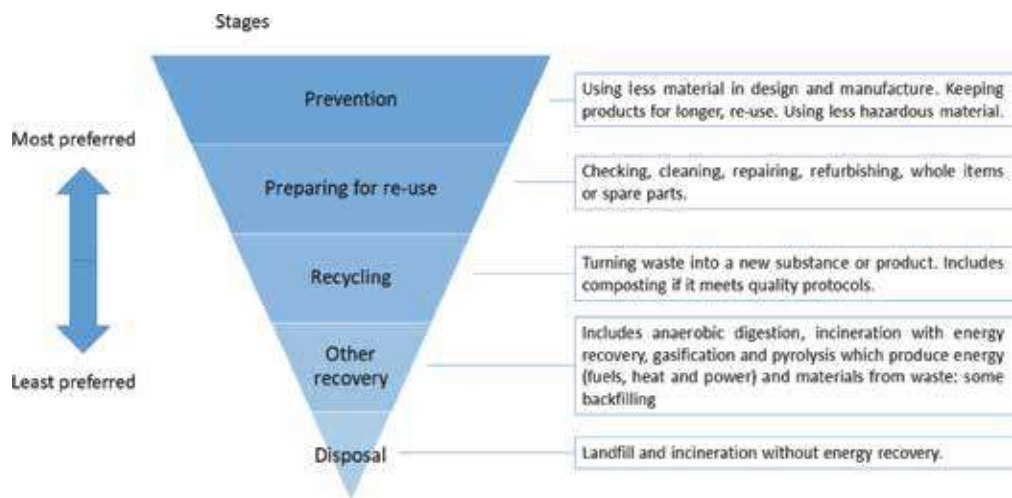

Figure 1. Waste hierarchy, adapted from [7].

Component	Fraction (%)
Organic	46
Metal	4
Plastic	10
Paper	17
Other	18

Table 1. Composition of global MSW [8].

Some studies have characterized the streams of materials involved in the RDF production process [9, 10], with descriptions on the characteristics of RDF in terms of composition and proximate and ultimate analysis [11, 12]. Also, the energy potential of RDF obtained from combustible solid waste has been evaluated by [13, 14].

Table 2 shows data compiled by [15] for the elemental composition of MSW and RDF.

The direct utilization of MSW in processes for the recovery of energy can lead to variable operation conditions, even unstable, with quality fluctuations in the final product. This is a consequence of the heterogeneity of the material regarding size, shape and composition. This is why firstly fuel is derived from waste, which is then utilized in the energy generation system [16]. For gasification and pyrolysis technologies, pretreatment is a fundamental requirement, which does not occur when considering plasma gasification and incineration.

With the objective of improving the handling characteristics and homogeneity of the material, the conversion process of MSW into fuels is constituted by different steps: trituration, sifting, selection, drying and/or pelletization. The least expensive and most

		MSW	RDF	RDF processed from landfill waste
Water content	wt% wet	34.2 [31.0–38.5]	10.8 [2.9–38.7]	14.4 [12–35.4]
Volatiles	wt% daf[a]	87.1 [87.1]	88.5 [74.6–99.4]	80.4
Ash	wt% dry	33.4 [16.6–44.2]	15.8 [7.8–34.5]	27.1
Net calorific value	MJ/kg daf	18.7 [12.1–22.5]	22.6 [1.1–29.3]	22
C	wt% daf	49.5 [33.9–56.8]	54.6 [42.5–68.7]	54.9
H	wt% daf	5.60 [1.72–8.46]	8.37 [5.84–15.16]	7.38
O	wt% daf	32.4 [22.4–38.5]	34.4 [15.8–43.7]	NA[b]
N	wt% daf	1.33 [0.70–1.95]	0.91 [0.22–2.37]	2.03
S	wt% daf	0.51 [0.22–1.40]	0.41 [0.01–1.27]	0.36

[a]Dry ash free.
[b]Not available.

Table 2. Composition of MSW and RDF: mean values and [min.–max.] [15].

http://dx.doi.org/10.5772/intechopen.79235

well-established current practice to produce RDF from MSW is mechanical pretreatment (MT); however, different schemes can be used, as presented by [17].

3. Energy conversion technologies

The characteristics of waste are important when selecting a specific WtE technology. The energy recovery efficiency depends on variables such as technology and quality of waste. An optimized plant that treats preselected waste can recover two or three times more electricity and heat than a more traditional plant that treats raw waste [18].

There is a wide range of WtE technologies, biochemical and thermochemical, for the conversion of solid waste into energy (steam or electricity). Fuels such hydrogen, natural gas, synthetic diesel and ethanol can be utilized [19, 20].

The biochemical route, in the case of MSW, refers to anaerobic digestion, which consists of controlled decomposition by microbes to reduce the organic material. Biochemical processes are used in the treatment of waste with high percentages of biodegradable organic matter and high moisture content. Methane, fuel for electricity generation, steam and heat can be produced.

One of the disadvantages of the biological treatment is the preprocessing required to separate MSW. Biochemical conversion of waste can be grouped into four categories: anaerobic digestion/fermentation, aerobic digestion, composting, and landfill gas power (LFG). These technologies are the most economic and environmentally safe means of obtaining energy from MSW [21].

In thermochemical conversion, both biodegradable and nonbiodegradable matters contribute to the energy output. Incineration, gasification and pyrolysis are types of thermochemical conversion processes, which are fundamental and necessary components of a comprehensive and integral urban solid waste management system [22].

The main advantages of thermochemical processes include lower masses and volumes of waste, decrease in the space occupied by landfills, destruction of organic pollutants such as halogenated hydrocarbons, and decrease in the emission of GHGs due to anaerobic decomposition. When considering the life cycle, the use of waste as a source of energy generates less environmental impacts than other conventional energy sources.

With incineration, the energy value of waste can be recovered; however, pyrolysis and gasification can be utilized to recover the chemical value of waste. The derived chemical products, in some cases, can be utilized as inputs in other processes or as secondary fuels.

With the conversion of MSW into fuels, higher calorific values are obtained along with more homogeneous physical and chemical compositions, lower levels of pollutants and ashes, less excess air required for combustion, and better conditions for storage, handling, and transportation. Therefore, it is recommended to establish a balance between increasing production costs and the potential reduction of costs associated with designing and operating the system. **Figure 2** shows thermochemical conversion processes, the products involved, and energy and material recovery systems.

In the next topic, the main aspects of each of the mentioned routes will be analyzed.

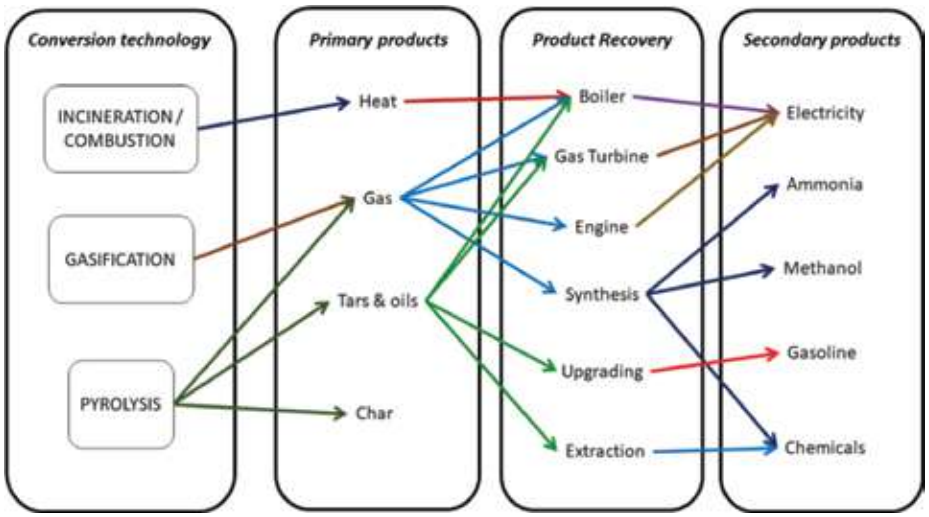

Figure 2. Thermochemical conversion processes and products, adapted from [23].

3.1. Thermochemical route

3.1.1. Incineration

Waste incineration is a specific treatment that reduces the volume of waste and its level of dangerousness, selecting and concentrating, or destroying the potentially harmful substances. Incineration processes can also offer the possibility of recovering the energy, mineral or chemical content of waste.

During recent decades, most industrialized countries with high population densities have employed incineration as an alternative procedure to controlled landfilling, for the treatment of MSW.

According to Ref. [24], the two main processes applied for the thermal treatment of waste are fluidized bed combustion and grate combustion. Another technological alternative is the rotary furnace or rotary kiln frequently employed in the field of waste treatment, for the combustion of hazardous waste in combination with other devices for gasification and pyrolysis [25].

Grate combustion, also known as mass burn combustion, is by far the most utilized, as it can handle larger items and only oversized materials have to be crushed. Fluidized bed combustion (as well as most pyrolysis and gasification processes) requires the waste to be shredded into small particles before being introduced in the combustion (pyrolysis/gasification) chamber [24].

The calorific value of the material to be incinerated and the polluting potential of the emissions generated are the main reasons for the evolution of incineration systems (higher combustion efficiencies and effective removal of contaminants).

Due to the heterogeneous nature of waste, some differences with respect to conventional fossil fuel power plants have to be considered in the energy conversion process. The efficiency

of a coal burning cycle is generally around 40%, while the efficiency of a garbage incineration cycle varies between 20 and 25%, if operating in a cogeneration mode, and up to 25–35% in the case of power production only [8, 26–28]. In general, fuel quality (i.e., waste) and other technical conditions (e.g., plant size, low temperature sources, etc.) limit the electrical efficiency of incinerators. This means that more than 70–80% of the heat generated by waste combustion is rejected to the environment.

The conversion efficiency of steam energy into electricity increases with higher steam temperatures and pressures. However, when increasing steam temperature, the heat transfer surfaces are submitted to severe high-temperature corrosion, caused by metal chlorides in the ash particles deposited on the gas tubes and by high concentrations of chlorine and sulfur in MSW. Most chlorines are present in plastics (e.g., PVC), while fluorines are present in polytetrafluoroethylene (PTEF), along with other inorganic compounds. Corrosion limits steam properties to maximums of 450–500°C and 4.0–6.0 MPa, while the steam temperature can reach 600°C in a coal cycle [27, 29].

HCl is highly corrosive at high (>450°C) and low (<110°C) temperatures. The heating surfaces of radiant parts are protected by a resistant refractory material and/or welded high-alloy to prevent corrosive attacks in the furnace of the boiler system. The feed water should be preheated to a minimum of 125°C, before being sent to the boiler, to prevent low-temperature corrosion [29].

Beyond corrosion problems, another negative aspect related to WtE plants is represented by erosion, especially the abrasion of surface material responsible for the vertical wear and tear. This is primarily caused by the ash particles present in flue-gas, and erosion appears mostly in the area of gas redirection. Tube wear is caused by a combination of corrosion and abrasion.

The pollutants released with exhaust gases after the burning of the waste affect the efficiency of the boiler. In an MSW incineration plant, efficiency is influenced by the heat lost with exhaust gases and by corrosion, which means that the temperature of exhaust gases cannot be significantly changed. For this reason, until 2013, the maximum efficiency of a boiler was approximately 87% [30].

The incineration of MSW emits GHG such as carbon dioxide (CO_2), methane (CH_4), nitric oxide (N_2O), hydrofluorocarbons (HFCs), polyfluorocarbons (PFCs), and sulfur hexafluoride (SF). When the furnace is maintained under high oxidizable conditions, there is no CH_4 being emitted in the gases exiting the chimney. When primary air is supplied from the storage tank, CH_4 is oxidized to CO_2 and H_2O.

The pollutants emitted during incineration hinder the improvement of the steam cycle, but new technologies developed for the recovery of energy have managed to improve the overall efficiency of the plant. Some of the factors that have contributed the most to the improvement of new plants include two-second increase in residence time for dioxin destruction, high performance with mobile grills, utilization of new metal alloys and high-performance exhaust gas cleaning systems [31].

Most recent data from the Eurostat database highlight that municipal waste was treated differently in the EU 28 in 2014: 16.1% is composted (Eurostat shows it as biological treatment),

27.3% is incinerated (total incineration including energy recovery), 28.2% is recycled and 28.4% is landfilled [32].

Japan has 1172 incinerators for the treatment of 80% of MSW; approximately 71% of MSW is incinerated with energy recovery generating 1770 MW [33]. In the United States, there are 77 WtE power plants, of which 78% employ mass burn technology (60 facilities), 17% refuse derived fuel (13 facilities), and 4% utilize modular combustion (4 facilities). Of these facilities, 77% produce electricity (59 units), 4% export steam (3 units), and 19% cogeneration—or combined heat and power (15 units) [32].

LFG power represents one of the most readily available, cheap and relatively simple forms of WtE options. However, the carbon dioxide emissions from landfills per ton of MSW processed are at least 1.2 t CO_2, much higher than WtE plants. Considering all environmental performance criteria (energy, material, and land consumption, air and water emissions, risks), WtE is the most favorable solution [24].

3.1.2. Gasification

Gasification is the thermal conversion of carbon-based material into a mixture of combustible gases, called syngas. Gasification is used to convert solid materials such as coal, coke, biomass and solid waste into a gas, with average composition 15–30% CO, 12–40% H, and 4.5–9% CH_4. The lower heating value (LHV) of syngas is between 4 and 13 MJ/Nm^3, depending on the oxidizing agent used in gasification, operating conditions, among other factors [34]. From the syngas gas produced, different chemical intermediate products can be obtained, with different industrial uses. Energy can also be obtained, in the form of power, heat or biofuel. Gasification temperature is one of the most important operation parameters that affects the performance of the process, due to the balance between endothermic and exothermic reactions involved.

Ref. [35] compared different thermochemical conversion processes, and verified that gasification technology is the best choice considering energy and environmental perspectives. Gasification has attracted attention and gained importance in recent years, presenting higher energy efficiency and being friendlier to the environment.

One of the challenges of MSW gasification is the characteristics of MSW, with variable size and moisture content, and highly variable on calorific value [36].

The gasification of MSW is an effective technique to reduce the amount of waste, and is relatively faster than the conventional processes (more residues can be treated in less time). The process of integrated gasification and combustion emits dioxin and furan within acceptable limits established by national and international agencies [37].

Although gasification has been employed for over 200 years, gasification of MSW is still in its early development stages. Some companies are developing smaller, compact gasifiers designed to be used by cities, towns, and military bases. Companies engaged in waste gasification and the characteristics of gasification plants can be consulted in the Global Syngas Technologies Council Database (GSTC) [38].

Plasma gasification is a technology suitable for MSW that uses a specific type of allothermal gasifiers. The heat that maintains the endothermic gasification reactions is provided by electrically generated thermal plasma (a plasma torch where an electric arc is created between two electrodes inside a vase and an inert gas is injected through this arc) [39].

The plasma torch temperature varies between 2700 and 4500°C, which is sufficient to crack the complex hydrocarbons in syngas, and all inorganic compounds (glass, metals, heavy metals) are melted in a volcanic-type lava that becomes a basaltic slag after cooling. The advantage of this system is that the syngas is produced in high temperatures, which ensures the destruction of all dioxins and furans. More information about this technology can be found in Refs. [40, 41].

Table 3 shows why gasification is attractive among other waste-to-energy technologies, due to its high efficiency for electricity generation at a lower unit cost.

3.1.3. Pyrolysis

Pyrolysis is the thermal degradation of organic material in an oxygen-deficient atmosphere at approximately 400–900°C, producing gas, liquid and solid products. The yield and composition of the products are influenced by a range of pyrolysis process parameters, including the type of waste, reactor system, gas residence time, contact time, heating rate, temperature, pressure ranges, and presence of catalysts [43].

Due to the different operation conditions, pyrolysis can be classified into three main categories: slow, fast and flash pyrolysis.

Pyrolysis is a promising technology and is currently utilized in many regions of the world for MSW disposal and energy generation. The objective of MSW pyrolysis is to treat waste, reduce its volume and associated hazards, destroying potentially harmful substances. Pyrolysis can also involve energy recovery from waste, in the form of heat, steam, electricity, or fuel (e.g., oil, char, and gas).

There are several types of pyrolysis reactors for MSW treatment operating in different countries, of which the most common are fixed-bed, fluidized bed, and rotary kiln reactors. Fixed-bed equipment is easy to operate and control, but presents disadvantages such as uneven

Performance parameter	Incineration	Pyrolysis	Plasma gasification	Conventional gasification
Capacity (t/day)	250	250	250	250
Conversion efficiency (MWh/t)	0.5	0.3	0.4	0.9
Power generation capacity (MWh/day)	160	180	108	224
Unit cost/kWh installed	435	222	1000	125
Unit cost (US$/nominal ton/day)	500	160	960	112

Table 3. Comparison between different MSW thermal treatment technologies [42].

heating and discontinuous running. The fluidized bed reactor can operate continuously and presents some advantages, such as high heat transfer efficiency and manageable temperature, but the resulting pyrolysis gas presents low calorific value. The rotary kiln reactor presents high internal heating and good adaptability to MSW; however, this technology presents a difficulty associated with the sealing of connectors [44].

More details on typical pyrolysis reactors, problems and MSW plants and products can be found in Refs. [42, 45, 46].

3.2. Biochemical route

3.2.1. Anaerobic digestion

Anaerobic digestion consists of a set of processes in which microorganisms consume the organic matter present in waste, in the absence of oxygen. This process occurs naturally in some types of soil and in the sediments settled on the bottom of a body of water (e.g., rivers, lakes, oceans, and swamps), where oxygen cannot penetrate. Decomposition of the submerse biomass occurs at the bottom of hydroelectricity reservoirs, producing methane.

There are several chemical reactions associated with conversion processes, which are in chemical balance. Generally, although some authors classify the anaerobic digestion process in two or even three steps, it is more common to utilize four steps to describe the process, as depicted in **Table 4**.

The main aspects that influence anaerobic digestion are [48, 49]:

pH/alkalinity: methanogenic bacteria are sensitive to acid environments, and an increase in the pH will inhibit their growth. pH varies throughout the different steps of the process due to the generation of fatty acids, CO_2, and bicarbonates. pH correction is accomplished through the addition of a basic compound ($CaCO_3$, NaOH). The optimal range of pH is between 6.6 and 7.4.

Temperature: temperature is related to the growth of microbes, and therefore, its control is very important for optimal growth/development of microorganisms and performance

Step	Description
Hydrolysis	Organic polymolecules are cracked into standard molecules such as sugars, amino, and fatty acids with the addition of hydroxyl groups. This is accomplished by hydrolytic bacteria.
Acidogenesis	Sugars, fatty, and amino acids are converted into smaller molecules, with the formation of volatile fatty acids (acetic, propionic, butyric, and valeric acids) and production of ammonia, carbon dioxide, and H_2S as subproducts.
Acetogenesis	The molecules produced during acidogenesis are digested, producing carbon dioxide, hydrogen, and acetic acid.
Methanogenesis	Formation of methane, carbon dioxide, and water.

Table 4. Description of the anaerobic digestion phases [47].

of anaerobic digestion. The process can occur in two ranges, mesophilic (25–40°C) and thermophilic (55–65°C). The mesophilic range is an interval of temperature conditions that enables bacteria to be more tolerant to changes in the environment, constituting more resistant microorganisms, but with higher retention times and lower production of biogas. This condition enables the use of simpler reactors, without complex control systems, with simpler operation strategies that entail lower capital costs. However, within thermophilic conditions, there is a higher production of biogas, with lower retention times. In these conditions, microorganisms are less tolerant to changes in the environment, which if occur, can compromise the production. A more complex, precise control system is required, with higher capital costs associated.

Substrate concentrations: an increase in the organic load can lead to an excessive production of acids, which can act as inhibitors for other reactions and cause lower biogas yield.

Partial H_2 pressure: an increase in pressure can lead to system collapse due to accumulation of acids.

C/N ratio: in the anaerobic digestion process, carbon corresponds to the source of energy, and nitrogen enables microbial growth. The optimal ratio between carbon (C) and nitrogen (N) varies between 20 and 30. High values of the C/N relationship are associated with a fast consumption of nitrogen, which can limit microbial growth and reduce gas production. Lower C/N values lead to accumulation of ammonia, which affects the pH of the reactor.

Anaerobic digestion adds value to MSW, generating an overall positive impact on the environment as it avoids a series of issues (negative impacts) associated with the natural decomposition process that occurs in landfills, besides enabling the substitution of other fossil raw materials.

The process of anaerobic digestion can occur in controlled environments, such as in biodigesters, which recover energy from waste, and in sanitary landfills. Sanitary landfills are locations for the controlled disposal of waste, reducing its negative environmental impact, and for the control of lixiviate material. Some landfills generate electricity from the biogas produced.

Biogas production from organics within the MSW stream is in the range of 100–150 m^3 of biogas per ton of source separated organics (SSO) [50].

3.2.1.1. Types of biodigesters

There are currently several commercially consolidated technologies for biodigestion, such as the Dranco, Valorga, Kompoga, BTA, and Linde-BRV systems. These technologies are widely employed in Europe, with 118 plants in operation, which totalize a combined treatment capacity 5.12 million tons of MSW per year. The Valorga system alone presents an installed capacity of 2.19 million tons of MSW [51, 52]. **Table 5** presents a summary of size, capacity and applications of anaerobic digestion systems.

More details about WtE such as biogas technologies, process, efficiencies, economic, and environment aspects can be found in Refs. [50, 54].

Size	Capacity (t/year)	Electricity production	Typical applications
Small	Up to 7500	25–250 kW_e	Residential and agricultural (farms) applications
Intermediate	7500–30,000	250–1 MW_e	Agricultural applications or digestible waste production facilities
Large	Above 30,000	Over 1 MW_e	Centralized, with several mixed raw materials (municipal, industrial)

Table 5. Size, capacity, and applications of anaerobic digestion systems [53].

3.2.2. Landfill gas

Landfill gas (LFG) is formed when organic wastes decompose anaerobically in a landfill. Although LFG gas is generated under aerobic and anaerobic conditions, the initial aerobic phase is short-lived and produces a gas with a much lower energy content than does the long-term anaerobic phase which follows.

There are several models developed to estimate the amount of biogas that can be produced from a sanitary landfill. According to Ref. [55], these models can be divided into:

Zero-order models: generation of biogas is considered constant throughout time, with no influence of age and type of waste.

First-order models: consider waste characteristics, such as humidity, carbon content, MSW availability.

Second-order models: utilize the reactions that occur during organic matter degradation, constituting a second-order kinetic model.

Numerical and mathematical models: consider the different variables involved in the process, and require a higher number of inputs.

The most utilized models for the estimation of biogas production from waste are the first-order models, of which the IPCC and LandGEM [55] are the most employed.

3.2.2.1. Intergovernmental panel on climate change (IPCC) model

Developed by the Intergovernmental Panel on Climate Change (IPCC), it is a first-order decay model (revised equations of IPCC-2006). It considers the degradation rates of waste and generation of methane throughout time. In the case of MSW, information on the different types of residues (food scraps, paper, wood, textiles, etc.) is required [56]. According to the IPCC model, the amount of methane produced is given by:

$$Q_{CH_4} = \sum_{t=S}^{E} n\left\{\left[\left(\frac{1-e^{-k}}{k}\cdot k\cdot RSUT_n\cdot RSUF_n\cdot L_{0(t)}\right)\cdot e^{-k(t-x)}\right]-R_x\right\}\cdot(1-OX) \quad (1)$$

Q_{CH_4} is the amount of methane generated per year (t CH_4/t waste), S refers to the beginning of landfill operation, E refers to the end of landfill operations, n is the considered year, and k is

the methane generation constant rate (y^{-1}). $RSUT_n$ is the amount of MSW generated in year n (t waste/year), $RSUF_n$ is the fraction of MSW destined to landfilling in year n (dimensionless).

$L_{0(t)}$ is the methane generation potential, expressed as:

$$L_{0(t)} = MCF_{(t)} \cdot DOC_{(t)} \cdot DOC_f \cdot F \cdot (16/12) \quad (2)$$

$MCF_{(t)}$ is the methane correction factor and reflects the management of the disposal locations (dimensionless), $DOC_{(t)}$ is the degradable organic carbon (t carbon/t waste), DOC_f is the fraction of degradable carbon (dimensionless), F is the methane fraction within biogas (dimensionless), 16/12 is the conversion ratio between carbon (C) and methane (CH_4) (dimensionless), $R(n)$ is the recovered methane (t CH_4/t waste), n are the years considered, and OX is an oxidation factor (reflects the amount of methane in the residual mass that is oxidized in the soil and cover layer (dimensionless).

3.2.2.2. LandGEM model

The Landfill Gas Emissions Model (LandGEM) was developed in 2005 by the Control Technology Center of the Environmental Protection Agency of the U.S.A. This mathematical model is utilized to estimate the amount of landfill gas generated in a specific location, allowing for variations to be introduced. Besides methane, 49 other compounds can be calculated. It is based on electronic worksheets that use a first-order decay equation. It is considered that methane generation peaks soon after initial disposal of waste and the methane generation rate decays exponentially as organic matter is consumed by bacteria [55]:

$$Q_{CH_4} = \sum_{i=1}^{n} \sum_{j=0.1}^{1} k \cdot L_0 \cdot \left[\frac{M_i}{10}\right] \cdot (e^{-k \cdot t_{ij}}) \quad (3)$$

Q_{CH_4} is the amount of methane produced per year (m^3/year), i is the time, in years, to be incremented, n is the inventory year, j is the time, in years/10, to be incremented, k is the methane generation rate ($year^{-1}$), L_0 is the potential methane generation (m^3 CH_4/t waste), M_i is the mass of solid waste received during year "I" (t/year), and t is the age of section "j" of waste M_i received during year "I" (years with decimal point, e.g., 3.2 years).

There is a great potential for electricity generation from landfill gas (biogas), as 1 ton of methane can be equivalent to 3.67 MWh—considering a conversion efficiency of 30%, this can be equivalent to 1.1 MWh_e [57]. This way, considering the ever-growing restrictions regarding MSW disposal along with the high volumes of MSW generated (with high energy potential), the use of anaerobic digestion has been the focus of several studies. The International Energy Agency (IEA) has a study group dedicated to biogas energy, Task 37: energy from biogas, with the objective of approaching the challenges related to economic and environmental sustainability of the production and utilization of biogas [58].

With the increasing necessity of promoting renewable energies, along with the emergence of new technologies that have lowered production costs, anaerobic digestion has been attracting the attention of developed European countries and also of populous countries such as India and China [1].

WTE technologies	Capital cost (US$/ton of MSW/year)	Operational cost (US$/ton of MSW/year)
Incineration	400–700	40–70
Pyrolysis	400–700	50–80
Gasification	250–850	45–85
Anaerobic digestion	50–350	5–35
Landfilling with gas recovery	10–30	1–3

Table 6. Cost estimates for different waste treatment technologies [60].

Another factor that contributes to the economic viability of anaerobic biodigestion is the progressive trend of countries adopting laws that prohibit the disposal of organic waste in sanitary landfills, demanding technologies that can effectively manage waste and recover the energy still contained within the covalent bonds of organic waste [58].

The study by Ref. [59] presented step-by-step, thorough calculations for landfill gas generation capacity, including the total amount of solid waste disposed, total organic matter, fractions of degradable organics, methane generated, methane captured, and finally, the amount of approximately 65,000 tons of captured LFG in 30 years. The leachate flow in the landfill was 8000 m^3/year. The landfill could produce approximately 135 GWh of electricity throughout its lifetime, with a global efficiency of almost 84%.

3.3. Economic aspects

Investment costs depend on the degree of complexity of the technology, as well as whether the system requires auxiliary processes such as pretreatment, gas cleaning, among others. **Table 6** presents cost estimated for different waste treatment technologies.

Regarding the costs associated with MSW disposal, biological routes present considerably lower costs than thermochemical routes. The facilities that utilize biological routes present simpler construction, when compared with thermochemical facilities. Besides, operational costs correspond to approximately 1% of the capital cost required.

4. Conclusions

Nowadays, it becomes more evident that mankind is facing serious difficulties regarding waste disposal and therefore can be its own victim. Waste disposal is unavoidable, but special, systematic efforts must be directed to establish a turnaround strategy.

One of the biggest challenges for modern society is establishing an effective strategy for the management and treatment of municipal solid waste. This strategy should consider, whenever possible, economic and environmental viewpoints. Global warming mitigation alternatives include the harvesting of landfill gas as an important waste management strategy.

There are currently different technological routes for municipal solid waste, which could transform these from a challenge or a problem into a source of clean energy and useful recyclable raw materials. At the same time, the impact of waste on the environment would decrease, benefitting human health and natural resources.

Acknowledgements

José Carlos Escobar Palacio wishes to express his thanks to the Brazilian National Research and Development Council (CNPq), grant no. 310674/2015-8 and the Foundation for Research Support of the State of Minas Gerais (FAPEMIG). Monica Carvalho would also like to acknowledge the support received by CNPq, grant no. 303199/2015-6. José Joaquim Conceição Soares Santos would like to thank the National Agency of Petroleum Gas and Biofuels (ANP) and the Foundation for Support to Research and Innovation of Espírito Santo (FAPES) for the financial support. Dimas José Rúa Orozco wish to express their thanks to the Coordination of Improvement of Higher Level Personnel (CAPES) for the financial support through the National Postdoctoral Program—PNPD/CAPES.

Author details

José Carlos Escobar Palacio[1]*, José Joaquim Conceição Soares Santos[2],
Maria Luiza Grillo Renó[1], Juarez Corrêa Furtado Júnior[3], Monica Carvalho[4],
Arnaldo Martín Martínez Reyes[1] and Dimas José Rúa Orozco[2]

*Address all correspondence to: jocescobar@unifei.edu.br

1 Federal University of Itajubá-UNIFEI, Itajubá, MG, Brazil

2 Federal University of Espírito Santo-UFES, Vitória, ES, Brazil

3 University of Campinas-UNICAMP, Campinas, SP, Brazil

4 Federal University of Paraíba, João Pessoa, Brazil

References

[1] The World Bank Group. What a Waste: A Global Review of Solid Waste Management [Internet]. 2018. Available from: http://web.worldbank.org/WBSITE/EXTERNAL/TOPICS/EXTURBANDEVELOPMENT/0,contentMDK:23172887~pagePK:210058~piPK:210062~theSitePK:337178,00.html [Accessed: 20-04-2018]

[2] Nowling U. Waste to Energy: An Opportunity Too Good to Waste, or a Waste of Time? [Internet]. 2016. Available from: http://www.powermag.com/waste-energy-opportunity-good-waste-waste-time/?pagenum=1 [Accessed: 20-04-2018]

[3] Geissdoerfer M, Savaget P, Bocken N, Hultink E. The circular economy—A new sustainability paradigm? Journal of Cleaner Production. 2017;**143**:757-768. DOI: 10.1016/j.jclepro.2016.12.048

[4] Tukker A. Product services for a resource-efficient and circular economy—A review. Journal of Cleaner Production. 2015;**97**:76-91. DOI: 10.1016/j.jclepro.2013.11.049

[5] Trindade A, Palacio J, González A, Rúa Orozco D, Lora E, Renó M, et al. Advanced exergy analysis and environmental assesment of the steam cycle of an incineration system of municipal solid waste with energy recovery. Energy Conversion and Management. 2018;**157**:195-214. DOI: 10.1016/j.enconman.2017.11.083

[6] US EPA, OSWER O of RC and R. Municipal Solid Waste [Internet]. 2018. Available from: https://archive.epa.gov/epawaste/nonhaz/municipal/web/html/ [Accessed: 19-04-2018]

[7] DEFRA—Department for Environment Food and Rrual Affairs. Guidance on Applying the Waste Hierarchy [Internet]. 2011. Available from: https://assets.publishing.service.gov.uk/government/uploads/system/uploads/attachment_data/file/69403/pb13530-waste-hierarchy-guidance.pdf [Accessed: 14-04-2018]

[8] WEC—World Energy Council. World Energy Resources: Waste to Energy. London: World Energy Council; 2013. pp. 1-14. DOI: 10.1080/09297040802385400. Available from: https://www.worldenergy.org/wp-content/uploads/2013/10/WER_2013_7b_Waste_to_Energy.pdf

[9] Caputo A, Pelagagge P. RDF production plants: I. Design and costs. Applied Thermal Engineering. 2002;**22**:423-437. DOI: 10.1016/S1359-4311(01)00100-4

[10] Rotter V, Kost T, Winkler J, Bilitewski B. Material flow analysis of RDF-production processes. Waste Management. 2004;**24**:1005-1021. DOI: 10.1016/j.wasman.2004.07.015

[11] Velis C, Wagland S, Longhurst P, Robson B, Sinfield K, Wise S, et al. Solid recovered fuel: Influence of waste stream composition and processing on chlorine content and fuel quality. Environmental Science & Technology. 2012;**46**:1923-1931. DOI: 10.1021/es2035653

[12] Velis C, Wagland S, Longhurst P, Robson B, Sinfield K, Wise S, et al. Solid recovered fuel: Materials flow analysis and fuel property development during the mechanical processing of biodried waste. Environmental Science & Technology. 2013;**47**:2957-2965. DOI: 10.1021/es3021815

[13] Srisaeng N, Tippayawong N, Tippayawong K. Energetic and economic feasibility of RDF to energy plant for a local Thai municipality. Energy Procedia. 2017;**110**:115-120. DOI: 10.1016/j.egypro.2017.03.115

[14] Consonni S, Giugliano M, Grosso M, Rigamonti L. Energy and environmental balances of energy recovery from municipal solid waste with and without RDF production. In: Proceedings of the Biomass Waste to Energy Symp.; 29 November-1 December 2006; Venice, Italy. 2006. pp. 1-12

[15] Bosmans A, Vanderreydt I, Geysen D, Helsen L. The crucial role of waste-to-energy technologies in enhanced landfill mining: A technology review. Journal of Cleaner Production. 2013;**55**:10-23. DOI: 10.1016/j.jclepro.2012.05.032

[16] Klein A. Gasification: An alternative process for energy recovery and disposal of municipal solid wastes [thesis]. Columbia University; 2002

[17] Sever Akdağ A, Atımtay A, Sanin F. Comparison of fuel value and combustion characteristics of two different RDF samples. Waste Management. 2016;**47**:217-224. DOI: 10.1016/j.wasman.2015.08.037

[18] Massarutto A. Economic aspects of thermal treatment of solid waste in a sustainable WM system. Waste Management. 2015;**37**:45-57. DOI: 10.1016/j.wasman.2014.08.024

[19] Valkenburg C, Gerber M, Walton C, Jones S, Thompson B, Stevens D. Municipal Solid Waste (MSW) to Liquid Fuels Synthesis, Volume 1: Availability of Feedstock and Technology [Internet]. 2008. Available from: http://www.pnl.gov/main/publications/external/technical_reports/PNNL-18144.pdf [Accessed: 04-05-2018]

[20] Karajgi SB, Yaragatti UR, Kamalapur GD. Modeling of power generation using municipal solid waste in India. International Journal of Electrical and Computer Engineering. 2012;**2**:197-202. DOI: 10.11591/ijece.v2i2.270

[21] Ofori-Boateng C, Lee KT, Mensah M. The prospects of electricity generation from municipal solid waste (MSW) in Ghana: A better waste management option. Fuel Processing Technology. 2013;**110**:94-102. DOI: 10.1016/j.fuproc.2012.11.008

[22] Mavrotas G, Skoulaxinou S, Gakis N, Katsouros V, Georgopoulou E. A multi-objective programming model for assessment the GHG emissions in MSW management. Waste Management. 2013;**33**:1934-1949. DOI: 10.1016/j.wasman.2013.04.012

[23] Begum S, Rasul MG, Akbar D. An investigation on thermo chemical conversions of solid waste for energy recovery. International Journal of Environmental and Ecological Engineering. 2012;**6**:624-630

[24] Babcock & Willcox Vølund. 21' Century Advanced Concept for Waste-Fired Power Plants [Internet]. 2012. Available from: http://www.volund.dk/~/media/Downloads/Brochures_-_WTE/Advanced_concept_for_waste-fired_power_plants.pdf [Accessed: 10-05-2018]

[25] Leckner B. Process aspects in combustion and gasification Waste-to-Energy (WtE) units. Waste Management. 2015;**37**:13-25. DOI: 10.1016/j.wasman.2014.04.019

[26] Di Maria F, Contini S, Bidini G, Boncompagni A, Lasagni M, Sisani F. Energetic efficiency of an existing waste to energy power plant. Energy Procedia. 2016;**101**:1175-1182. DOI: 10.1016/j.egypro.2016.11.159

[27] Meratizaman M, Amidpour M, Jazayeri SA, Naghizadeh K. Energy and exergy analyses of urban waste incineration cycle coupled with a cycle of changing LNG to pipeline gas. Journal of Natural Gas Science and Engineering. 2010;**2**:217-221. DOI: 10.1016/j.jngse.2010.08.005

[28] Lombardi L, Carnevale E, Corti A. A review of technologies and performances of thermal treatment systems for energy recovery from waste. Waste Management. 2015;**37**:26-44. DOI: 10.1016/j.wasman.2014.11.010

[29] Branchini L. Advanced waste-to-energy cycles [thesis]. Università di Bologna; 2012

[30] Wood S, Fanning M, Venn M, Whiting K. Review of State-of-the-Art Waste-to-Energy Technologies—Stage two, Case Studies [Internet]. 2013. Available from: http://www.wtert.com.br/home2010/arquivo/noticias_eventos/WSP%20Waste%20to%20Energy%20Technical%20Report%20Stage%20Two.pdf [Accessed: 08-05-2018]

[31] Porteous A. Energy from waste incineration—A state of the art emissions review with an emphasis on public acceptability. Applied Energy. 2001;**70**:157-167. DOI: 10.1016/S0306-2619(01)00021-6

[32] Cucchiella F, D'Adamo I, Gastaldi M. Sustainable waste management: Waste to energy plant as an alternative to landfill. Energy Conversion and Management. 2017;**131**:18-31. DOI: 10.1016/j.enconman.2016.11.012

[33] Lino F, Ismail K. Incineration and recycling for MSW treatment: Case study of Campinas, Brazil. Sustainable Cities and Society. 2017;**35**:752-757. DOI: 10.1016/j.scs.2017.09.028

[34] Násner A, Lora E, Palacio J, Rocha M, Restrepo J, Venturini O, et al. Refuse derived fuel (RDF) production and gasification in a pilot plant integrated with an Otto cycle ICE through aspen plusTM modelling: Thermodynamic and economic viability. Waste Management. 2017;**69**:187-201. DOI: 10.1016/j.wasman.2017.08.006

[35] Consonni S, Viganò F. Waste gasification vs. conventional waste-to-energy: A comparative evaluation of two commercial technologies. Waste Management. 2012;**32**:653-666. DOI: 10.1016/j.wasman.2011.12.019

[36] Panepinto D, Tedesco V, Brizio E, Genon G. Environmental performances and energy efficiency for MSW gasification treatment. Waste and Biomass Valorization. 2015;**6**:123-135. DOI: 10.1007/s12649-014-9322-7

[37] Thakare S, Nandi S. Study on potential of gasification technology for municipal solid waste (MSW) in Pune city. Energy Procedia. 2016;**90**:509-517. DOI: 10.1016/j.egypro.2016.11.218

[38] GSTC—Global Syngas Technologies Council. Worldwide Syngas Database [Internet]. 2018. Available from: https://www.globalsyngas.org/resources/world-gasification-database [Accessed: 10-05-2018]

[39] Mazzoni L, Ahmed R, Janajreh I. Plasma gasification of two waste streams: Municipal solid waste and hazardous waste from the oil and gas industry. Energy Procedia. 2017;**105**:4159-4166. DOI: 10.1016/j.egypro.2017.03.882

[40] Fabry F, Rehmet C, Rohani V, Fulcheri L. Waste gasification by thermal plasma: A review. Waste and Biomass Valorization. 2013;**4**:421-439. DOI: 10.1007/s12649-013-9201-7

[41] Sanlisoy A, Carpinlioglu M. A review on plasma gasification for solid waste disposal. International Journal of Hydrogen Energy. 2017;**42**:1361-1365. DOI: 10.1016/j.ijhydene.2016.06.008

[42] Wilson B, Williams N, Liss B, et al. A Comparative Assessment of Commercial Technologies for Conversion of Solid Waste to Energy. Boca Raton, Florida: Enviro Power Renewable, Inc; 2013. Available from: https://pdfs.semanticscholar.org/92ba/d2a1a1d4870a57b6fc2263e2e9a9fd882647.pdf

[43] Velghe I, Carleer R, Yperman J, Schreurs S. Study of the pyrolysis of municipal solid waste for the production of valuable products. Journal of Analytical and Applied Pyrolysis. 2011;**92**:366-375. DOI: 10.1016/j.jaap.2011.07.011

[44] Wu D, Zhang A, Xiao L, Ba Y, Ren H, Liu L. Pyrolysis characteristics of municipal solid waste in oxygen-free circumstance. Energy Procedia. 2017;**105**:1255-1262. DOI: 10.1016/j.egypro.2017.03.442

[45] Chen D, Yin L, Wang H, He P. Pyrolysis technologies for municipal solid waste: A review. Waste Management. 2014;**34**:2466-2486. DOI: 10.1016/j.wasman.2014.08.004

[46] Al-Salem S, Antelava A, Constantinou A, Manos G, Dutta A. A review on thermal and catalytic pyrolysis of plastic solid waste (PSW). Journal of Environmental Management. 2017;**197**:177-198. DOI: 10.1016/j.jenvman.2017.03.084

[47] Igoni A, Sepiribo I, Harry K. Modelling continuous anaerobic digestion of municipal solid waste in biogas production. Energy and Environmental Engineering. 2016;**4**:30-43. DOI: 10.13189/eee.2016.040302

[48] Khalid A, Arshad M, Anjum M, Mahmood T, Dawson L. The anaerobic digestion of solid organic waste. Waste Management. 2011;**31**:1737-1744. DOI: 10.1016/j.wasman.2011.03.021

[49] Themelis N. Anaerobic Digestion of Biodegradable Organics in Municipal Solid Wastes. New York: Found Sch Eng Appl Sci Columbia Univ; 2002. pp. 1-56. DOI: 10.1016/j.biotechadv. 2010.10.005. Available from: http://www.seas.columbia.edu/earth/wtert/sofos/Verma_thesis.pdf

[50] Environment Canada. Technical Document on Municipal Solid Waste Organics Processing. Ottawa: Government of Canada; 2013. Available from: http://www.compost.org/English/PDF/Technical_Document_MSW_Organics_Processing_2013.pdf

[51] Arsova L. European Technology Overview: Anaerobic Digestion (AD) of the Organic Fraction of the MSW. New Jersey: Rutgers University; 2016. Available from: http://eco-complex.rutgers.edu/FEW_Ljupka_Arsova.pdf

[52] Nalo T, Tasing K, Kumar S, Bharti A. Anaerobic digestion of municipal solid waste: A critical analysis. International Journal of Innovative Research in Science, Engineering and Technology. 2014;**3**:224-234

[53] GMI—Global Methane Initiative. Overview of Anaerobic Digestion for Municipal Solid Waste [Internet]. 2016. Available from: https://www.globalmethane.org/documents/AD-Training-Presentation_Oct2016.pdf [Accessed: 10-05-2018]

[54] Mutz D, Hengevoss D, Hugi C, Gross T. Waste-To-Energy Options in Municipal Solid Waste Management: A Guide for Decision Makers in Developing and Emerging Countries. Eschborn: Deutsche Gesellschaft für Internationale Zusammenarbeit; 2017. pp. 27-29. Available from: https://www.giz.de/en/downloads/GIZ_WasteToEnergy_Guidelines_2017.pdf

[55] Kamalan H, Sabour M, Shariatmad N. A review on available landfill gas models. Journal of Environmental Science and Technology. 2011;**4**:79-92. DOI: 10.3923/jest.2011.79.92

[56] Bianek J, Schirmer WN, Cabral AR, Mayer CLD, Eurich PHM, Martins EH. Comparação entre metodologias USEPA e IPCC para estimativa teórica de produção de biogás em aterro municipal. Biofix Scientific Journal. 2018;**3**:34-40. DOI: 10.5380/biofix.v1i1.56038

[57] Seadi TA, Rutz D, Prassl H, Köttner M, Finsterwalder T, Volk S, et al. Biogas Handbook. Esbjerg, Denmark: University of Southern Denmark; 2008. DOI: 10.1533/9780857097415.1.85. Available from: http://www.lemvigbiogas.com/BiogasHandbook.pdf

[58] IEA—International Energy Agency. Annual Report 2016. Paris: IEA Bioenergy; 2017. 126 pp. Available from: http://www.ieabioenergy.com/wp-content/uploads/2017/04/IEA-Bioenergy-Annual-Report-2016.pdf

[59] Chacartegui R, Carvalho M, Abrahão R, Becerra J. Analysis of a CHP plant in a municipal solid waste landfill in the south of Spain. Applied Thermal Engineering. 2015;**91**:706-717. DOI: 10.1016/j.applthermaleng.2015.08.069

[60] Kumar A, Samadder SR. A review on technological options of waste to energy for effective management of municipal solid waste. Waste Management. 2017;**69**:407-422. DOI: 10.1016/j.wasman.2017.08.046

Edited by Ibrahim H. Al-Bahadly

Energy conversion technology has always been a main focus for researchers in order to meet the increasing demand as well as securing a clean, consistent and reliable energy supply. The constantly rising fuel price is another good reason to develop alternative systems such as wind turbines, hydropower, photovoltaic systems and other renewable energy solutions. This book contains a collection of selected research works in the areas of electric energy generation, renewable energy sources, hybrid system, electromechanical energy conversion, electric machines, power electronic converters and inverters, energy storage, smart grid and traditional energy conversion systems. The book intends to provide academic and industry professionals working in the field of energy conversion and related applications with an update in energy conversion technology, particularly from the applied perspective.

Published in London, UK

IntechOpen

ISBN 978-1-83881-739-8